IN THE UNITED STATES PATENT AND TRADEMARK OFFICE

Appl. No.	:	10/501,842	Confirmation No. 8958
Applicant	:	Gerhard Bonnet	
Filed	:	January 18, 2005	
Title	:	PROCESS AND DEVICE FOR	
	:	MEASURING DISTANCE	
TC/A.U.	:	3662	
Examiner	:	Timothy A. Brainard	
Atty. Docket No.	:	PTK0025	
Customer No.	:	0832	

MAIL STOP AF
Commissioner for Patents
P.O. Box 1450
Alexandria, VA 22313-1450

DECLARATION OF PROF. DR. KLASS. BERGMANN ON THE FREQUENCY-SHIFTED FEEDBACK LASER WITH INJECTION OF NARROW BAND PHASE-MODULATED RADIATION FOR HIGH RESOLUTION RANGING

In the Office Action several documents have been cited that will be considered irrelevant to the average skilled person.

Since it is believed that this might stem from the mentioning of terms used in the US patent application, like "seed laser", "modulation", "phase control" and "frequency-shifted feedback-cavity", certain aspects of the physics involved will be briefly explained to show that the principles and objectives of the present invention are entirely different. In addition, a list of peered publications analyzing the principles in detail is given.

Only the work using an FSF-laser (Shattil, Phillips and Takeuchi) seems to warrant more detailed comments in the official reply as the average skilled person surely and easily realizes that the teachings of the other patents are completely unrelated to our scheme.

I. THE PRESENT INVENTION AND THE UNDERLYING PHYSICAL PRINCIPLES

1. Major Elements of the current invention are ...

a) ... **for the laser source:**

a cavity, a gain medium, a frequency shifter (usually an acousto-optical modulator),

a narrow band seed laser and a modulator in the path of the seed laser (with the latter being the key of the invention, see below),

b) ... **for the measurement set-up**:

a beam splitter, which separates the laser beam into two parts, one sent along a reference path, the other one sent to the object, the distance of which is to be measured, light collecting elements which collect light reflected (or scattered) back from the reference surface and the surface of the object, means to direct the reflected radiation towards a photo-detector followed by suitable electronics. The beam splitting and recombination is typically, but not necessarily, done in a set-up similar to a Michelson interferometer.

The combination of detector and electronics records the light power.

2. **Comments on the major elements:**

a) The cavity and the gain medium

The combination of cavity and gain medium exhibits net effective gain over a certain bandwidth. The larger the bandwidth, the higher the resolution and the signal enhancement due to the phase modulation (see below). Because radiation circulating in the cavity will always suffer from losses, "net effective gain" means that the gain medium itself must allow for an amplification factor larger than unity.

The frequency shifter imposes a frequency shift Δ_{shift} per roundtrip on radiation circulating in the cavity. The shift leads to a comb of spectral components (order of 10^4 components are typical), separated by Δ_{shift}, which extends over a certain bandwidth away from the seed frequency. Depending on the sign of Δ_{shift} the comb can either extend to higher or to lower frequencies. The value of Δ_{shift} is chosen different from the free spectral range Δ_{FSR} of the cavity. For $\Delta_{shift} = \Delta_{FSR}$ mode locking will occur, what is to be avoided.

Normally, the effective gain is positive over a certain spectral range and negative outside this range. Typically, the seed laser frequency is set to a region with small positive (or negative) gain, but near one of the frequencies for which the effective gain is zero. The frequency shifter then shifts the frequency towards the other frequency, for which the gain is zero. As the frequency is shifted, the spectral components are amplified and reach their maximum power at the frequency (away from the frequency of the seed laser) for which the effective gain is zero. The comb will extend beyond that frequency, but the components will be successively attenuated

Technical considerations lead to the conclusion that it is best, but not required for the method to work, that the net gain (i.e. "gain" minus "losses") is positive near

and around the seed wavelength and zero over an as large as possible bandwidth beyond the seed wavelength in the region covered by the spectral comb induced by the frequency-shifter. The power of the spectral components remains unchanged over the spectral range with "zero net gain".

Such a cavity with a gain medium and a cavity-internal frequency shifter is known as a "frequency shifted feedback (FSF)" cavity. When the device shows positive effective gain, lasing will occur and the system is called a FSF-laser.

This FSF-laser set-up is a central element in our ranging scheme, but is not claimed per se . The FSF-laser concept has previously been described by Kowalski Furthermore, the use of an FSF-laser (although without external phase-modulated seed) for ranging has been published by Nakamura et.al..

b) The measurement set-up:

The Michelson-type setup is also central to our ranging scheme but - by itself - is not part of the patent claims, as it is a well-known text-book type concept.

c) The effect of the seed laser and its modulation:

Injection of a seed laser into the FSF-cavity will modify the laser operation as the output spectrum of the FSF-laser will be dominated by the frequency comb starting at the frequency of the injected photons. Without seeding, the spectrum is a combination of many frequency combs, each one started by a spontaneously emitted photon within the gain medium. Seeding the FSF-cavity without phase-modulating the seed will not improve the performance of the system for ranging.

The seed laser is referred to as "narrow band", but no specific limit to the bandwidth is set. It is the phase-modulation of the seed laser, in combination with the FSF-laser cavity and the Michelson-interferometer type setup, which leads to an orders-of-magnitude improvement of the performance in distance measurement.

Understanding the physics requires a detailed analysis of the radiation field reaching the detector. The spectral characteristics of the field (frequency, amplitude and phase) are determined by the features of the FSF-laser, the seed laser including its phase-modulation and the relevant propagation distances. The field at the detector is a superposition of the two fields delayed in time by the difference in propagation time along the reference path and the path to the object.

The signal at the detector can be represented as a sum of terms [see eq. 22 in Opt. Commun. 282, 2212 (2009).]. Each term, labelled by an index n, has an amplitude and a time dependent phase. The detailed analysis of the latter term shows

that for a specific modulation frequency $\Omega = \Omega^*$ of the phase of the seed laser – and only for this modulation frequency- all terms have the same phase.

Theory furthermore shows the relation of Ω^* to the desired path difference ΔL. The experimental signature for finding Ω^* is the maximum of the signal as Ω is varied. When Ω is different from Ω^*, then the phase of the (order of) 10^4 terms changes from term to term.

The situation can be visualized by interpreting each one of the term (of eq. 22, see above) as a vector with amplitude and phase (the phase being the angle in a complex plane). Adding many such vectors with varying phase will lead to a sum-vector with is small. However, when the phases of all terms are equal, the vectors all line up parallel and the sum of the vectors will increase by orders of magnitude.

In conclusion, it is the phase modulation of the seed laser radiation and the option to vary the frequency of it that allows the finding of the frequency Ω^*, which leads to a dramatically enhanced signal and thus leads to the determination of ΔL.

The phase modulation of the seed laser, which is the key element of this invention, works towards a dramatic improvement of the ranging scheme *when combined* with a FSF-laser and a Michelson-type optical arrangement. This scheme is entirely different from any other scheme which was referred to by the US patent officer, even when terms such as FSF-laser or seed laser or phase modulation are used in the cited documents.

II NON-OBVIOUSNESS OF THE PRESENT INVENTION

The reasons for and the consequences of imposing phase modulation on the seed are far from obvious or trivial.

As a senior research professor at a technical university I am well familiar with the knowledge and experience of the average skilled person such as a PH.D. student or a postdoctorate. According to my conviction, the average skilled person would not have been able to find and implement the scheme proposed, not even in a trial and error process, based on the knowledge of an FSF-laser and the ranging concept, as demonstrated by e.g. Nakamura and any of the cited documents.

The physics behind this particular ranging scheme is subtle, but well understood by now. Even to a trained person with relevant experience (not to speak of the average skilled person) the reason for the dramatic improvement of the signal for ranging with an FSF-laser, when phase modulated narrow band radiation is injected into a FSF-laser cavity, is not at all

obvious. Most importantly, it can not be derived from any of the teachings of the cited documents, as the underlying physics is, in each case, entirely different. It is the complexity of the physics involved which classifies the phase-modulation scheme as a true invention.

The suggested scheme was found only after several years of work on FSF-Lasers and their use for ranging applications at the University of Kaiserslautern and after extensive discussions among the inventors in Kaiserslautern including a careful analysis of the work by Nakamura et.al., who showed that an FSF-laser (without seed) can be used for ranging, although with rather poor performance.

The present scheme was first identified by rather involved analytical and numerical calculations. It was only after the availability of those results that the intuitively understandable physics, underlying the concept was identified. Based on those discussions and results, the physics behind the success of our ranging concept with orders-of-magnitude improvement over ranging with only an FSF-laser is now well understood.

Only detailed expert-analysis of how the phase-variation, imposed on the seed laser, propagates through the components of the set-up and how it shows up in the sum of the two field at the detector, reveals the underlying physics.

The detailed scientific analysis extends far beyond the scope of the present remark and has been subject of a number of scientific papers, all published in the mean time in reknowned journals after peer-reviewing

Among the coauthors are the following inventors which all are prominent scientists :

Yatsenko: Ukrainian State Prize Winner 1998 for his work in laser-based metrology

Shore: Humboldt-Research Award winner 1997/1998,
25-year employee of Lawrence Livermore National Laboratories ,
specializes in optics and laser physics
single author of the "bible" of coherent excitation:
"The Theory of Coherent Atomic Excitation", John Wiley (1990), 2 Volumes, Total of 1700 pages.

Bergmann Senior research Professor of the Technical University of Kaiserslautern,
Chair to the "Laserzentrum Kaiserslautern" between 1997 - 2002
Chair to the special doctoral training program("Graduiertenkolleg") "Nonlinear Optics and Ultrafast Physics" between 2002-2006,

Chair to the center for "Optical Technologies and Laser- controlled Processes" between 2002 - 2008
has coordinated the Marie-Curie Trainingsite : Coherent Control in Matter Waves and Quantum Optics
1972 Gödecke Forschungspreis for the thesis work (topic: one of the first applications of lasers to collision dynamics), awarded by the University of Freiburg and sponsored by local industry (Gödecke).
1981 ***Physik-Preis*** (Physics - Prize) of the Deutsche Physikalische Gesellschaft (German Physical Society) "for his ground breaking work in laser state selection and the application of the method to scattering experiments using crossed molecular beams"
1992 ***Fellow*** of the American Physical Society (fellow status awarded "for his development of innovative laser systems and their application to molecular scattering processes")
2000-2004 Coordinator of European Research Training Networks:"Coherent Control of Molecular Systems and Processes - COCOMO",
2006-2010 Coordinator of European Research Training Networks: "Engineering of Quantum States of Matter and Light - EMALI",.
2003 **Robert-Wichard-Pohl-Award** of the Deutsche Physikalische Gesellschaft (German Physical Society) "in recognition of his outstanding scientific achievements, especially in molecular physics, which had an impact on a broad range of fields in physics"
2003 **Honorary Doctorate** of the Latvian University of Riga
2003 **Max-Planck**-Researchprize **for International Collaboration** awarded jointly by the Alexander von Humboldt-Foundation and the Max-Planck-Society "for outstanding research achievements"
2005 Honored by the Ministerpresident of Rheinland-Palatinate Kurt Beck on December 8th with the "Verdienstorden des Landes Rheinland-Pfalz" (order of merit). The "Verdienstorden" is the highest honor awarded by the state of Rheinland-Palatinate. It is given for outstanding service for the state and its citizens.

The following attached publications in peered journals explain the theory of the present invention:

1. L.P. Yatsenko, B.W. Shore and K. Bergmann
"Theory of a Frequency Shifted Feedback Laser"
Opt. Commun. 236, 183 – 202 (2004)
A new and thorough theoretical treatment of FSF-laser, however not yet including the competition between coherent radiation evolving from spontaneous emission and injected photons. In particular: showing the equivalence of the two pictures "stationary comb" and "moving comb".

2. L.P. Yatsenko, B.W. Shore, and K. Bergmann
"Ranging and Interferometry with a Frequency Shifted Feedback Laser"
Opt. Commun., 242, 581 - 598 (2004)
First discussion of the principles of laser ranging based on a FSF-laser, emphasizing the relevance of injection seeding by frequency- (or phase-) modulated narrow band radiation.

3. V.V. Ogurtsov, L.P. Yatensko, V.M. Khodakovskyy, B.W. Shore, G. Bonnet, and K. Bergmann
"High Accuracy Ranging with Yb^{3+}-doped Fiber-Ring Frequency-shifted Feedback Laser with Phase-modulated Seed"
Opt. Communications 266, 266-273 (2006)
First discussion of experimental ranging results based on an FSF-laser with injection by phase-modulated narrow band radiation, confirming the theory presented in paper 2.

4. V.V. Ogurtsov, L.P. Yatensko, V.M. Khodakovskyy, B.W. Shore, G. Bonnet, and K. Bergmann
"Experimental Characterization of an Yb^{3+}-doped Fiber Ring Laser with Frequency-shifted Feedback"
Opt. Commun., 266, 627-637 (2006)
Experimental characterization of an FSF-laser with injection seeding, confirming theoretical results of paper 1.

5. V.V. Ogurtsov, V.M.Khodakovsky, L.P.Yatsenko, G.Bonnet, B.W.Shore, and K. Bergmann
An all-fiber frequency-*shifted feedback laser for optical ranging; signal variation with distance*
Optics Commun. 281, 1679 – 1685 (2008)

Experimental verification of a specific feature of the ranging method using a FSF-laser with injection of phase-modulated narrow band radiation, namely the variation of the signal with distance.

6. L.P.Yatsenko, B.W.Shore, and K.Bergmann
Coherence in the output *spectrum of frequency shifted feedback lasers*
Optics Commun. 282, 300-309 (2009)
The full ab initio theory of FSF-laser operation with treatment of growth starting from spontaneous emission and from injection seeding on equal footing.

7. L.P.Yatsenko, B.W.Shore, and K. Bergmann
An intuitive picture of optical *ranging using frequency shifted feedback lasers seeded by a phase modulated field*
Optics Commun. 282, 2212 – 2216 (2009)
Explaining the physics behind the dramatic enhancement of the signal by injection seeding of phase-modulated radiation on the basis of an intuitively accessible picture.

These documents explain the theory behind the invention should the explanation given above should not be considered sufficient.

III COMMENTS ON PATENTS CITED BY THE U.S. PATENT OFFICER:

As indicated in the introduction to this remark, only the work using an FSF-laser (Shattil, Phillips and Takeuchi) seems to warrant more detailed comments as the average skilled person surely and easily realizes that the teachings of the other patents are completely unrelated to our scheme.

a) **Documents unrelated to the principles of the present invention**

Palese: 6 570 704 B2 "High average power chirped pulse fiber amplifier array"

This patent is about a high power fiber amplifier allowing the production of nearly arbitrary pulse shapes. The term "seed" is used but it means the radiation which is to be amplified after spectral dispersion by an array of fiber amplifiers. The terms "phase" and "phase modulator" are used but in an entirely different context. Like in a liquid crystal pulse shaper (also called modulator) the phase of the different spectral components are controlled (NOT modulated) by phase modulators in order to achieve a certain pulse shape.

Goldberg: 5 745 284 "Solid-state laser source of tunable narrow-bandwidth ultraviolet radiation"

I have no idea why this patent is cited in the given context. The patent is about frequency conversion starting from a diode laser, which is usually considered too weak for efficient conversion into the UV. Talk is about "seed laser" (3/7) and the "amplitude modulator" (3/15). The seed laser is very standard in the context of frequency conversion, as one typically starts from a source with low power and narrow bandwidth, which is then amplified and converted. The amplitude modulation serves to increase the peak power without enhancing the average power of the diode laser radiation in order to increase the efficiency in the non-linear conversion step. Thus, the teaching of this text is not even remotely related to our FSF-scheme for ranging.

Gabl: 5 592 327 "Regenerative amplifier incorporating a spectral filter within the resonant cavity"

Like the Goldberg text, the teaching of this invention is absolutely unrelated to our approach. The invention is about pulse amplification of radiation, called "seed". It describes means to allow for high amplification factors without reaching destructive intensity levels. This is done by stretching the pulse of the radiation to be amplified in time and recompress it after amplification. Also, the inclusion of a spectral filter is proposed to prevent or reduce amplification of spontaneous emission, which would reduce the gain in the wanted spectral region. Thus, the teaching of this text is not even very remotely related to our FSF-scheme for ranging.

Mocker: 5 394 238 "Look ahead windshear detector by filtered Rayleigh and/or aerosol scattered light"

Windshear detection relies on the measurement of the frequency shift of reflected (incoming) light with respect to the outgoing light. A simple mean to measure such a shift is to set the frequency of the outgoing light at the edge of a steep transmission filter and send the reflected light through the same or an equivalent filter. The frequency shift can be derived from the change of the transmission, provided appropriate normalization procedures are applied. The essential teaching of this patent is about improved ways of generating the outgoing radiation and locking it to a frequency filter. Except for mentioning the name "seed", it has no connection to our scheme and objective.

b) Documents closer related to the present invention

Shattil: 5 955 992 "Frequency-shifted feedback cavity used as a phased array antenna controller and carrier interference multiple access spread-spectrum transmitter"

This patent is about controlling the emission properties (in particular the direction of emission) of an antenna array and the processing of received signals through such an array. Although it does rely on an FSF cavity but it has no modulated seed laser and has entirely different objectives and works on different principles. Ranging and phase modulation of a narrow band seed laser is not mentioned and not used. It does mention phase control (see e.g. column 12, line 50 and before) only in order to achieve mode locking, a regime which our scheme avoids.

Phillips: 5 835 199 "Fiber-based ladar transceiver for range/Doppler imaging with frequency comb generator"

This patent is about measuring jointly distance and velocity. Pulsed radiation is used with long pulse duration for high velocity resolution and wide spectral band width for high spatial resolution. A frequency shifter is used to derive radiation with a larger bandwidth (through discrete frequency components) from a narrow band laser. As in our case, the frequency shifter plays an essential role in their scheme. It is stated, however, that best performance is achieved when the phases of the spectral components of the comb are random (column 12, line 15 and 16/57) and incommensurate spacing of the frequency components is wanted (12/19). These statements alone provide clear cut documentation that not only the objective but also the approach is entirely different from ours, since well-set phases, controlled through the phase-modulation of the seed, are essential in our case. At 16/26 it is also said that ideally the spectrum should be of white light character. This scheme seems to rely on waveform detection and the ranging scheme is of the time-of-flight type.

Takeuchi: 5 394 235 "Apparatus for measuring distortion position of optical fibers"

Surprisingly the English of this text is of rather poor quality and suffers from ambiguous or unclear statements. The claimed invention is about an improved diagnostics for optical fibers. It relies on amplification through Brillouin scattering and is thus, in any case, limited to solid state material. In a similar (known) version of the scheme light with frequencies f_o (pulsed) and f_m (continuous) is coupled to one and the other end, respectively, of the optical fiber to be measured. When the difference frequency f_o-f_m equals the Brillouin shift frequency (given by phonon

modes in the material) the continuous laser is amplified by the other, counter-propagating, laser. The amplified radiation is displayed (I assume: as a function of time, thus correlating via suitable timing circuits any deviation from expected growth of the intensity to a location within the fiber, thus localising a defect region). The accuracy relies on a stable frequency difference. The essential teaching of this patent is how to best create the two frequencies. This is done by a frequency shifter which derives the frequency f_m from the laser of frequency f_o with the main benefit that frequency fluctuations of the radiation source do not affect the relevant frequency difference. As stated above, this technique relies on non-linear mixing within the medium and has no element of phase control or phase modulation as in our scheme.

In summary, none of the cited documents relate to the physical principles underlying the present invention.

The enhancement of the measurement signal obtained by the use of a modulated seed laser could not be expected by an average skilled person and was predicted only after very thorough analysis and long discussions among a number of very experienced scientists.

I hereby declare that all statements made herein of my own knowledge are true and that all statements made on information and belief are believed to be true and further that these statements were made with the knowledge that willful false statements and the like so made are punishable by fine or imprisonment, or both, under §1001 of Title 18 of the United States Code and that such willful false statements may jeopardize the validity of the application or any patent issued thereon.

Date: July 27, 2009

K. Bergmann

Prof. Dr. Klaas. Bergmann

Available online at www.sciencedirect.com
SCIENCE DIRECT®
Optics Communications 236 (2004) 183–202
OPTICS COMMUNICATIONS
www.elsevier.com/locate/optcom

Theory of a frequency-shifted feedback laser

L.P. Yatsenko [a], B.W. Shore [b,*], K. Bergmann [b]

[a] *Institute of Physics, Ukrainian Academy of Sciences, prospect Nauki 46, 03650, Kiev-39, Ukraine*
[b] *Universität Kaiserslautern, 67653 Kaiserslautern, Germany*

Received 11 November 2003; received in revised form 10 February 2004; accepted 11 March 2004

Abstract

We present a new approach to the description of the output from a frequency-shifted feedback (FSF) laser seeded by a phase-fluctuating but stationary continuous-wave (CW) laser. We illustrate the new analysis by showing how short frequency-chirped pulses arise for appropriate operating conditions. We show the equivalence of two common viewpoints of the FSF laser output as either a moving comb of equidistant frequencies or as a fixed set of discrete frequencies. We also consider operation of a FSF laser when there is no external seeding laser, and instead the cavity radiation originates with spontaneous emission.

PACS: 42.55.–f; 42.60.Da; 42.55.Ah

Keywords: Optics; Lasers; Frequency-shifted feedback

1. Introduction

Conventional lasers rely on multiple passes through a gain medium to reinforce a preselected frequency, thereby obtaining near-monochromatic output. For many purposes, such as excitation of Doppler-broadened atomic transitions, it is desirable to have light spread over a broader range of frequencies. One means of fulfilling that objective is to introduce a frequency shifting element into the laser feedback loop such that successive passes of a wavepacket take place with different carrier frequencies. The operation of such a frequency shifting feedback (FSF) laser has been considered by several research groups [1–46] and it has been used for a number of practical applications [12,21,36,41,47,48]. Although much is known about the behavior of FSF lasers and some of their surprising properties (see e.g. [20,24]), there remain some fundamental questions. Even the precise nature of the field emerging from such a laser remains a matter for discussion and confusion [33].

Although all authors agree on the elements that comprise a FSF device, there are conflicting approaches concerning detailed description of the electric field $E(t)$ that emerges from the device. In part this is because a FSF laser can operate in a variety of regimes: the output may range from

* Corresponding author.
E-mail address: shore@physik.uni-kl.de (B.W. Shore).

0030-4018/$ - see front matter © 2004 Elsevier B.V. All rights reserved.
doi:10.1016/j.optcom.2004.03.049

extreme irregularity to very regular pulse trains (cf. [24,46]), depending on such controllable properties as the amount of gain (controlled by the pump power) and the relative values of various time constants or frequency bandwidths of the device.

In this paper we reexamine some of the properties of this device, as deduced from equations that describe the time dependence of the (complex-valued) electric field amplitude. We also provide further clarification of the relationship between two apparently conflicting views of the output electric field. We are here concerned with steady-state operation, and will not consider the very interesting possibilities of irregular behavior.

The terms "steady state" and "stationary" deserve some comment when applied to pulsed lasers. As an example, one can consider the operation of a conventional mode-locked laser whose output consists of a train of short pulses. On a short time scale (that of one pulse) the intensity, and even the frequency, depends on time and thus on this time scale the output appears nonstationary. Nevertheless, on a time scale that encompasses many pulses the properties of the output is unchanged, and one can consider this as a stationary process.

We begin, in Section 2, with a general description of a prototype FSF layout. In Section 3 we derive equations of motion describing the two coupled systems that comprise the laser, namely the electric field (including both a seeding field and spontaneous emission as well as the stimulated emission) and the atomic inversion. Our field equations deal with complex-valued amplitudes, not just with photon numbers, as in rate equation treatments (e.g. [24]). Thus our formulation of the FSF laser equations includes phases. These are important for the injection seeded FSF: all the pulse chirping effects considered in Sections 4–6 rely on phase relationships. For the FSF laser seeded by spontaneous emission phase is not important.

In Section 4 we present solutions to these equations, allowing for seeding by a noisy but otherwise continuous-wave signal. We show here some special cases and some specific examples, and we reconcile (see Section 6.2) two common but apparently conflicting views of the FSF laser (as discrete frequencies, Section 5 or as a moving comb of frequencies, Section 6). Section 7 briefly discusses operation of a FSF laser whose field originates entirely from spontaneous emission, and Section 8 connects the present formalism to the earlier rate-equation model.

2. The FSF laser layout

We consider a simple idealized model of a frequency-shifted feedback laser: a ring cavity of perimeter L in which there is a section having gain, some elements that provide spectral filtering, and, most importantly, an element that induces a frequency shift (of angular frequency Δ) on each wavepacket that passes through it. The round trip time is $\tau_r = L/c$. For definiteness we assume that the frequency shift is provided by an acousto-optic modulator (AOM) and that this acts as a grating, to deflect light (into first order) that has been frequency shifted from ω to $\omega + \Delta$. The light that remains in the undeflected beam (zero-order diffraction) leaves the cavity as output.

We follow common practice and idealize the cavity field as having spatial variation only along the longitudinal coordinate z (i.e. we unwind the mirror action). We take the entrance face of the AOM to be $z = 0$ and regard the various optical elements, such as the gain medium and the AOM, as having negligible length.

Fig. 1 shows a prototype schematic layout for a seeded FSF cavity. The input is through the AOM and the output is light that is undeflected by the AOM. With each pass around the cavity some light is lost. The most important loss sources are

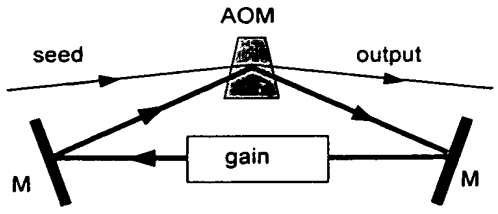

Fig. 1. Schematic diagram of a ring cavity showing mirrors (M), frequency shifting AOM , amplifier (gain), as well as input (seed) and output beams.

the mirror transmittance and the loss to the output beam (through the AOM), both of which are frequency dependent. Often the cavity will include a filter that introduces controllable frequency-dependent loss. To simplify the presentation and to avoid unnecessary model-dependent details, we will consider only the case of a cavity whose loss varies negligibly within the frequency interval Δ. In this case the ordering of the elements (AOM, mirrors, broadband gain and filter) are not important, and we can lump all losses into one element, which we call the filter. We consider this to be infinitesimally thin, time independent, and to decrease the field amplitude entering it with frequency ω by a factor $\mathscr{T}(\omega) = \exp[-f(\omega)]$. We assume that the filter function $f(\omega)$ varies slowly with frequency. Such broadband operation is found in almost all experimentally realized FSF lasers, and it is a prerequisite for use in high-resolution interferometry. In keeping with this requirement, we assume that the effect of the losses can be expressed in quadratic form

$$f(\omega) = f_m + \frac{1}{2}\left(\frac{\omega - \omega_f}{\Gamma_f}\right)^2. \quad (1)$$

The filter function $f(\omega)$ has its *minimum* value, f_m, when $\omega = \omega_f$, and it increases from that value quadratically with the frequency difference $\omega - \omega_f$. The parameter Γ_f characterizes the bandwidth of the filter while the central frequency ω_f provides a convenient fiducial for defining frequency detunings.

In order to sustain operation and produce a steady-state output, the cavity must include a section having gain, where amplification replaces the light lost to the output beam. As with the loss, we consider the gain to be localized in an infinitesimally thin element, having the property that a field entering it with frequency ω will be increased in amplitude by a factor $\exp[g(\omega)]$. We assume that the gain $g(\omega)$, like the loss $f(\omega)$, varies slowly and smoothly with frequency.

3. The coupled field-atom equations

As in all dynamical descriptions of a laser, we require an equation relating the time evolution of the electric field amplitude in the presence of polarizable atoms (some form of the Maxwell equations), and equations describing the time evolution of atomic properties in the presence of a given field (some form of a density-matrix equation). We here derive the needed coupled equations by considering the passage of a pulse through the region of gain (the amplifier), and then considering the effects of the filter and the frequency shift.

Our model of the FSF laser differs in essential respects from some previous models, and readers familiar with those may question how one can consider the output of the FSF laser to be stationary. Where we to consider (as we do not) just a single pulse in the FSF laser, then this pulse will evolve with each round trip, changing frequency repetitively and undergoing growth through gain. The output in such a scenario is clearly not stationary, for each output pulse differs in amplitude and frequency from all others.

Although it is useful to describe the frequency shifting properties of a FSF laser by following the succession of frequency shifts occurring to a specific pulse, our mathematical treatment does not follow such a single pulse. Instead we consider a system in which the FSF laser is continuously seeded, either by spontaneous emission or by continuous injection of a seeding laser. We then examine the characteristics of the FSF output after startup transients have ceased. Because the seeding source is assumed to be stationary the FSF output, after some initial transient time development, is also stationary; operation of the FSF laser reaches a steady state in which the statistical properties of the output signal do not change.

We assume that the properties of the filters, though frequency dependent, are independent of time and of the intracavity field. However, we allow the gain to be influenced by both the pump power and by the cavity field; time variations of the cavity field will then induce time-dependent changes in the gain.

We assume that the relaxation time of the gain-medium polarization is much shorter than all other relaxation times under consideration, so that we can use standard techniques of adiabatic elimination and neglect the time derivative of the medium polarization. With this approximation we deal

only with rate equations for number densities or probabilities (populations), rather than with the Bloch-type equation for a density matrix. We assume that the population is spatially uniform within the (infinitesimally thin) gain medium, and that during one round trip within the cavity there is at most only a small change in the population (and so the gain can change only slowly with time).

In keeping with our interest in Ti:Sapphire as the gain medium we idealize the amplifier as a collection of identical four-level atoms (cf. [49], whose notation we follow), with the lasing transition between levels 1 and 2, while the pump radiation moves population between levels 0 and 3. Rapid decay from level 3 fills the upper lasing level 2, and rapid decay from level 1 to the ground state 0 ensures that the lower-level probability $P_1(t)$ is negligible, and the population inversion $w(t) \equiv P_2(t) - P_1(t)$ can be replaced by the population $P_2(t)$.

The FSF laser is a system where the Fourier transform in its normal form does not appear particularly useful. As one learns in Fourier analysis, sampling a signal for a time interval τ gives a valid representation of the spectral properties of the signal if τ is long enough so that the effect of the discontinuities at the beginning and end of the segment are insignificant. Then the Fourier transform, from which one evaluates the spectrum, will be independent of any change in τ.

Our goal is different. We want to obtain equations which describe all regimes of FSF laser operation – steady state, transient, or pulse evolution.

3.1. The field amplitude equation

We take the center frequency of the effective filter, ω_f, as a carrier frequency and express the time dependence of the complex-valued electric field $E(t)$ at position $z = 0$, taken to be just prior to the AOM in a path around the cavity, by the complex envelope $\mathscr{E}(t)$

$$E(t) = \mathscr{E}(t)\exp(-i\omega_f t). \tag{2}$$

The FSF laser is one of many examples where the frequency content of a signal changes with time and conventional Fourier transform methods are not sufficient. This problem, of explicitly time-dependent spectra, has been discussed by Eberly and Wodkiewicz [51]. We overcome the difficulties by using a sliding-window Fourier transform (SWFT). For any fixed fiducial reference time T we introduce a Fourier decomposition of the envelope $\mathscr{E}(t)$, valid in the time window $T - \tau_r < t < T$,

$$\mathscr{E}(t) = \int_{-\infty}^{\infty} d\varpi \mathscr{E}(\varpi, T)\exp(-i\varpi t) \quad \text{for } T - \tau_r < t < T. \tag{3}$$

Note that the Fourier frequency ϖ is *not* the optical frequency; it is a *detuning* from the carrier frequency ω_f. The windowed Fourier components are obtained from the integral

$$\mathscr{E}(\varpi, T) = \frac{1}{2\pi}\int_{T-\tau_r}^{T} dt \mathscr{E}(t)\exp(+i\varpi t). \tag{4}$$

It should be understood that our choice of the window duration as the round trip time is not related to any requirements of Fourier transforms, nor is it to impose any phase closure condition, for example, a requirement that accumulated phase during a round trip must be an integral multiple of 2π.

Because we deal with a SWFT rather than a conventional FT, the value of the frequency shift relative to the fiducial time T is not important. We obtain a set of finite-difference equations which can be used to describe the FSF laser. The smallness of the frequency shift can subsequently be used to simplify these finite-difference equations as approximate differential equations.

The intensity $I(t)$ at $z = 0$ during the time interval $T - \tau_r < t < T$ is expressible either as the absolute square of the time-dependent electric field envelope or as a double Fourier integral

$$I(t) = \frac{c}{8\pi}|\mathscr{E}(t)|^2 = \frac{c}{8\pi}\int_{-\infty}^{\infty}\int_{-\infty}^{\infty} d\varpi_1\, d\varpi_2 \mathscr{E}(\varpi_1, T)\mathscr{E}(\varpi_2, T)^* \times \exp[-i(\varpi_1 - \varpi_2)t]. \tag{5}$$

The windowed Fourier components $\mathscr{E}(\varpi, T)$, based on windowed Fourier analysis, serve as the basic quantities for theory: we derive the desired equations by considering the connection between $\mathscr{E}(\varpi, T)$ and $\mathscr{E}(\varpi, T - \tau_r)$. Prior to arriving at the reference position, this Fourier component $\mathscr{E}(\varpi, T)$

has made a circuit in which it was filtered, underwent a frequency shift, and underwent gain. It began that circuit with frequency $\varpi - \Delta$ at time $T - \tau_r$, and after immediately shifting frequency it acquired a phase increment $(\omega_f + \varpi)\tau_r$ from spatial propagation. We express this behavior by writing

$$\mathscr{E}(\varpi, T) = \mathscr{E}(\varpi - \Delta, T - \tau_r)\exp[+i(\omega_f + \varpi)\tau_r + g(\omega_f + \varpi, T) - f(\omega_f + \varpi)]. \quad (6)$$

We assume that there is little change in the gain during one round trip and we assume the filter has only a slight frequency dependence

$$g(\omega_f + \varpi, T - \tau_r) \simeq g(\omega_f + \varpi, T),$$
$$f(\omega_f + \varpi + \Delta) \simeq f(\omega_f + \varpi).$$

To emphasize the discreteness of the periodic frequency shift it proves useful to consider a two-dimensional time-frequency space

$$\vec{X} = (\varpi, T), \quad (7)$$

in which successive circulations involve a change by the vector $\vec{X}_0 = (\Delta, \tau_r)$. Then the basic equation (6) for the field change in one round trip can be written as

$$\mathscr{E}(\vec{X}) = \mathscr{E}(\vec{X} - \vec{X}_0)\exp\left[G(\vec{X})\right] + \varepsilon(\vec{X}) + \xi(\vec{X}), \quad (8)$$

where the effect of gain (and loss) is present through the function

$$G(\vec{X}) = i(\omega_f + \varpi)\tau_r + g(\omega_f + \varpi, T) - f(\omega_f + \varpi) \quad (9)$$

and the two additional terms represent various sources of radiation (in Fourier space):

- $\varepsilon(\vec{X})$ is the seeding field source (if present),
- $\xi(\vec{X})$ is the source of the spontaneous emission field during a time interval τ_r.

Eqs. (8) and (9) are our basic equations for the field amplitude emerging from the FSF cavity. Missing from our treatment is any explicit nonlinearity, such as four-wave mixing due to Kerr effect or gain saturation. Because we neglect such nonlinearities our resulting theory cannot explain results such as those of Ito and coworkers [29,32] where the chirped comb (though a very small component of the FSF laser output) was observed in an unseeded FSF laser.

The source terms have the following properties.

3.1.1. The seed laser source

The seeding laser produces the source term $\varepsilon(\vec{X})$. We take this to be a source of continuous radiation at the frequency

$$\omega_s = \omega_f + \varpi_s \quad (10)$$

(that is, ϖ_s is a frequency offset from the central filter frequency ω_f of the carrier field). We allow a finite bandwidth to this laser by taking the windowed Fourier transform to have the form

$$\varepsilon(\vec{X}) = \varepsilon_c \frac{1}{2\pi}\int_{T-\tau_r}^{T} dt \exp[-i\varpi_s t - i\varphi_s(t) + i\varpi t]. \quad (11)$$

The time varying phase $\varphi_s(t)$ appearing here represents the phase of the seed laser. To permit treatment of the unavoidable finite bandwidth of any seed laser we treat this phase as a stochastic process. The quantity ε_c is the amplitude of the seeding laser field within the cavity. It parametrizes the seeded intensity I_c within the cavity,

$$I_c = \frac{c}{8\pi}|\varepsilon_c|^2. \quad (12)$$

3.1.2. Spontaneous emission source

Spontaneous emission (within the gain medium) is described by the term $\xi(\vec{X})$. This is similar to a Langevin force [50]. This frequency domain source term relates to the time domain source via Fourier integral within one round trip time

$$\xi(\vec{X}) \equiv \xi(\varpi, T) = \frac{1}{2\pi}\int_{T-\tau_r}^{T} dt \xi_{sp}(t)\exp(+i\varpi t). \quad (13)$$

The time-varying emission source $\xi_{sp}(t)$ describes the field created from spontaneous emission events. These occur at random times, and successive emissions are completely uncorrelated. This property will be quantified in Section 7.

3.2. The population inversion equation

To complete the description of the atom-field system we require an equation for the time dependence of the gain coefficient $g(\omega, T)$. This is

directly proportional to the population inversion $w(t) = P_2(t) - P_1(t) \approx P_2(t)$ of the lasing transition (assuming the two levels have equal degeneracies). We express this by the equation

$$g(\omega, T) = g_0(\omega)w(T). \tag{14}$$

We take the frequency dependence of $g_0(\omega)$ to be of Lorentzian form

$$g_0(\omega) = \frac{g_m}{1 + (\omega - \omega_g)^2/\Gamma_g^2}, \tag{15}$$

where ω_g is the frequency of maximum gain and $1/\Gamma_g$ is the relaxation time for the off-diagonal terms of the density matrix.

To avoid unnecessarily complicated formulas we assume that the width of the frequency-dependent loss, as incorporated into the filter $f(\omega)$, is much smaller than the gain width: $\Gamma_g \gg \Gamma_f$. With this assumption we can regard the gain as being independent of frequency, and set $g_0(\omega) = g_m$. This simplification is not essential, and the results are readily adapted to the case when only the gain, but not the filter, has significant frequency dependence. For simplification we have taken $g_0(\omega)$ and $f(\omega)$ to be purely real functions of frequency. It can be shown that, in the quadratic approximation, the inclusion of imaginary parts (dispersion) would lead only to a redefinition of the round trip time.

Within the approximations discussed here, the inversion $w(T)$ changes from its value at the earlier time $T - \tau_r$ due to the following effects, each of which acts for time τ_r:

- growth by pumping (into level 3 with rapid decay to 2) at rate R;
- loss by spontaneous emission at rate $\gamma_s w(T - \tau_r)$;
- loss by stimulated emission at rate $\gamma_s I(t)/I_{sat}$.

Taking these effects into account we write the following expression for the inversion after one round-trip time:

$$w(T) = w(T - \tau_r)\left[1 - \gamma_s \int_{T-\tau_r}^{T} \frac{I(t)}{I_{sat}}\,dt - \gamma_s \tau_r\right] + R\tau_r. \tag{16}$$

In the absence of lasing, $I(t) = 0$, this equation gives the stationary inversion $w(T) = w(T - \tau_r) = w_m = R/\gamma_s$. Then the inversion equation reads

$$\frac{w(T) - w(T - \tau_r)}{\tau_r} = -\gamma_s\left[w(T - \tau_r) - w_m + w(T - \tau_r)\int_{T-\tau_r}^{T} \frac{I(t)}{I_{sat}}\frac{dt}{\tau_r}\right]. \tag{17}$$

In traditional treatments of population inversion one considers the limiting case of an infinitesimal time increment (here the fixed increment τ_r)

$$\frac{w(T) - w(T - \tau_r)}{\tau_r} \to \frac{dw}{dT}$$

and thereby obtains an equation for the time derivative of the inversion. However, in the present work the discreteness of the round trip time is an essential part of the physics of the field, and so we here retain also a similar discrete form for the evolution equation for the inversion.

The time integral over intensity can be taken as the definition of the average intensity during a round trip

$$\bar{I}(T) = \frac{1}{\tau_r}\int_{T-\tau_r}^{T} dt I(t) \equiv \int_{-\infty}^{\infty} d\varpi I(\varpi, T), \tag{18}$$

where, in the frequency domain,

$$I(\varpi, T) = \frac{c}{8\pi}\int_{-\infty}^{\infty} d\varpi' \mathscr{E}(\varpi, T)\mathscr{E}(\varpi + \varpi', T)^* \times \frac{1 - \exp[-i\varpi'\tau_r]}{i\varpi'\tau_r}\exp[i\varpi' T]. \tag{19}$$

With this definition we can write the equation for the inversion as

$$w(T) = w(T - \tau_r)\left[1 - \gamma_s\tau_r\frac{\bar{I}(T)}{I_{sat}} - \gamma_s\tau_r\right] + R\tau_r. \tag{20}$$

This equation completes the necessary set of equations for the FSF laser.

3.3. Steady-state operation

We are interested in steady-state operation of the FSF laser, as contrasted with irregular or transient behavior. We therefore carry out a stochastic average $\langle\cdots\rangle$ of the inversion and the average intensity

$$\bar{w} \equiv \langle w(T)\rangle = \langle w(T-\tau_r)\rangle, \quad \bar{I} \equiv \langle \bar{I}(T)\rangle. \tag{21}$$

This step rules out possible relaxation oscillations of the inversion, but it does not require that the phase be constant. With this approximation we deal with the average gain coefficient $g_m\bar{w}$.

In this work we consider a laser whose spectrum has a width much larger than the free spectral range $\Delta\omega_{axial} = 2\pi/\tau_r$. Under this restriction we can replace $w(T)$ and $w(T+\tau_r)$ with $\bar{w}$ and $\bar{I}(T)$ with $\bar{I}$ in Eq. (20). Then we find that the stationary average inversion $\bar{w}$ and the average intensity $\bar{I}$ are related by the equation

$$\bar{w} = \frac{w_m}{1+\bar{I}/I_{sat}}. \tag{22}$$

3.4. Solving the coupled equations

The dynamics of a laser with frequency-shifted feedback can be described by two stochastic finite-difference equations: Eq. (8) for the time-dependent spectral component $\mathscr{E}(\vec{X})$ and Eq. (20) for the inversion $w(T)$. The procedure for solving the equations is as follows.

1. We find the solution $\mathscr{E}(\vec{X})$ of Eq. (8) with $\bar{w}$ treated as an unknown parameter.
2. Using $\mathscr{E}(\vec{X})$ in Eq. (19) we obtain $I(\varpi, T)$.
3. We do the stochastic averaging of $I(T)$ over realizations of the spontaneous emission source $\zeta(\vec{X})$ and (or) realizations of the stochastic phase $\varphi_s(t)$ of the seeding laser, and from these we obtain $\bar{I}$.
4. We solve Eq. (22) for $\bar{w}$.
5. Using the expression obtained for $\bar{w}$ we obtain $\mathscr{E}(\vec{X})$ and the intensity $I(T)$ of items 1 and 2. We also obtain the spectral density of the intensity, $I(\varpi, T)$.

The following sections discuss implementations of this program with various approximations and simplifications for the following important cases:

- A laser with injection seeding, but without spontaneous emission, $\varepsilon(\vec{X}) \neq 0$, $\xi(\vec{X}) = 0$.
- A laser with spontaneous emission, but without seeding, $\varepsilon(\vec{X}) = 0$, $\xi(\vec{X}) \neq 0$.

4. The FSF laser with (noisy) seeding

An important simple case of the FSF laser occurs when a seeding laser provides the only source term. We take this to be a CW laser, of frequency ω_s, but we allow finite bandwidth by including phase noise $\varphi_s(t)$.

4.1. The electric field

We here neglect the spontaneous emission source $\xi(\vec{X})$, so that Fourier components of the laser field are determined by the equation

$$\mathscr{E}(\vec{X}) = \mathscr{E}(\vec{X}-\vec{X}_0)\exp\left[G(\vec{X})\right] + \varepsilon(\vec{X}). \tag{23}$$

Here we use the function $G(\vec{X})$, defined by Eq. (9), with stationary and frequency-independent gain coefficient $g_m\bar{w}$, so that it becomes

$$G(\vec{X}) = i(\omega_f + \varpi)\tau_r + g_m\bar{w} - f(\omega_f + \varpi). \tag{24}$$

As in Eq. (11) we take $\varepsilon(\vec{X})$ to have only phase variation (i.e. constant amplitude).

The solution to the difference equation (23) is the infinite sum

$$\mathscr{E}(\vec{X}) = \varepsilon(\vec{X}) + \sum_{n=1}^{\infty} \exp\left[\sum_{l=0}^{n-1} G(\vec{X}-l\vec{X}_0)\right] \times \varepsilon(\vec{X}-n\vec{X}_0), \tag{25}$$

where

$$\varepsilon(\vec{X}-n\vec{X}_0) = \frac{\varepsilon_c}{2\pi}\int_{T-\tau_r-n\tau_r}^{T-n\tau_r} dt' \exp\left[-i\varpi_s t' - i\varphi_s(t') + i(\varpi - n\Delta)t'\right]. \tag{26}$$

From the windowed Fourier transform of expression (25), over the time interval $T-\tau_r < t < T$, one finds (after straightforward but lengthy algebra) the time-dependent envelope of the field to be

$$\mathscr{E}(t) = \varepsilon_c \exp[-i\varpi_s t - i\varphi_s(t)] + \varepsilon_c \sum_{n=1}^{\infty}\int_{-\infty}^{\infty} d\varpi \exp(-i\varpi t) \times r_n(\varpi) \times q_n(\varpi), \tag{27}$$

where $r_n(\varpi)$ incorporates all consequences of gain and loss

$$r_n(\varpi) \equiv \exp\left[in(\omega_f + \varpi_s + [n+1]\Delta/2)\tau_r + \sum_{l=0}^{n-1}[g_m\bar{w} - f(\omega_f + \varpi - l\Delta)]\right] \quad (28)$$

and $q_n(\varpi)$ expresses all the effects of phase fluctuations (seed-laser bandwidth)

$$q_n(\varpi) \equiv \frac{1}{2\pi}\int_{T-\tau_r}^{T} dt' \exp[-i\varphi_s(t' - n\tau_r) + i(\varpi - \varpi_s - n\Delta)t']. \quad (29)$$

The function $q_n(\varpi)$ is maximum near $\varpi = \varpi_s + n\Delta$. The width of this maximum is roughly $1/\tau_r + \delta\omega_s$, where $2\pi/\tau_r$ is the free spectral range and $\delta\omega_s$ is the bandwidth of the seeding laser. We assume that the width of the filter Γ_f is much larger than these

$$\Gamma_f \gg 1/\tau_r + \delta\omega_s. \quad (30)$$

This equation says that the function $r_n(\varpi)$ is a slowly varying function of the detuning ϖ compared with the narrow function $q_n(\varpi)$. Thus one can replace $r_n(\varpi)$ by its value at the point $\varpi = \varpi_s + n\Delta$. After integration over ϖ and using the expression (1) one can write the electric field envelope $\mathscr{E}(t)$ as a sum over terms with constant real-valued amplitudes a_n

$$\mathscr{E}(t) = \varepsilon_c \sum_{n=0}^{\infty} a_n \exp[-i\Phi_n - i\varphi_s(t - n\tau_r) - i(\varpi_s + n\Delta)t]. \quad (31)$$

Section 4.2 provides a simple interpretation of this expression, and of the indexing integer n. The constant real-valued amplitudes are expressible as $a_n = \exp(S_n)$ with

$$S_n = n\left[g_m\bar{w} - f_m - \frac{6\varpi_s^2 + 6\varpi_s n\Delta + 6\varpi_s\Delta + 2n^2\Delta^2 + 3\Delta^2 n + \Delta^2}{12\Gamma_f^2}\right]. \quad (32)$$

As defined earlier, f_m is the filter loss at maximum transmission ($\omega = \omega_f$) and ϖ_s is the detuning of the seed laser frequency from ω_f. The phase of the nth component has a stochastic portion $\varphi_s(t)$ and a time-independent part that is quadratic in n

$$\Phi_n = -\tau_r n[\omega_s + (n+1)\Delta/2]. \quad (33)$$

The steady population inversion $\bar{w}$ affects only the amplitudes a_n of Eq. (31), not the phases of the Fourier expansion (31). The inversion depends upon the steady mean intensity $\bar{I}$ through the condition of steady-state operation, Eq. (22). In turn, the mean intensity $\bar{I}$,

$$\bar{I} = \frac{c}{8\pi}\overline{|\mathscr{E}(t)|^2} = I_c\sum_{n=0}^{\infty}|a_n|^2, \quad (34)$$

involves $\bar{w}$ through the dependence of a_n shown in Eq. (32). Eqs. (22) and (34) combine to give a single transcendental equation for either $\bar{w}$ or $\bar{I}$.

4.2. Simplified interpretation

For the specific case of a seeded FSF laser the expression (31) for the envelope $\mathscr{E}(t)$ of the intracavity field $E(t) = \mathscr{E}(t)\exp(-i\omega_f t)$ can be interpreted in the following way. At any time t the field $E(t)$ inside the cavity at $z = 0$ is the superposition of fields entering the cavity at earlier times that underwent at least one round trip. For simplicity we assume the incident field to be perfectly monochromatic at frequency ω_s, meaning that there is no random phase, $\varphi_s(t) = 0$. Then the incident seed field (prior to passing through the input mirror) can be written as

$$E_{in}(t) = \mathscr{E}_s\exp(-i\omega_s t). \quad (35)$$

In this case the amplitude ε_c of the seeding source is $\varepsilon_c = \mathscr{E}_s\mathscr{T}_{in}$, where $\mathscr{T}_{in}$ is the transmittance of the input mirror for the incoming light.

The cavity field entering the AOM at time t is expressible as the sum

$$E(t) = \sum_{n=0}^{\infty} E_n(t), \quad (36)$$

where component $E_n(t)$ at time t has, by definition, made n round trips and has undergone n frequency shifts. The field emerging at time t as the output beam is evaluated by considering the transmittance of each beam, $\mathscr{T}_n \equiv \mathscr{T}(\omega_s + n\Delta)$, through the AOM without frequency shifting

$$E_{out}(t) = \sum_{n=0}^{\infty}\mathscr{T}_n E_n(t). \quad (37)$$

The amplitude of an individual component is determined by the effective gain $Q(\varpi)$,

$$Q(\varpi) = g_m\bar{w} - f_m - \frac{\varpi^2}{2\Gamma_f^2} \equiv Q_m\left(1 - \frac{\varpi^2}{\varpi_0^2}\right), \quad (38)$$

defined as the difference between saturated gain and filter losses. Here Q_m is the maximum of the effective gain and ϖ_0 is the larger of the two frequency detunings for which the effective gain is equal zero

$$Q_m \equiv g_m\bar{w} - f_m, \quad \varpi_0 \equiv \sqrt{2Q_m}\Gamma_f. \quad (39)$$

It is well known that for a conventional laser, in CW operation, the saturated gain is equal to the loss. However for a FSF laser the gain is not saturated completely, even when the laser operates in the stationary regime.

The field components can be evaluated from the following consideration. The component $E_n(t)$ entered the cavity at time $t - n\tau_r$, with frequency ω_s. It decreased in amplitude by the factor $\mathscr{T}_{in}$, shifted frequency by Δ, and underwent attenuation or gain [depending on the sign of the effective gain $Q(\omega_s + \Delta)$] by a factor $R_1 = \exp(Q(\omega_s + 1\Delta))$. On the next round trip it underwent frequency shift from $\omega_s + \Delta$ to $\omega_s + 2\Delta$ and again underwent attenuation or gain, this time by the factor $\mathscr{R}_2 = \exp(Q(\omega_s + 2\Delta))$. It makes n such round trips, on each of which it changes amplitude by a factor $\mathscr{R}_i(\omega)$ and acquires a phase shift $\omega\tau_r$ because it propagates the distance τ_r/c. It follows that the various components are

$$E_0(t) = \mathscr{E}_s\mathscr{T}_{in}\exp[-i\omega_s t], \quad (40)$$

$$E_1(t) = \mathscr{E}_s\mathscr{T}_{in}\mathscr{R}_1\exp[-i(\omega_s + \Delta)t] \times \exp[+i(\omega_s + \Delta)\tau_r], \quad (41)$$

$$E_2(t) = \mathscr{E}_s\mathscr{T}_{in}\mathscr{R}_1\mathscr{R}_2\exp[-i(\omega_s + 2\Delta)t] \times \exp[+i(\omega_s + \Delta)\tau_r + i(\omega_s + 2\Delta)\tau_r], \quad (42)$$

$$\vdots \quad (43)$$

$$E_n(t) = \mathscr{E}_s\mathscr{T}_{in}\mathscr{R}_1\mathscr{R}_2\cdots\mathscr{R}_n exp[-i(\omega_s + n\Delta)t] \times \exp\left[i\sum_{m=1}^{n}(\omega_s + m\Delta)\tau_r\right], \quad (44)$$

where the reflectivity $\mathscr{R}_n$ is

$$\mathscr{R}_n = \exp\left[Q_n - \frac{(\omega_s + n\Delta)^2}{2\Gamma_f^2}\right]. \quad (45)$$

The first exponential factor describes the time variation appropriate to frequency $\omega_n = \omega_s + n\Delta$. The last exponential factor describes the spatial phase $\sum_n (\omega_n/c)L$ acquired by propagating n full round trips through the cavity, each of length $L = \tau_r/c$ but at a different frequency ω_n.

Note that in the absence of any frequency shift, in the absence of the gain, and with $\mathscr{R}(\omega_s) = \mathscr{R} < 1$, the individual components have the form $E_n(t) = \mathscr{E}_s\mathscr{T}_{in}\mathscr{R}^n\exp[-i\omega_s t + in\omega_s\tau_r]$ and the field has the construction

$$E(t) = \frac{\mathscr{E}_s\mathscr{T}_{in}\exp[-i\omega_s t]}{1 - \mathscr{R}\exp[+i\omega_s\tau_r]}. \quad (46)$$

The maximum of this field occurs when $\tau_r\omega_s = 2\pi q$, for any integer q. This is the standard Fabry–Perot cavity condition for axial modes.

5. The discrete frequency model

Comparison of the heuristically derived Eqs. (35) and (44) with the field presented in Eq. (31) is done by introducing an envelope $\mathscr{E}_{DF}(t)$ as in Eq. (2),

$$E(t) = \exp[-i\omega_f t]\mathscr{E}_{DF}(t). \quad (47)$$

Using Eq. (10) and the definitions (32) and (33) of S_n and Φ_n we find

$$\mathscr{E}_{DF}(t) = \sum_n^{\infty}\mathscr{E}_s\mathscr{T}_{in}\exp[S_n - i\Phi_n] \times \exp[-i(\varpi_s + n\Delta)t] = \exp[-i\omega_s t]\sum_{n=0}^{\infty}A_n\exp[-in\Delta t]. \quad (48)$$

This is just the amplitude of Eq. (31) with $\varphi_s = 0$ (i.e. a monochromatic seed) and $\varepsilon_c = \mathscr{E}_s\mathscr{T}_{in}$.

The amplitude $\mathscr{E}_{DF}(t)$ defined by the summation (48) is periodic, with the period $T_p = 2\pi/\Delta$, and hence the expression is in the form of a Floquet series: a time-dependent prefactor $\exp[-i\omega_s t]$ multiplying a periodic function, expressed as a Fourier series with constant complex-valued

Fourier coefficients $A_n = \varepsilon_c a_n \exp[-i\Phi_n]$. Therefore the field in the seeded FSF cavity is *a comb of discrete frequency components, separated by the increment* Δ, and starting from the seed frequency ω_s. The phase Φ_n varies quadratically with n, whereas the exponent of S_n, defined in Eq. (32), varies cubically. However, in practice the variation of S_n is significant only near its maximum $S_{max} = S_{n_{max}}$ where it also is quadratic.

The magnitude of A_n is governed by the real-valued exponent S_n the sign of which is determined critically by the saturated inversion $\bar{w}$. In turn, $\bar{w}$ depends on the total intensity and hence on the seed detuning ϖ_s and on other parameters of the laser. We will show in Section 5.1 that, for wide range of parameters, $\bar{w}$ is determined mainly by the filter width Γ_f and the frequency shift Δ. Using the definitions of Eq. (39) for the peak effective gain Q_m and ϖ_0 we rewrite the real-valued exponent S_n of Eq. (32) as

$$S_n = Q_m n\left(1 - \frac{6\varpi_s^2 + 6\varpi_s n\Delta + 6\varpi_s\Delta + 2n^2\Delta^2 + 3\Delta^2 n + \Delta^2}{6\varpi_0^2}\right). \tag{49}$$

If the seeding laser is tuned near the lower frequency where the effective gain is zero, so $\varpi_s \geqslant -\varpi_0$, then starting from $n = 0$, the value of S_n grows steadily with n as long as the gain exceeds the loss, i.e. $Q(\varpi_s + n\Delta) > 0$. Eventually, for $n > (\varpi_0 + |\varpi_s|)/\Delta$, the loss dominates the gain, and the exponent S_n falls with further increase of n. Thus there is a maximum of S_n, determined from the solution of the equation $(d/dn)S_n = 0$. This value, S_{max}, occurs for the index $n = [n_{max}]$, where $[\ldots]$ means the integer part. For large $\varpi_0 \gg \Delta$ the peak occurs at

$$n_{max} \approx (\varpi_0 + |\varpi_s|)/\Delta. \tag{50}$$

This is a value of n for which $Q(\varpi_s + n\Delta) = 0$. The variation of the magnitude $a_n = \exp[S_n]$ of the frequency component with index n is therefore very nearly of Gaussian shape centered around $n = n_{max}$; the exponential argument S_n departs from quadratic form in n only when n is large or small compared with n_{max}.

Fig. 2(b) illustrates the variation of the components a_n with n, normalized to unit value at the maximum. The peak of a_n is very close to the location of the value $Q(\varpi_s + n\Delta) = 0$. For reference, Fig. 2(a) shows the effective gain $Q(\varpi)$ associated with these components. Fig. 5 of [8] shows an experimentally observed spectrum which looks exactly like our Fig. 2(a).

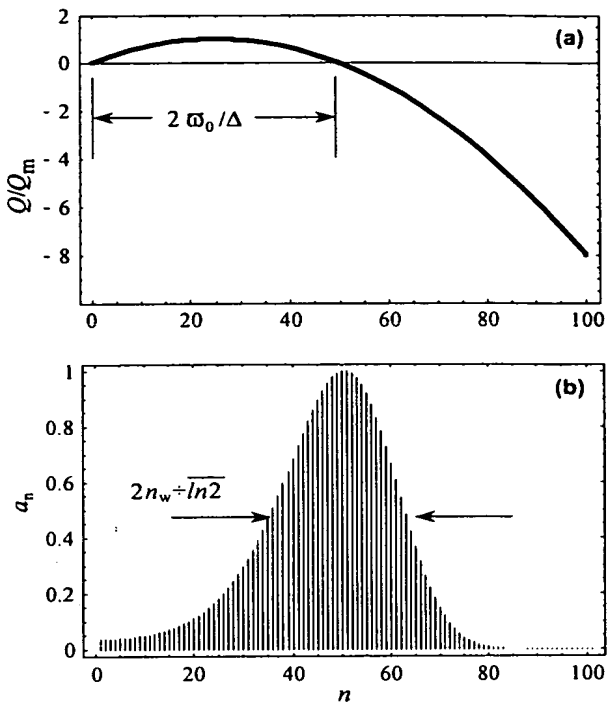

Fig. 2. (a) The relative effective gain function Q/Q_m vs. n, showing the definition of ϖ_0. (b) The magnitudes a_n of the field components $E_n(t)$ vs. n, normalized to unity at the maximum. The parameters $1/(n_w)^2 = 240$. For clarity only every second component is plotted. One can see, from comparing the two frames, that the peak of the component distribution occurs where the effective gain changes from positive to negative.

5.1. Gaussian approximation

The S_n of Eqs. (32) or (49) follows a quadratic dependence on n for appropriate conditions. This gives the amplitude a_n a Gaussian form. To identify those conditions, we consider the field given by Eq. (31) when the seeding laser is detuned far away from the central frequency of the laser spectrum. In this case the first frequency component is very

weak and the shape of the laser output spectrum is close to Gaussian. To quantify this relationship we express S_n as a Taylor series around n_{max}, where $dS_n/dt = 0$, retaining only the quadratic term. The magnitudes a_n can then be written as

$$a_n \simeq \mathscr{A} \exp\left[-\left(\frac{n-n_{max}}{n_w}\right)^2\right], \tag{51}$$

where the width parameter n_w obeys the relationship

$$(n_w)^2 = \frac{2(\Gamma_f)^2}{\varpi_0 \Delta} \tag{52}$$

and n_{max} is given by Eq. (50). The common amplitude $\mathscr{A}$ is expressible as

$$\mathscr{A} = \exp\left[\frac{2\varpi_0^3 + \varpi_s^3 - 3\varpi_s\varpi_0^2}{6\gamma^3}\right], \tag{53}$$

where the frequency parameter γ is defined as

$$\gamma \equiv (\Delta\Gamma_f^2)^{1/3}. \tag{54}$$

The Gaussian approximation of Eq. (51) is valid if n_w is large enough, meaning

$$n_w \gg \Gamma_f^2/\varpi_0^2. \tag{55}$$

This condition depends, through ϖ_0 and Eq. (39), on the still-unknown saturated inversion $\bar{w}$,

$$\bar{w} = \frac{f_m}{g_m} + \frac{(\varpi_0)^2}{2g_m(\Gamma_f)^2}. \tag{56}$$

To find $\bar{w}$ we assume that the Gaussian approximation is valid, so that the mean number n_w of discrete components is large, $n_w \gg 1$. Then we replace the summation over n in Eq. (34) by an integration

$$\bar{I} = I_c\mathscr{A}^2 \int_{-\infty}^{\infty} dx \exp\left(-\frac{2x^2}{n_w^2}\right) = I_c\sqrt{\frac{\pi}{2}}\mathscr{A}^2 n_w. \tag{57}$$

Taking into account the condition $|\Delta| \ll \Gamma_f$, we have from Eq. (22) the result

$$\exp\left[\frac{2\varpi_0^3 + \varpi_s^3 - 3\varpi_s\varpi_0^2}{3\gamma^3}\right]\sqrt{\frac{2\gamma}{\varpi_0}} = \frac{1}{\beta}. \tag{58}$$

The small parameter $\beta \ll 1$ introduced here is

$$\beta \equiv \sqrt{\frac{\pi}{2}}\frac{I_c}{I_{sat}}\frac{1}{(\eta-1)}\left(\frac{\Gamma_f}{\Delta}\right)^{2/3} \tag{59}$$

with the threshold parameter η being defined as

$$\eta = \frac{g_m}{f_m}. \tag{60}$$

Eq. (58) gives an implicit relationship between the value of ϖ_0 (and hence of $\bar{w}$) and the parameters γ, β and ϖ_s. Fig. 3 shows the numerical solution of this equation for different values of detunings ϖ_s of the seeding laser as a function of the parameter β. The dependence on β is very weak.

A simple approximation, based on inspection of this figure, is to take the parameters of the Gaussian profile to be

$$\varpi_0 \approx 3\gamma, \quad \bar{\Gamma} \approx \sqrt{\frac{2}{3}}\gamma, \quad n_w \approx \sqrt{\frac{2}{3}}\frac{\gamma}{\Delta}. \tag{61}$$

With this approximation the amplitudes of the Fourier components depend only on the detuning Δ and the filter bandwidth Γ_f, through the combination γ.

More detailed calculations, taking into account the parameters I_c, I_s and η, make only a small change. When β is extremely small (so $1/\ln(1/\beta)$ is also small) the transcendental equation (58) can be solved approximately for the specific choice of detuning $\varpi_s = 0$. In this case one obtains the approximation

$$\varpi_0 \approx \left[\frac{3}{2}\ln\frac{1}{\beta}\right]^{1/3}\gamma. \tag{62}$$

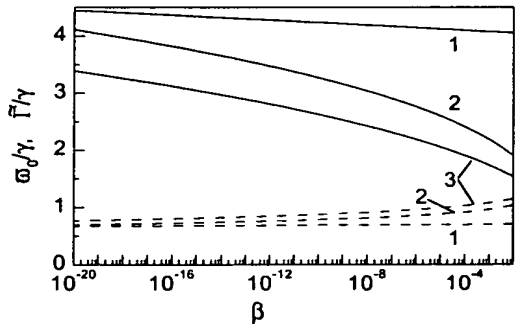

Fig. 3. The shift ϖ_0 of the position of the spectrum maximum (solid lines) and the width $\bar{\Gamma}$ of the spectrum (dashed lines) in units of γ as a function of the parameter β. The detuning of the seeding laser is: (1) $\varpi_s = -8\gamma$; (2) $\varpi_s = 0$; (3) $\varpi_s = -2\gamma$.

The maximum of the spectrum is located at

$$\omega_{\max} = \omega_f + \varpi_0. \tag{63}$$

The mean number of components (the "width parameter" n_w) is given by the formula

$$n_w = \frac{\sqrt{2}}{[(3/2)\ln(1/\beta)]^{1/6}} \frac{\gamma}{\Delta} \tag{64}$$

and the mean intensity $\bar{I}$ is

$$\bar{I} = I_{sat}(\eta - 1). \tag{65}$$

The spectral width, $\tilde{\Gamma} = \Delta n_w$, and the mean intensity are both nearly independent of the seeding laser intensity.

We have derived here, from first principles, formulas for the width and the peak of the discrete-frequency model. The important parameters are Δ, the frequency shift per round trip, and the filter width Γ_f; this latter has only a weak dependence on β, which incorporates the saturation intensity, on the threshold parameter η, on the intensity of the seeding laser in the cavity and on the ratio of the filter width to the AOM frequency. In principle the values of these quantities are known for any particular laser, and so the operation of the FSF laser can be fully described.

5.2. Explicit Fourier formula

When the Gaussian approximation is justified for the amplitude of Eq. (48), the construction for the electric field $E(t)$ reads

$$E(t) = \exp[-i\omega_s t]\varepsilon_c \mathscr{A} \times \sum_{n=0}^{\infty} \exp\left[-\frac{(n-n_{\max})^2}{n_w^2} + i\tau_r n[\omega_s + (n+1)\Delta/2]\right] \exp[-in\Delta t]. \tag{66}$$

Because the frequency width of the spectrum $\tilde{\Gamma}$ is much smaller than the filter width Γ_f one can neglect the frequency dependence of the AOM efficiency near $\omega_{\max}$. Then the output field $E_{out}(t)$ is directly proportional to the intracavity field $E(t)$.

Because we assume n_w to be very large we can approximate $n_{\max}$ by the integer $n_{\max} \simeq [n_{\max}]$. For purposes of display, the largest-magnitude Fourier component, which occurs for $n = n_{\max}$, serves as a useful reference point for expressing the others. We rewrite the argument of the exponential,

$$S_n - i\Phi_n = -\frac{(n-n_{\max})^2}{n_w^2} + i\tau_r n[\omega_s + (n+1)\Delta/2],$$

in terms of the difference between n and $n_{\max}$, using the variable m

$$S_{n_{\max}+m} = -(m/n_w)^2, \tag{67}$$

$$\Phi_{n_{\max}+m} = \Phi_{n_{\max}} - m[\omega_s\tau_r + (n_{\max}+1)\Delta\tau_r/2] - m^2(\Delta\tau_r/2). \tag{68}$$

We eliminate the occurrence $n_{\max}$ from this formula by shifting the time $t \to t - t_0$ with an appropriately chosen initial time t_0 appropriately. The choice

$$t_0 = \tau_r\left[(n_{\max}+1)/2 + \frac{\omega_s}{\Delta}\right] \tag{69}$$

available when $\Delta \neq 0$, eliminates the linear variation with m from the phase, and eliminates also the dependence on the seed frequency ω_s. This choice leads to the expression

$$E(t) = \exp[-i(\omega_s + n_{\max}\Delta)(t-t_0)] \times \sum_{m=-\infty}^{\infty} A'_m \exp[-im\Delta(t-t_0)] \tag{70}$$

with

$$A'_m = A_0 \exp[-(m/n_w)^2 - im^2(\Delta\tau_r/2)], \tag{71}$$

where the new normalization constant A_0 incorporates all constant phases and the factor $\varepsilon_c\mathscr{A}$. With this choice the seed frequency ω_s appears only in the common time-dependent prefactor $\exp[-i\omega_s(t-t_0)]$, but not in the summation. The prefactor does not affect the intensity of the output radiation, $|E(t)|^2$, and it gives only a constant contribution to the instantaneous frequency $\Omega(t)$, defined by

$$\Omega(t) = \frac{d}{dt}\arctan(\mathrm{Re}[E(t)]/\mathrm{Im}[E(t)]). \tag{72}$$

The right-hand side of Eq. (70) is a Floquet series in which the coefficients are Gaussians with a phase that varies quadratically with the index m. Apart from normalization, the amplitudes depend on only two parameters: the phase change in one

round trip, $\Delta\tau_r$, and the width of the effective gain distribution, n_w.

5.3. Examples of pulsing output

It is instructive to examine illustrative examples of the output, Eq. (70). For that purpose we introduce the dimensionless time variable $x = t/T_p$, thereby expressing time in units of the basic repetition period $T_p = 2\pi/\Delta$. We then deal with the function

$$F(x) = F_0 \sum_{m=-M}^{+M} \exp[-im2\pi(x - x_{ref}) - (m/n_w)^2 - im^2(\pi\tau_r/T_p)]. \quad (73)$$

The function $F(x)$ depends on three parameter combinations: n_w, $x_{ref} = t_0/T_p$ and τ_r/T_p. The first of these determines the width of the Gaussian distribution of Fourier amplitudes, and thereby controls the number of components that can add coherently. The relative time x_{ref} merely adjusts the position of the pulse peaks along the x axis. The most important parameter combination is $\tau_r/T_p = 2\pi\Delta\tau_r$. Whenever the parameter τ_r/T_p is an integer, the field is a sequence of short pulses, one per period. Such pulses are described by the function

$$F(x) = F_0 \sum_{m=-M}^{+M} \exp[-im2\pi(x - x_{ref}) - (m/n_w)^2]. \quad (74)$$

The duration of an individual pulse is inversely proportional to the number of Fourier components that contribute significantly to the sum. The present work parameterizes this number by n_w, the width of the Gaussian distribution of Fourier components. Thus as the n_w increases, the pulse durations can become shorter. The time-dependent frequency of such pulses, defined by Eq. (72), remains constant during the presence of a pulse.

Fig. 4 shows examples of these short pulses, for several values of n_w. Earlier such pulses were reported in [20]. For uniformity of plots we normalize the field by taking the quantity $1/F_0$ to be real and equal to the sum (we take the summation limits to be $M = 4n_w$)

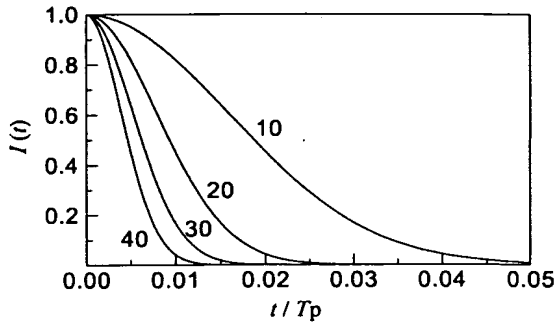

Fig. 4. The relative intensity $I(t)$ of the output field vs. time t, in units of the period $T_p = 2\pi/\Delta$. Plots are for $n_w = 10$, 20, 30 and 40.

$$1/F_0 = \sum_{m=-M}^{+M} \exp[-(m/n_w)^2]. \quad (75)$$

More generally, trains of short pulses occur whenever τ_r/T_p is the ratio of two integers. These become less intense as they become more numerous in one period. Fig. 5 presents examples of such

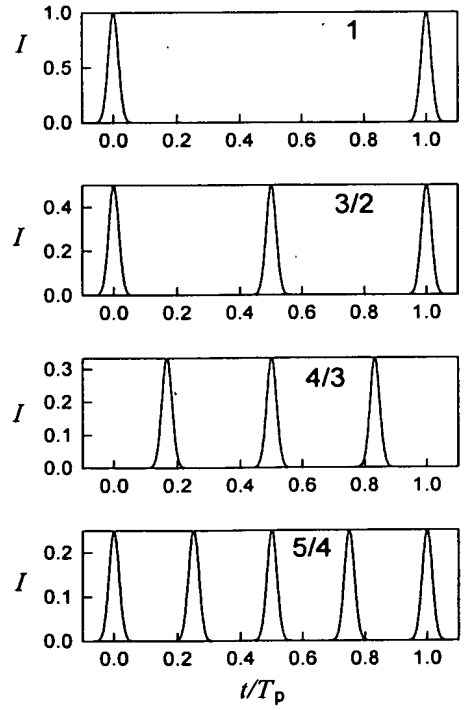

Fig. 5. Intensity I vs. time t, in units of T_p, for values of $\tau_r/T_p = 1$, 3/2, 4/3, and 5/4.

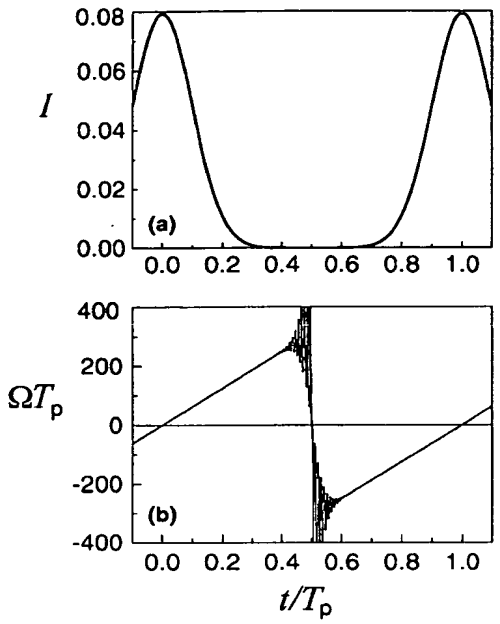

Fig. 6. (a) The relative intensity I of the output field vs. time, in units of the period T_p, for $n_w = 20$ and $\tau_r/T_p = 1.01$. (b) The instantaneous frequency vs time, in units of T_p.

pulses, for several choices of τ_r/T_p. As the difference between τ_r/T_p and an integer increases, the pulses become longer, and the instantaneous frequency develops a chirp. The chirp rate increases until adjacent pulses begin to overlap. Fig. 6 illustrates the chirp. With further increase of $|\tau_r/T_p|$ the overlapping pulses interfere, and a more complex structure develops.

The predicted chirp rate for the frequency chirp shown in Fig. 6 can be estimated from the following argument. The spectral width of the short pulses does not depend on the difference between round trip time τ_r and the time interval $T_p = 2\pi/\Delta$. Thus, for $\tau_r = T_p$ we have short pulses with duration T_p/n_ω and with the spectral width $n_\omega\Delta$. If τ_r is not equal to T_p (as it is in Fig. 6) the duration of a pulse is about τ_r, but the spectral width is the same, $n_\omega\Delta$. This width is due entirely to chirp, and so one can estimate the chirp rate as $n_\omega\Delta/\tau_r$.

6. The moving comb model

The preceding section presented a description of the FSF laser as a static comb of frequency components. An alternative viewpoint of the FSF laser output is that in stationary operation the output electric field $E_{MC}(t)$ consists of a moving comb of chirped frequencies [14,18,29,36,39]. There are an infinite number of frequency components ("teeth") in this comb, each with a time varying amplitude $B_n(t)$

$$E_{MC}(t) = \mathscr{E}_0 \sum_{n=-\infty}^{+\infty} B_n(t) \exp[-ip_n(t)]. \tag{76}$$

Associated with the real-valued amplitude $B_n(t)$ is a phase $p_n(t)$, whose time derivative is the instantaneous frequency of the nth component

$$\omega_n(t) = \frac{d}{dt} p_n(t). \tag{77}$$

The moving comb model assumes that each frequency $\omega_n(t)$ increases linearly with time; for the nth component one can write the time-dependent frequency as

$$\omega_n(t) = \omega_{max} + \frac{\Delta}{\tau_r}(t - n\tau_s). \tag{78}$$

That is, starting from a very large negative value in the remote past (as $t \to -\infty$), this chirped frequency increases steadily, exceeding the value ω_{max} when $t = n\tau_s$. The frequency continues to increase indefinitely thereafter, while the amplitude $B_n(t)$ is vanishingly small in the remote past, when its instantaneous frequency lies outside the range for which the gain exceeds the loss. As time progresses the chirp brings the frequency into the frequency domain of net amplification, and the amplitude grows. The amplitude reaches a maximum, by definition, when $t = n\tau_s$; the frequency $\omega_n(t)$ then is ω_{max}. As time increases the instantaneous frequency grows beyond the region of net gain, and losses cause the amplitude to diminish. In the remote future, when the instantaneous frequency has become very large, the amplitude again becomes negligible.

It is generally assumed, e.g. [32], that the amplitude $B_n(t)$ has a Gaussian form

$$B_n(t) = \exp\left[-\frac{(t - n\tau_s)^2}{(n_0\tau_r)^2}\right], \tag{79}$$

peaking at $t = n\tau_s$ and with a Gaussian width parameter of $n_0\tau_r$. We take the phase $p_n(t)$ to be

$$p_n(t) = \frac{\Delta}{2\tau_r}(t - n\tau_s)^2 + \omega_{max}(t - n\tau_s). \quad (80)$$

From Eq. (80) we determine the instantaneous frequency to be equal to the value given by Eq. (78). Combining the amplitude with the phase, and summing over all possible comb components, we obtain the field

$$\mathscr{E}_{MC}(t) = \mathscr{E}_0 \sum_{n=-\infty}^{+\infty} \exp\left[-\frac{(t - n\tau_s)^2}{(n_0\tau_r)^2} - i\frac{\Delta}{2\tau_r}(t - n\tau_s)^2 - i\omega_{max}(t - n\tau_s)\right]. \quad (81)$$

This is the fundamental expression for the field in the moving comb picture, when individual amplitudes are idealized as Gaussians.

6.1. Interpretation

It is customary to depict this moving-comb field by presenting a density plot of the (real) amplitude $B_n(t)$ as a function of time t (along the horizontal axis) and of instantaneous frequency ω (along the vertical axis). Such a plot appears as a set of slanted ridges, each corresponding to one of the frequency components. Fig. 7 illustrates a portion of such a comb. The intensity distribution shown in the picture has the following properties.

- For fixed frequency (a horizontal line), one finds a set of peaks, spaced evenly with time interval $\tau_s = 2\pi/\Delta$, the repetition period of the field.
- At a fixed time (a vertical line), one finds a set of ridges separated in frequency by the mode spacing, $2\pi/\tau_r$. This set of ridges forms a comb in frequency space. As time increases, the peaks shift toward higher frequency.
- The nth ridge peaks at time $t = n\tau_s$, at which moment the instantaneous frequency is ω_{max}. The ridges all become negligibly small as the instantaneous frequency becomes very different from ω_{max}.
- Each ridge has the same slope, $(d/dt)\omega_n(t)$, equal to the frequency-chirp rate $\gamma_c = \Delta/\tau_r$.

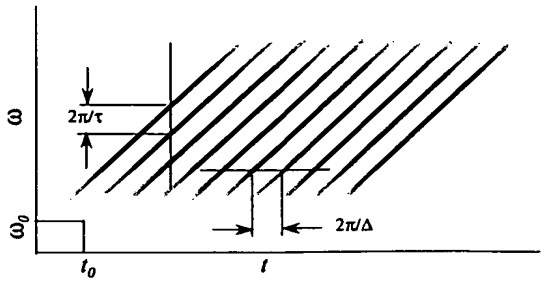

Fig. 7. Schematic diagram of a portion of intensities of FSF laser output as a function of frequency ω and time t. At any fixed time there are a finite number of equidistant frequency components separated by the free spectral range, $2\pi/\tau_r$. At fixed frequency there is an infinite succession of pulses, with period $2\pi/\Delta$.

This model, of a moving comb of frequencies, explains a number of observed properties of FSF lasers. However, it has been questioned by some authors. In particular, it seems puzzling that, although the frequency shift occurs only within a single short segment of the ring cavity (namely the length of the AOM), the output field shows only a smoothly increasing instantaneous frequency [33].

The model has been used to describe the output of an *unseeded* FSF laser [37], that is, one in which the internal field originates with amplified spontaneous emission. Presumably a set of discrete-frequency components such as shown by a fixed-time slice of Fig. 7 derive from a single spontaneous emission event. These are thereafter phase coherent with this initial phase. But many spontaneous emission events occur, each at random times, and so it is not obvious, for example, what sets the time t_0 at which any component has a specified reference frequency. It is likely that frequency feedback may offer a similar means of stabilizing a comb pattern, by selecting one discrete comb out of a continuum of combs that differ only in the time t_0. Any irregularities or noise will introduce a departure from the regular pattern depicted in Fig. 7. A *seeded* FSF laser deals with this ambiguity by providing a definite phase and frequency of the input signal.

6.2. Unification of models

In the model presented in Section 5 there is no continuously varying frequency, no comb apparently steadily advancing with time. Instead, the frequency takes a succession of constant values, being shifted by Δ with each round trip. The output field $E_{DF}(t)$, where DF refers to the discrete-frequency model, is the superposition of the original seed field and fields that have made all possible round trips within the cavity.

A glance at Eq. (81) shows that the field associated with the moving-comb model is unchanged when t is replaced by $t + m\tau_s$, where m is any integer. This field therefore shares with the field of the discrete-frequency model a periodicity, of period $\tau_s = 2\pi/\Delta$. We therefore know that this field can be represented as a Fourier series. We write this series representation of the moving-comb model in the form

$$E_{MC}(t) = \mathscr{E}_0 \sum_m C_m \exp[-im\Delta(t - t_{MC})], \tag{82}$$

where t_{MC} is a reference time. The Fourier coefficients C_m are determined by integrating over one period

$$\mathscr{E}_0 C_m = \frac{\Delta}{2\pi} \int_{t_0}^{t_0+\tau_s} dt E_{MC}(t). \tag{83}$$

For the moving-comb model defined by Eq. (81) the Fourier components can be evaluated in closed form. They are

$$C_m = \frac{\Delta}{2\pi} \frac{\sqrt{\pi}}{\sqrt{(n_0\tau_r)^{-2} + i(\Delta/2\tau_r)}} \times \exp\left[\frac{(\omega_{max} - m\Delta)^2}{4((n_0\tau_r)^{-2} + i(\Delta/2\tau_r))} - im\Delta t_{MC}\right]. \tag{84}$$

We are interested in the case where there are many Fourier components, which occurs when $n_0 \gg 1$. We also assume that the frequency shift Δ is comparable to the cavity mode separation, meaning that $\Delta\tau_r/2\pi$ is comparable with unity. In this case, with the choice of reference time as $t_{MC} = \omega_{max}\tau_r/\Delta$, the Fourier components can be written as

$$C_m = C_0 \exp\left[-\left(\frac{m - (\omega_{max}/\Delta)}{n_0}\right)^2\right] \times \exp[+im^2(\Delta\tau_r/2)]. \tag{85}$$

Here the factor C_0 incorporates the common phase, the first exponential describes a Gaussian distribution of amplitudes, and the final exponential describes the (quadratic) dependence of phase upon m.

Although the discrete frequency model of the previous section deals with a seeded laser, there is no such reference frequency for the moving-comb model. Nevertheless, the two pictures have the same Fourier transforms, and hence they describe the same output field, if only one assumes that the frequency of the seed laser of the discrete-frequency model is some large integer multiple of Δ. The connection between the two models is completed with the identification of the Gaussian widths, $n_0 = n_w$.

6.3. Comments

Our analytical expressions of the earlier sections provide a first-principles derivation of the width and the peak of the discrete-frequency model and, from the proven equivalence of the two models, the moving-comb model as well. The quadratic m-dependence of the phases of the Fourier components of the moving-comb model, C_m, given in Eq. (85) are identical with the phases of the amplitudes A_m of the discrete-frequency model. With simple assumptions about the gain and loss properties of the device, one obtains in both cases Gaussian distributions of amplitudes. Thus the two models are identical when they both describe a FSF laser seeded by a CW field. Then Eq. (85) is exactly the field of a seeded FSF laser whose seed frequency is equal to some (very large) integer multiple of Δ.

The equivalence of the two descriptions means, in particular, that even though the moving comb model appears to have a continuously varying linearly chirped frequency, in fact the field contains only discrete frequencies when it is seeded.

The moving comb model has been applied not only to a seeded system but to a system that grows

from spontaneous emission. In this case there is no identifiable seed carrier frequency ω_s. Nevertheless, the system retains the same periodicity established by the presence of a fixed frequency shift Δ at regular intervals.

In all cases only these discrete frequencies $n\Delta$ are present in the field. This means that unless the field passes through some nonlinear element, then it cannot acquire any additional frequencies. This implies that for use in interferometry that depends on measuring a beat frequency whose value is proportional to delay time between two paths [28,29,36] such a field can not be used directly.

7. The FSF laser with spontaneous emission

The procedure used to solve Eq. (23) is also applicable to the treatment of a FSF laser based on the growth of spontaneous emission – the laser acts as a regenerative amplifier of spontaneous emission. The relevant equation is

$$\mathscr{E}(\vec{X}) = \mathscr{E}(\vec{X} - \vec{X}_0)\exp\left[G(\vec{X})\right] + \xi(\vec{X}). \tag{86}$$

The solution to Eq. (86) is

$$\mathscr{E}(\vec{X}) = \xi(\vec{X}) + \sum_{n=1}^{\infty}\exp\left[\sum_{l=0}^{n-1} G(\vec{X} - l\vec{X}_0)\right] \times \xi(\vec{X} - n\vec{X}_0). \tag{87}$$

We now use the properties of our assumed noise model to evaluate stochastic averages.

7.1. Stochastic averages

We are interested in the intensity $I(\omega, T)$ of Eqs. (18) and (19) averaged over stochastic realizations of the Langevin force $\xi(\vec{X})$

$$J(\varpi, T) \equiv \langle I(\varpi, T)\rangle. \tag{88}$$

For the steady-state cases considered in most of this paper, this average is independent of T; in Section 8 we consider more general situations. To carry out the stochastic average $\langle\cdots\rangle$ and obtain the spectrum $J(\varpi, T)$, we assume that the spontaneous emission process $\xi_{sp}(t)$ is a delta- correlated (Wiener–Levy) stochastic process

$$\langle\xi_{sp}(t_1)\xi^*_{sp}(t_2)\rangle = \xi_0^2\delta(t_1 - t_2). \tag{89}$$

The parameter ξ_0^2 that characterizes the spontaneous emission intensity depends on the inversion w, the spontaneous emission rate γ_s, and the geometry of the laser cavity. Because the width of the filter is much larger than the free spectral range $\Gamma_f \gg 1/\tau_r$, the result of this averaging is the spectrum

$$J(\varpi, T) = \frac{c\tau_r}{16\pi^2}\xi_0^2\sum_{n=1}^{\infty}\exp\left[2\sum_{l=0}^{n-1}\left[g_m\bar{w} - f_m - \frac{1}{2}\left(\frac{\varpi - l\Delta}{\Gamma_f}\right)^2\right]\right]. \tag{90}$$

After integrating Eq. (90) over ϖ we obtain the averaged intensity

$$\bar{I} \equiv \int_{-\infty}^{+\infty} d\varpi J(\varpi, T) = \frac{c\tau_r\Gamma_f\xi_0^2}{16\pi^{3/2}}\sum_{n=1}^{\infty}\frac{1}{n^{1/2}}\exp\left[n\left(2\left[g_m\bar{w} - f_m\right] - \frac{\Delta^2}{12\Gamma_f^2}(n^2 - 1)\right)\right]. \tag{91}$$

7.2. Simplification

We assume, as before, that $\Delta \ll \Gamma_f$. In this case we can replace the summation over n in (91) by integration and write

$$\bar{I} = I_{sp}F(X), \quad X \equiv \frac{\Delta}{\sqrt{12}\Gamma_f}[2[g_m\bar{w} - f_m] + \Delta^2/(12\Gamma_f^2)]^{-3/2}, \tag{92}$$

where the function $F(x)$ is defined as

$$F(x) = x^{1/3}\int_0^{\infty} dt\exp[t^2(1 - x^2t^4)] \tag{93}$$

and the magnitude of the spontaneous emission source is characterized by the parameter

$$I_{sp} = \frac{c\tau_r\xi_0^2}{\sqrt{\pi^3}}\left(\frac{\sqrt{3}\Gamma_f^4}{2^8\Delta}\right)^{1/3}. \tag{94}$$

By taking into account that $g_m\bar{w} \simeq f_m$ one can transform Eq. (22) for $\bar{w}$ into

$$\beta_{sp}F(X) = 1, \tag{95}$$

where we have introduced the (small) parameter

$$\beta_{sp} = \frac{I_{sp}}{I_{sat}(\eta - 1)} \ll 1. \tag{96}$$

Under typical operating conditions the parameter β_{sp} is very small: $\beta_{sp} \simeq 10^{-18}$. Then we can use the asymptotic form of the function $F(x)$ for large $x \gg 1$

$$F(x) \simeq \frac{\pi^{1/2}}{2} x^{1/3} \exp\left(\frac{2}{3^{3/2}x}\right). \tag{97}$$

In this case the initial inversion w_0 can be found from the condition

$$\frac{\sqrt{\pi}}{3^{1/2}2^{2/3}} \beta_{sp} \exp(Y) = Y^{1/3}, \tag{98}$$

where

$$Y \equiv \frac{2}{3^{3/2}X} = \frac{4\Gamma_f}{3\Delta}[2(g_m\bar{w} - f_m) + \Delta^2/(12\Gamma_f^2)]^{3/2}.$$

The solution to Eq. (98) for $\beta_{sp} \ll 1$, and thus for $\ln(1/\beta_{sp}) \gg 1$, is

$$Y \simeq \ln\frac{1}{\beta_{sp}}. \tag{99}$$

Then the requirement for inversion is

$$2(g_m\bar{w} - f_m) = -\frac{\Delta^2}{12\Gamma_f^2} + \left[\frac{3\Delta}{4\Gamma_f}\ln\frac{1}{\beta_{sp}}\right]^{2/3}. \tag{100}$$

Taking into account the condition $\Delta \ll \Gamma_f$ we find that $g_m\bar{w} \simeq f_m$, as is expected. The spectrum $J(\varpi, T)$ can be written now as

$$J(\varpi, T) = \frac{c\tau_r}{16\pi^2}\xi_0^2 \sum_{n=1}^{\infty} \exp\left[\sum_{l=0}^{n-1}\left(-\left(\frac{\varpi - l\Delta}{\Gamma_f}\right)^2 - \frac{\Delta^2}{12\Gamma_f^2} + \left[\frac{3\Delta}{4\Gamma_f}\ln\frac{1}{\beta_{sp}}\right]^{2/3}\right)\right]. \tag{101}$$

In Eq. (101) one can replace the summation over n by integration. Taking into account the condition $\ln(1/\beta_{sp}) \gg 1$ we can carry out the integration, with the result that the spectrum takes the form of a Gaussian

$$J(\varpi, T) = I_{sat}(\eta - 1)\frac{1}{\sqrt{\pi}\tilde{\Gamma}} \exp\left[-\frac{(\varpi - \delta\omega)^2}{\tilde{\Gamma}^2}\right], \tag{102}$$

whose width $\tilde{\Gamma}$ is

$$\tilde{\Gamma} = \gamma/\sqrt{\sigma} \tag{103}$$

and whose peak is offset from $\varpi = 0$ by

$$\delta\omega = \sigma\gamma \tag{104}$$

with

$$\sigma = \left(\frac{3}{4}\ln\frac{1}{\beta_{sp}}\right)^{1/3}. \tag{105}$$

Recall that ϖ is the frequency offset from the filter center ω_f, meaning that the spectral maximum occurs at $\omega_{max} = \omega_f + \sigma\gamma$. This result for the continuous spectrum is to be compared with that of Section 5.1 for the distribution of discrete frequency components within a Gaussian envelope.

As in the case of the seeded laser we have here a first-principles derivation of the width and the peak of the spectrum. Again there is only a weak dependence on β_{sp} and the only important parameter is $\gamma = [\Delta\Gamma_f^2]^{1/3}$. It is noteworthy that parameter σ can be easily determined from the ratio $\delta\omega/\tilde{\Gamma} = \sigma^{3/2}$. In principle these are known for a particular laser, and so the operation of the FSF laser can be determined from these known quantities [24].

8. Rate equations

A previous paper [24] has used a rate-equation model to describe the operation of the FSF laser. This model is based on two sets of coupled equation, one for the population inversion and another for the spectral density of photons. It is interesting to compare our approach based on the Fourier expansion of the electric field with the rate-equation model.

Considering the FSF laser with spontaneous emission and using Eq. (86) for $\mathscr{E}(\vec{X})$ in the model of spontaneous emission, Eq. (89), we obtain an equation for the averaged spectral density $J(\varpi, T)$:

$$J(\varpi,T)=J(\varpi-\Delta,T-\tau_r)\times\exp(2[g_0(\varpi)w(T)-f(\varpi)])+\frac{c}{8\pi}\frac{\xi_0^2}{(2\pi)}. \quad (106)$$

This equation was derived earlier using the condition of broad loss $\Gamma_f \gg 1/\tau_r$. Here we do not assume steady-state operation and we allow the averaged spectral density $J(\varpi,T)$ to be time dependent (on the time scale of inversion relaxation). In traditional treatments of laser dynamics one assumes changes of $J(\varpi,T)$ are small during one round trip, $J(\varpi,T)\simeq J(\varpi-\Delta,T-\tau_r)$. In this limiting case Eq. (106) can be written as

$$\left[\frac{\partial}{\partial T}+\frac{\Delta}{\tau_r}\frac{\partial}{\partial\varpi}\right]J(\varpi,T)=J(\varpi,T)(2[g_0(\varpi)w(T)-f(\varpi)])+\frac{c}{8\pi}\frac{\xi_0^2}{(2\pi)}. \quad (107)$$

With the same assumptions the differential equation for the inversion reads

$$\frac{\partial}{\partial T}w(T)=-w(T)\left[\frac{\gamma_s}{\tau_r}\frac{\int d\varpi J(\varpi,T)}{I_{sat}}+\gamma_s\right]+\gamma_s. \quad (108)$$

Here γ_s, as defined in Section 3.2, is the spontaneous emission rate and ξ_0^2, defined in Eq. (89), parameterizes the spontaneous emission intensity. Apart from notational changes, these equations differ from the earlier rate equations of [24] only in the presence of the partial frequency derivative in Eq. (107) for the spectral density. In [24] the authors discretized the frequency space. For a smooth spectrum, which we assumed here, this discretization replaces Eqs. (107) and (108) with partial difference equations, leading to the approximate solutions discussed in [24].

9. Summary and conclusions

We have presented a formalism for treating the coupled equations linking electric field output and population inversion for a frequency-shifted feedback laser. The equations take full account of the phase of the field, and include a possible seed laser, which may have arbitrary phase modulation or fluctuation.

Using these equations we have derived simple expressions for the steady-state output electric field. These have a simple interpretation in terms of multiple passes of a wavepacket through the system, gaining or losing energy while undergoing a periodic frequency shift Δ.

We show that the distribution of spectral components follows a Gaussian form, as is often assumed. The width of this distribution determines the minimum duration of pulses. The characteristic parameters of the Gaussian amplitudes are almost entirely determined by the frequency shift Δ and the filter bandwidth Γ_f, through the combination $\gamma=(\Delta\Gamma_f)^{1/3}$.

The form of the output varies with the relative phases of these spectral components, and depends critically on the ratio of the cavity round-trip time $\tau_r=L/c$ to the repetition period $T_p=2\pi/\Delta$. We have presented illustrative examples of the steady-state output in which there occur various forms of short pulses. Under appropriate conditions these pulses exhibit a linear frequency chirped.

We have also shown the equivalence of two popular models for the output field of the FSF laser, one in which there is a moving comb of frequencies and the other in which there is a fixed discrete set. Our analytical expressions provide a derivation from first principles of the width and the peak of the spectrum of the moving comb model. We also show that the rate equations used previously in modeling the FSF laser can be recovered from the equations presented in this paper.

Acknowledgements

LPY acknowledges support by the stiftung Rheinland-Pfalz für Innovation and the Deutsche Forschungsgemeinschaft (436-UKR-113/16).

References

[1] F. Kowalski, J.A. Squier, J.T. Pinckney, Appl. Phys. Lett. 50 (1987) 711.

[2] F.V. Kowalski, S.J. Shattil, P.D. Hale, Appl. Phys. Lett. 53 (1988) 734.
[3] F.V. Kowalski, P.D. Hale, S.J. Shattil, Opt. Lett. 13 (1988) 622.
[4] P.D. Hale, F.V. Kowalski, IEEE J. Quantum Electron. 26 (1990) 1845.
[5] I.C.M. Littler, S. Balle, K. Bergmann, J. Opt. Soc. Am. B 8 (1991) 1412.
[6] P.I. Richter, T.W. Hänsch, Opt. Commun. 85 (1991) 414.
[7] C.C. Cutler, IEEE J. Quantum Electron. 28 (1992) 60.
[8] I.C.M. Littler, S. Balle, K. Bergmann, Opt. Commun. 88 (1992) 514.
[9] I.C.M. Littler, K. Bergmann, Opt. Commun. 88 (1992) 523.
[10] I.C.M. Littler, J.H. Eschner, Opt. Commun. 87 (1992) 44.
[11] I.C.M. Littler, K. Bergmann, R. Roy, Opt. Commun. 87 (1992) 53.
[12] D.T. Mugglin, A.D. Streater, S. Balle, K. Bergmann, Opt. Commun. 104 (1993) 165.
[13] S. Balle, I.C.M. Littler, K. Bergmann, F.V. Kowalski, Opt. Commun. 102 (1993) 166.
[14] M.W. Phillips, G.Y. Liang, J.R.M. Barr, Opt. Commun. 100 (1993) 473.
[15] H. Sabert, E. Brinkmeyer, Electron. Lett. 29 (1993) 2122.
[16] F.V. Kowalski, S. Balle, I.C.M. Littler, K. Bergmann, Opt. Eng. 33 (1994) 1146.
[17] J. Martin, Y. Zhao, S. Balle, K. Bergmann, M.P. Fewell, Opt. Commun. 112 (1994) 109.
[18] I.R. Perry, R.L. Wang, J.R.M. Barr, Opt. Commun. 109 (1994) 187.
[19] H. Sabert, E. Brinkmeyer, J. Lightwave Technol. 12 (1994) 1360.
[20] S. Balle, K. Bergmann, Opt. Commun. 116 (1995) 136.
[21] K. Nakamura, K. Kasahara, M. Sato, H. Ito, Opt. Commun. 121 (1995) 137.
[22] A.P. Willis, A.I. Ferguson, D.M. Kane, Opt. Commun. 116 (1995) 87.
[23] K.W. Benoist, IEEE Photon. Technol. Lett. 8 (1996) 25.
[24] G. Bonnet, S. Balle, T. Kraft, K. Bergmann, Opt. Commun. 123 (1996) 790.
[25] G. Mussi, P. Stamp, N. Gisin, R. Passy, J.P. von der Weid, IEEE Photon. Technol. Lett. 8 (1996) 1513.
[26] S. Wabnitz, IEEE J. Quantum Electron. 32 (1996) 925.
[27] K. Kasahara, K. Nakamura, M. Sato, H. Ito, Opt. Rev. 4 (1997) 180.
[28] K. Nakamura, F.V. Kowalski, H. Ito, Opt. Lett. 22 (1997) 889.
[29] K. Nakamura, F. Abe, K. Kasahara, T. Hara, M. Sato, H. Ito, IEEE J. Quantum Electron. 33 (1997) 103.
[30] A. Uchida, T. Sato, M. Takeoka, F. Kannari, Jpn. J. Appl. Phys. 2 36 (1997) L912.
[31] S.H. Yun, D.J. Richardson, D.O. Culverhouse, B.Y. Kim, IEEE J. Sel. Top. Quantum Electron. 3 (1997) 1087.
[32] K. Kasahara, K. Nakamura, M. Sato, H. Ito, IEEE J. Quantum Electron. 34 (1998) 190.
[33] F.V. Kowalski, K. Nakamura, H. Ito, Opt. Commun. 147 (1998) 103.
[34] T. Latz, F. Aupers, V.M. Baev, P.E. Toschek, Opt. Commun. 156 (1998) 210.
[35] M.J. Lim, C.I. Sukenik, T.H. Stievater, P.H. Bucksbaum, R.S. Conti, Opt. Commun. 147 (1998) 99.
[36] K. Nakamura, T. Miyahara, M. Yoshida, T. Hara, H. Ito, IEEE Photon. Technol. Lett. 10 (1998) 1772.
[37] K. Nakamura, T. Miyahara, H. Ito, Appl. Phys. Lett. 72 (1998) 2631.
[38] O.G. Okhotnikov, Electron. Lett. 34 (1998) 1493.
[39] A. Yoshizawa, H. Tsuchida, Opt. Commun. 155 (1998) 51.
[40] K.A. Shore, D.M. Kane, IEEE J. Quantum Electron. 35 (1999) 1053.
[41] M. Cashen, V. Bretin, H. Metcalf, J. Opt. Soc. Am. B 17 (2000) 530.
[42] K. Nakamura, T. Hara, M. Yoshida, T. Miyahara, H. Ito, IEEE J. Quantum Electron. 36 (2000) 305.
[43] P. Oberson, B. Huttner, O. Guinnard, L. Guinnard, G. Ribordy, N. Gisin, IEEE Photon. Technol. Lett. 12 (2000) 867.
[44] J.M. Sousa, O.G. Okhotnikov, Opt. Commun. 183 (2000) 227.
[45] S.K. Kim, M.J. Chu, J.H. Lee, Opt. Commun. 190 (2001) 291.
[46] M. Stellpflug, G. Bonnet, B.W. Shore, K. Bergmann, Opt. Express 11 (2003) 2060.
[47] I.C.M. Littler, H.M. Keller, U. Gaubatz, K. Bergmann, Z. Phys. D 18 (1991) 307.
[48] M. Yoshida, K. Nakamura, H. Ito, IEEE Photon. Technol. Lett. 13 (2001) 227.
[49] P. Milonni, J.H. Eberly, Lasers, Wiley, New York, 1988, p. 304.
[50] H. Haken, Laser Theory, Springer, Berlin, 1984, p. 46.
[51] J.H. Eberly, K. Wodkiewicz, J. Opt. Soc. Am. A 67 (1977) 1252.

Available online at www.sciencedirect.com
SCIENCE DIRECT®
Optics Communications 242 (2004) 581–598
OPTICS COMMUNICATIONS
www.elsevier.com/locate/optcom

Ranging and interferometry with a frequency shifted feedback laser

L.P. Yatsenko [a], B.W. Shore [b,*], K. Bergmann [b]

[a] *Institute of Physics, Ukrainian Academy of Sciences, Prospect Nauki 46, Kiev-39, 03650, Ukraine*
[b] *Universität Kaiserslautern, 67653 Kaiserslautern, Germany*

Received 15 May 2004; accepted 30 August 2004

Abstract

The potential advantages of chirped pulses for very precise measurement of distance, through frequency-domain ranging, has prompted consideration of frequency shifted feedback (FSF) lasers as sources of interferometer light. We here derive theoretical limitations to the spatial accuracy one can expect in such applications, by considering analytical expressions for the electric field emerging from a frequency shifted feedback (FSF) laser seeded by a CW laser whose finite bandwidth originates in phase fluctuations. We also consider consequences of fluctuations in cavity size. We show that, for surfaces flat within the laser footprint, such a system can provide the subwavelength accuracy of conventional interferometry but without dependence on material-dependent phase shifts. Although noise has been important for previous uses of FSF lasers in optical ranging and interferometry, we here show that a frequency modulated seeding laser can be used to better advantage than noise.

PACS: 42.55.–f; 42.60.Da; 42.55.Ah
Keywords: Optics; Lasers; Frequency shifted feedback; Interferometry; Profilometry; Frequency-domain ranging

1. Introduction

Rapid and nonintrusive measurements of distances from millimeter to kilometer with accuracies of microns or less are now feasible using techniques of optical frequency domain ranging (OFDR) wherein a measurement of distance is obtained from a measurement of frequency differences [1–5]. The technique can be regarded either as a form of chirped optical radar [6] or as a form of interferometry using chirped laser input. As has been demonstrated, [7,8] the needed interferometer seed laser can use the technique of frequency-

* Corresponding author. Present address: Department of Physics, 618 Escondido Cir, Livermore, CA 94550, USA. Tel.: +1 925 455 0627.
E-mail address: bwshore@alum.mit.edu (B.W. Shore).

0030-4018/$ - see front matter © 2004 Elsevier B.V. All rights reserved.
doi:10.1016/j.optcom.2004.08.051

shifted feedback (FSF) [9–17]. In such a device feedback introduces a fixed frequency shift Δ with each passage of a wave packet around the cavity (during the round-trip time $\tau_r = L/c$ in a cavity of perimeter L). By interpreting the output as a moving comb of frequencies [18,19,15,20–22] Nakamura et al. [7,8] analyzed the use of FSF for distance measurements. A key parameter of their approach is the chirp rate $\gamma_c = \Delta/\tau_r$: the difference in lengths of the two interferometer arms h can be found from the measured beat frequency ω_B as $h = c\omega_B/2\gamma_c$.

An alternative view is also possible. Under proper conditions the output of a seeded FSF laser can be a regular train of pulses [9,10,18,23,13,24] and the individual pulses can exhibit a frequency chirp [26]. The apparent similarity with the longer-wavelength pulses used in chirped radar for accurate ranging suggests that operation at optical wavelengths could offer accuracy adequate for nanoscale structures. However, this simplistic view of FSF laser output is misleading. The chirp of individual pulses from a FSF laser is not connected with the average chirp rate γ_c but, as was shown in [26], is instead determined by the deviation of the frequency increment Δ from c/L.

Although the literature on FSF lasers is extensive, there remain some fundamental questions [25]. Some of these concern the ultimate limits on accuracy attainable when such a laser is used in interferometry. Earlier we have developed a first-principles treatment of the FSF laser [26]. In the present paper, we reexamine some of the properties of this device, with particular emphasis on interferometric applications. Our results provide useful estimates of the limiting accuracy one can achieve using a FSF laser for distance measurement. We clarify the importance of noise in providing the beat frequency that is used in the frequency-domain ranging, and we suggest an alternative approach, using controlled frequency modulation rather than uncontrolled noise, to produce the desired signal.

The present paper is organized as follows.

In Sections 1.1 and 1.3, we present a simple discussion of relevant aspects of interferometry and of frequency-domain ranging based on chirped pulses.

In Section 2, we discuss the properties of the FSF laser, and the form of the output field. The analytic expressions given here provide the basis for our discussion of FSF interferometry that follows.

In Section 3, we consider interferometry using the field presented in Section 2. We point out the importance of phase fluctuations in providing the frequencies needed for range measurement.

In Section 4, we consider the FSF laser seeded by a phase-noisy cw input field. We derive expressions for the beat-frequency spectrum. The width of this spectrum determines the accuracy with which the peak position (the beat frequency) can be measured, and hence the accuracy with which one can measure the distance.

In Section 5, we consider the effects of unavoidable fluctuations in the cavity length, and the effects these have on the accuracy of beat-frequency measurement.

In Section 6, we consider using a frequency-modulated seed to the FSF laser. We show that this has advantages for improved accuracy. We consider both phase sensitive and phase insensitive detection of the interference intensity.

Section 7 discusses the accuracy obtainable, using either a noisy seed or deliberate frequency modulation to provide the needed frequencies.

Section 8 summarizes our results.

An appendix provide details of our noise model.

1.1. Interferometry

Interferometry offers a means for obtaining extremely accurate distance measurements, such as are needed for determining the heights of nanometer-scale features on lithographed surfaces [27]. In a typical Michelson implementation, a laser beam passes through a beam splitter from which one beam travels a fixed distance in a fixed reference arm. The other beam travels to a sample, where it is reflected. The field of the returning beam is combined with that of the reference beam and the resulting intensity pattern is recorded; changes of intensity provide a measure of phase difference between the two beams. Apart from a fixed (but important) phase increment upon reflection, the phase is proportional to the difference in

lengths of the two paths. Thus a measurement of intensity, converted to a measurement of phase, gives a measurement of distance.

One standing difficulty with interferometric techniques applied to surfaces comprising several materials, often of unknown composition, is the presence of a material-dependent phase shift of the reflected field. For reliable measurements of surface heights to tolerances of a few nanometers, it is essential that this material phase shift be accurately known [28]. This shift is particularly difficult to determine when the surface comprises granules embedded in a substrate, unless the granules are either much smaller than a wavelength, so that the surface can be characterized by a complex index of refraction for an effective medium, or are much larger than a wavelength, so that they can be resolved readily. Even then it is difficult to evaluate the phase shift. A recent paper offers one means of overcoming this limitation [27]. As we will show, chirped pulse interferometry also offers the potential to overcome these handicaps.

1.2. Ranging

Conventional interferometry with a single wavelength λ provides subwavelength accuracy of path differences, but because phase has an intrinsic periodicity, it can only provide this accuracy modulo λ, i.e., it cannot distinguish between distance h and $h + \lambda$. Various techniques are used to overcome this limitation, such as the use of two different wavelengths.

For measurements of distances of meters or miles, radar techniques are often used. Typically these transmit a train of pulses and measure the time delay before a return pulse is observed. The requirement for very precise measurement of time intervals makes it difficult to obtain positions of even stationary objects with micron accuracy. The technique of chirped radar [29] replaces time measurements with beat-frequency measurements, but has much in common with interferometry. The technique described here can be used for measurements of large distances, as is done with optical ranging, as well as for small distances; all distances are measured with equal accuracy.

1.3. Chirped-pulse interferometry

It is easy to show that if one has a chirped frequency as input to a Michelson interferometer, see Fig. 1, then the Fourier transform (i.e., the spectrum) of the beat intensity includes a frequency equal to the product of the chirp rate and the delay time between the two arms. Thus one can anticipate construction of an interferometer in which a measurement of frequency gives a measurement of distance. To show this connection consider a simple model of a field whose carrier frequency varies linearly with time (a chirped frequency) at rate γ_c during the time interval $0 < t < T_0$. Assume a constant amplitude $\mathscr{E}$. Then the complex-valued field at a fixed position is

$$E(t) = \mathscr{E}\exp[-\mathrm{i}(\omega_0 + \gamma_c t/2)t]. \quad (1)$$

We use this field as input to a Michelson interferometer in which one arm has length z and the other has length $z + h$, where h is to be determined. Fig. 1 illustrates the general layout of the interferometer. Our interest here is in sub-micron metrology of surfaces, such as occur with lithography, wherein the reference beam can be reflected from the substrate that holds the sample; in other work the arms are often of very different lengths [7,8].

Upon reflection the electric field of beam j acquires a phase shift ϕ_j, which depends on the properties of the surface. The difference in arm lengths gives a relative time delay

$$T = 2h/c. \quad (2)$$

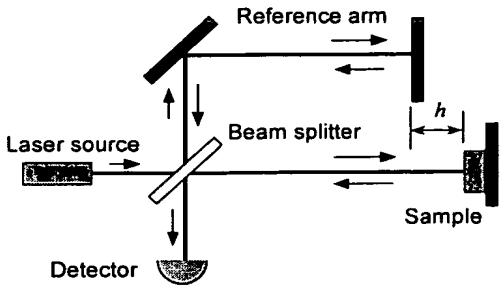

Fig. 1. Schematic diagram of interferometer. Laser source passes through beam splitter, and then along two arms, one of which contains the unknown height to me measured. The height h is relative to the reference arm length, as shown.

For simplicity, we assume perfect reflection at the reference and target surfaces and $T < T_0$. Then the interferometer output intensity is

$$I(t,T) = |E(t) + \exp(i\Delta\phi)E(t+T)|^2 = |E(t)|^2 + |E(t+T)|^2 + 2\mathrm{Re}[\exp(i\Delta\phi)E^*E(t+T)]. \quad (3)$$

where $\Delta\phi$ is the difference between the material-dependent phase shifts ϕ_j in the two arms. We are interested in the interference-term signal

$$S(t) = 2\mathrm{Re}[\exp(i\Delta\phi)E^*E(t+T)] = 2|\mathscr{E}|^2\cos[(2h\gamma_c/c)t + \Delta\phi + \Phi(T)]. \quad (4)$$

This expression shows that a measurement of the beat frequency [the oscillation frequency of $S(t)$]

$$\omega_B \equiv 2\pi\nu_B \equiv \gamma_c T = (\gamma_c/c)2h \quad (5)$$

converts, using the chirp rate γ_c, directly into a measure of T and thence to a measurement of distance h. The material-dependent phase difference $\Delta\phi$ adds a constant to the geometrical phase increment

$$\Phi(T) \equiv \omega_0 T - \gamma_c T^2/2 \quad (6)$$

to produce the interferometer phase $\Phi(t) + \Delta\phi$. Thus any determination of T from the *phase* of the interference term must rely on values of the material phase shift $\Delta\phi$. By contrast, measurements based on beat *frequency* determination are insensitive to this phase.

As will be explained, interferometry with the FSF laser also offers a means of avoiding dependence of distance measurements upon the material phase shift $\Delta\phi$, and hence it offers the potential for accurate surface topography measurements without knowledge of surface characteristics. Furthermore, by giving a measurement of heights of both reflecting and partially reflecting surfaces, it can reveal structure underlying a partially transparent layer with known refractive index but of arbitrary thickness.

The FSF laser is particularly suitable for optical ranging: it provides a strictly linear chirp that can have a very large chirp rate, say 100 MHz in 5 ns, or $5 \times 10^{17}\ s^{-2}$. The FSF laser also functions without an external seed, driven by spontaneous emission in the gain medium. The work of Nakamura et al. [7,8] is done with such a laser. Our work demonstrates that, when the properties of the laser are dominated by an external seed, then much improved accuracy of distance measurements can be achieved. The bandwidth of the seeding laser determines the accuracy, but the origin of the bandwidth is also significant. We show that bandwidth from controlled phase modulation is particularly useful.

1.4. Accuracy and resolution

When the laser beam covers a surface pattern having several heights, then a histogram of distance values displays several peaks. To resolve these using frequency chirping the difference in heights must be greater than half a wavelength. This limitation can be understood in the following way.

From the relationship (5) between the measured feature height h and beat frequency ω_B it follows that the height error δh is proportional to the beat-frequency error, $\delta h = (c/2\gamma_c)\delta\omega_B$. This error is approximated as $\delta\omega_B \approx 2\pi/T$, where T is the duration of a pulse. During a pulse the frequency changes by $\gamma_c T$. This change cannot be larger than the optical frequency $\omega = 2\pi c/\lambda$, and hence the frequency error cannot be less than $\delta\omega \approx (\gamma_c/c)\lambda$. From this limit it follows that the resolution limit is set by the optical wavelength λ,

$$\delta h > \lambda/2. \quad (7)$$

When the laser beam covers a flat surface then, as we will note, the error in a measurement of surface height relative to a reference surface can be significantly less than a wavelength. This error, the accuracy of interferometer measurement, is determined by the accuracy with which one can measure the location of the peak value of a spectral profile, i.e., by the error $\delta\omega_B$ in the beat frequency ω_B. In turn, this is set by the resonance width Γ_{res} of the spectral profile. As we will note (see section 7), accuracy of 100 nm appears possible.

2. The FSF laser

In brief, a FSF laser contains a feedback cavity (which is typically either a closed loop, of perime-

ter L, or a Fabry–Perot cavity of length $L/2$) in which there is a section having gain, one or more spatial or frequency filters and, most importantly, an element that induces a frequency shift (of angular frequency Δ) on each wavepacket that passes through it. Typically the frequency shift is provided by an acousto-optic modulator (AOM), acting as a grating that feeds the first order diffraction back into the cavity, while the zero-order light emerges as the output of the ring cavity. Fig. 2 illustrates an example of such a ring cavity [25].

The properties of such a laser have been extensively reported, e.g., [30–37,13,24,14,38]. The important parameters of the FSF cavity itself, apart from gain and loss, are as follows:

Δ = the frequency shift (rad/s) per round trip;
$\tau_r = L/c$ = the round trip time in the cavity; the free spectral range is $2\pi/\tau_r$.
$\tau_s = 2\pi/\Delta$ = the repetition period of the field;
$\gamma_c = \Delta/\tau_r$ = the average chirp rate of the instantaneous frequency of the cavity field.

Another set of parameters describe the net gain within the cavity and the loss due to reflection and filters. These are distributed over some finite range of frequencies. We treat them as localized in an infinitesimally thin segment of the path. Fig. 3 shows the distribution of gain and loss as a function of frequency (discretized by n).

A key parameter controlling the beat spectrum, from which follows the achievable accuracy of beat frequency measurement, is

n_w = the effective number of discrete frequency components within the output spectrum from the seeded FSF laser. (The output bandwidth divided by the the frequency shift).

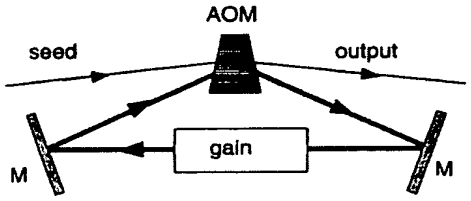

Fig. 2. Schematic diagram of ring cavity showing mirrors (M), frequency shifting AOM (FS), beam splitter (BS), amplifier (G), and input and output beams.

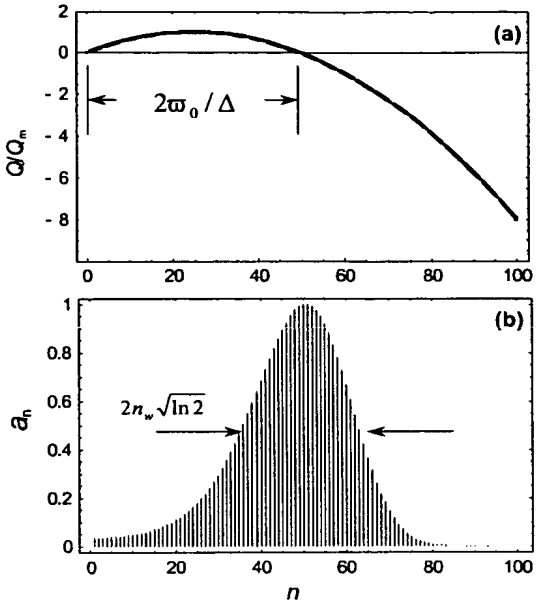

Fig. 3. (a) The relative effective gain function $Q(n)/Q_m$ vs. n. (b) The magnitudes a_n of the field components $E_n(t)$ vs. n, normalized to unity at the maximum. The parameter $1/(n_w)^2 = 240$. The frequency range of positive net gain is $2\varphi_0$, and Q_m is the maximum of $Q(n)$. For clarity only every second component is plotted. One can see, from comparing the two frames, that the peak of the component distribution occurs where the effective gain changes from positive to negative. From [26] Fig. 2.

Γ_f = the bandwidth of the frequency limiting elements of the cavity (a filter).
$\gamma = (\Delta^2\Gamma_f)^{1/3}$ = a frequency parameter largely determining the properties of the FSF laser output.

A FSF laser can operate in a variety of regimes: the output may range from extreme irregularity to very regular pulse trains or even cw, depending on such controllable properties as the amount of gain and the relative values of various time constants or frequency bandwidths of the device. We are here concerned only with steady-state operation (i.e., infinite pulse trains or cw).

2.1. The moving-comb model of FSF output

One viewpoint of the FSF laser output, used extensively by Nakamura et al. [15,16], is that in

stationary operation the output electric field $E_{MC}(t)$ consists of a moving comb of chirped frequencies. There are an infinite number of frequency "teeth" in this comb, each with a time varying amplitude $B_n(t)$:

$$E_{MC}(t) = \mathscr{E}_0 \sum_{n=-\infty}^{+\infty} B_n(t) \exp[-ip_n(t)]. \tag{8}$$

Associated with the real-valued amplitude $B_n(t)$ of tooth n is a phase $p_n(t)$ whose time derivative, the instantaneous frequency $\omega_{n(t)}$, varies linearly with time (a frequency chirp)

$$\omega_n(t) \equiv \frac{d}{dt} p_n(t) = \omega_{max} + \frac{\Delta}{\tau_r}(t - n\tau_s). \tag{9}$$

Typically the amplitude $B_n(t)$ is taken to be of Gaussian form,

$$B_n(t) = \exp\left[-\frac{(t - n\tau_s)^2}{(n_w\tau_r)^2}\right], \tag{10}$$

peaking at $t = n\tau_s$ and with a Gaussian width parameter $n_w\tau_r$.

Because the output of the FSF laser can be viewed as a comb of chirped frequencies, it is natural to consider using it as a source of radiation for chirped-pulse interferometry. However, this use is not as direct as one might think. In reference [26] we showed that this output of the FSF laser can also be written in the form of a Floquet series

$$E_{MC}(t) = \mathscr{E}_0 \sum_m C_m \exp[-im\Delta(t - t_{MC})], \tag{11}$$

where t_{MC} is a reference time. We take $t_{MC} = \omega_{max}\tau_r/\Delta$ and $n_w \gg 1$ and thereby write the Fourier coefficients as

$$C_m = C_0 \exp\left[-\frac{(m - (\omega_{max}/\Delta))^2}{(n_w)^2}\right] \exp\left[+im^2\frac{\Delta\tau_r}{2}\right]. \tag{12}$$

Here the factor C_0 incorporates the common phase, the first exponential describes a Gaussian distribution of amplitudes with width n_w, and the final exponential describes the (quadratic) dependence of phase upon m. This decomposition shows that the field comprises a discrete set of time-independent frequencies, separated by the frequency shift Δ. By contrast, the field needed for interferometry should comprise a continuum of frequencies if it is to include the beat frequency $2\gamma_c T$ for arbitrary delay time T.

In [26] we have shown that, because of the discreteness of the frequencies actually present in the moving comb model, it can be viewed as a discrete-frequency model (our term) seeded by a cw laser whose frequency is some integer multiple of the frequency shift Δ.

2.2. FSF cavity seeded with variable phase

The frequencies required for frequency-domain interferometry can be supplied in several ways. To observe a beat signal at some frequency it is essential that the seed laser spectrum contain this frequency. Noise fluctuations provide one potential source of the desired bandwidth. Previous authors [15,16], have relied on random amplitude fluctuations to provide seed bandwidth. Here we discuss the use of a modulated seed pulse, of carrier frequency ω_s. When we allow a variable phase $\varphi_s(t)$ on this input to the FSF cavity, the output field has the form

$$E(t) = \sum_{n=0}^{\infty} E_n(t) \exp[-i(\omega_s + n\Delta)t], \tag{13}$$

where the complex-valued time-dependent amplitude is

$$E_n(t) = \varepsilon_c a_n \exp[-i\Phi_n - i\varphi_s(t - n\tau_r)]. \tag{14}$$

The factor ε_c provides a normalization: it is related to the seeding-laser intensity inside the cavity I_c through the formula

$$I_c = \frac{c}{8\pi}|\varepsilon_c|^2. \tag{15}$$

The dimensionless amplitude a_n is, in the limit of interest here (large n_w, see [26]),

$$a_n \simeq \mathscr{A} \exp\left[-\left(\frac{n - n_m}{n_w}\right)^2\right] \tag{16}$$

where amplitude $\mathscr{A}$, width n_w and central position n_m are determined by laser parameters (see [26]). Here we assume that $n_w \gg 1$. The phase has a time-independent contribution that is quadratic in n,

$$\Phi_n = -\tau_r n[\omega_s + (n+1)\Delta/2]. \quad (17)$$

The field of Eq. (13) also receives a contribution from time varying phases $\varphi_s(t)$, either random or deterministic.

3. Interferometry with a FSF laser

We are interested in the homodyne beat signal created by the interference between two electric field amplitudes with relative time delay $T = 2h/c$ and with a phase difference $\Delta\phi$ originating in the difference between the material dependent phase shifts of reflected light in the two arms. This signal is proportional to the real part of the complex-valued product $\exp(i\Delta\phi)E(t)E^*(t+T)$:

$$\begin{aligned} S(t) &= \exp(i\Delta\phi)E(t)E^*(t+T) + \text{c.c.} \\ &= \sum_{n,l=0}^{\infty} E_n(t)E_l^*(t+T)\exp[i\Delta\phi - i(\omega_s + n\Delta)t \\ &\quad + i(\omega_s + l\Delta)(t+T)] + \text{c.c.} \\ &= \exp[i\Delta\phi + i\omega_s T]\sum_{n=0}^{\infty}\sum_{m=-\infty}^{\infty} E_n(t)E_{n-m}^*(t+T) \\ &\quad \times \exp[i(n-m)\Delta T - im\Delta t] + \text{c.c.} \end{aligned} \quad (18)$$

(Note that we need not consider the spectrum of $E(t)E^*(t)$ or $E(t+T)E^*(t+T)$ because these contain no information about the distance.) This signal contains many harmonics m, originating with combinations of the various frequencies in the sum. We will assume that the frequency $T\gamma_c = T\Delta/\tau_r$ produced during the time T is much less than the frequency shift Δ. This implies that $T \ll \tau_r$ and, in turn, that the possible beating frequency is small. For application to surface profilometry, where one is interested in measuring small variations in height, it is always possible, in principle, to adjust the reference arm relative to the sample so that $T \ll \tau_r$. For use with large distances, in optical ranging, this is not always possible and it is necessary to resolve the phase ambiguity of successive chirped pulses. That is, the time T is determined by interferometry only within some multiple of the repetition time τ_s. To resolve this ambiguity one can use a second AOM frequency to determine the order m to be used with Eq. (18), as was done by Nakamura et al. [8].

Without loss of generality we will here consider only the terms in (18) for which $l = n$ or $m = 0$. The signal is therefore

$$\begin{aligned} S(t) &= \sum_{n=0}^{\infty} E_n(t)E_n^*(t+T) \\ &\quad \times \exp[i\Delta\phi + i(\omega_s + n\Delta)T] + \text{c.c.} \end{aligned} \quad (19)$$

The only time dependence of this signal originates in phase variation of the seeding laser, as described by $\varphi_s(t)$ in $E_n(t)$.

Note that in the absence of phase variation, $\varphi_s(t) = 0$, *only discrete frequencies contribute to the electric field*: these differ from the seed frequency by n increments of the AOM frequency shift Δ. In particular, the interferometer generates no new frequencies. The time shift T leads only to a phase shift of beating at the frequency Δ and at the higher harmonics.

We emphasize that when there is no variation of the laser phase (e.g., no noise and no deliberate modulation), then there is no beat signal. Experimental observations [14] have confirmed that, when feedback in the FSF laser causes mode locking (and a consequent removal of noisy phase fluctuations), then any interferometric beat signal disappears. Thus to understand the characteristics of the beat signal, and the accuracy attainable in interferometry, we must consider the effect of noise of the seed laser. As we will show, it is possible to produce a beat signal whose power spectrum has a very sharply defined maximum at the frequency $\omega_B = T\gamma_c$. We also consider the possibility of introducing frequency modulation of the seeding laser, rather than relying on noise. We will show that this technique offers promise of high accuracy.

Our task now is to compute the power spectrum $J_S(\omega)$ of the beat signal $S(t)$. This is determined as the Fourier transform

$$\begin{aligned} J_S(\omega) &= 2\int_0^{\infty} d\tau\, G(\tau)\cos\omega\tau \\ &= \int_{-\infty}^{\infty} d\tau\, G(\tau)\exp(i\omega\tau) \end{aligned} \quad (20)$$

of the autocorrelation function $G(\tau)$,

$$G(\tau) \equiv \langle S(t)S(t+\tau)\rangle. \tag{21}$$

Here and elsewhere $\langle\cdots\rangle$ denotes a stochastic average. Because we deal with steady state, the autocorrelation function is independent of time t.

4. FSF interferometry with a noisy seed

In the presence of phase variation of the seed laser the autocorrelation function $G(\tau)$ can be written as

$$\begin{aligned} G(\tau) = &\sum_{n=0}^{\infty}\sum_{l=0}^{\infty} |\varepsilon_c|^4 |a_n|^2 |a_l|^2 F_+(\tau - l\tau_r + n\tau_r, T) \\ &\times \exp[i2\Delta\phi + i(2\omega_s + n\Delta + l\Delta)T] \\ &+ \sum_{n=0}^{\infty}\sum_{l=0}^{\infty} |\varepsilon_c|^4 |a_n|^2 |a_l|^2 F_-(\tau - l\tau_r + n\tau_r, T) \\ &\times \exp[+i(n-l)\Delta T] + \text{c.c.} \end{aligned} \tag{22}$$

where we define

$$\begin{aligned} F_\pm(t_1, t_2) \equiv \langle \exp[&-i\varphi_s(t) + i\varphi_s(t+t_1) \\ &\mp i\varphi_s(t+t_2) \pm i\varphi_s(t+t_2+t_1)]\rangle. \end{aligned} \tag{23}$$

Note that the only dependence upon the material phase shift $\Delta\phi$ occurs with the first summation, in the exponential associated with F_+.

We now consider the Fourier transform of this correlation function. From the above expressions we obtain the formula

$$\begin{aligned} J_S(\omega) = &F_+(\omega, T)\mathscr{L}(\omega + \gamma_c T)\mathscr{L}(-\omega + \gamma_c T) \\ &\times \exp[+i\Delta\phi + i2\omega_s T] + F_+(\omega, T) \\ &\times \mathscr{L}(\omega - \gamma_c T)\mathscr{L}(-\omega - \gamma_c T) \\ &\times \exp[-i\Delta\phi - i2\omega_s T] + 2F_-(\omega, T) \\ &\times \mathscr{L}(\omega - \gamma_c T)\mathscr{L}(-\omega + \gamma_c T) \end{aligned} \tag{24}$$

where all of the dependence upon phase fluctuation occurs in the factors

$$F_\pm(\omega, T) = \int_{-\infty}^{\infty} d\tau\, F_\pm(\tau, T)\exp[i\omega\tau], \tag{25}$$

while the remaining factors

$$\mathscr{L}(\omega) \equiv \sum_{n=0}^{\infty} |a_n|^2 \exp[+i\omega\tau_r n] \tag{26}$$

serve as profile functions independent of any phase fluctuation.

4.1. The profile function

Using formula (16) we write the profile function $\mathscr{L}(\omega)$ as

$$\mathscr{L}(\omega) \simeq A^2 \sum_{n=0}^{\infty} \exp[+i\omega\tau_r n] \exp\left[-2\left(\frac{n-n_m}{n_w}\right)^2\right]. \tag{27}$$

When the number of frequency components becomes large this is a very narrow function of ω. In this situation, with $n_w \gg 1$ and $n_m \gg 1$ the summation in this expression can be replaced by integration from $-\infty$ to $+\infty$, with the result

$$\mathscr{L}(\omega) \simeq n_w A^2 \sqrt{\frac{\pi}{2}} \exp[+i\omega\tau_r n_m] \exp\left[-\frac{(\omega\tau_r n_w)^2}{8}\right]. \tag{28}$$

In this case, we can extract a phase and an amplitude from the profile function $\mathscr{L}(\omega)$ and introduce a normalized Gaussian profile function

$$\mathscr{L}_g(\omega) \equiv \exp\left[-\frac{(\omega\tau_r n_w)^2}{8}\right]. \tag{29}$$

Then the spectrum takes the form

$$\begin{aligned} J_S(\omega) = \pi(n_w A^2)^2 |\varepsilon_c|^4 \Big[&F_+(\omega, T)\cos[2\Delta_0 T + 2\Delta\phi]. \\ &\times \mathscr{L}_g(\omega + \gamma_c T)\mathscr{L}_g(\omega - \gamma_c T) + F_-(\omega, T) \\ &\times [\mathscr{L}_g(\omega - \gamma_c T)]^2\Big]. \end{aligned} \tag{30}$$

In this formula, like the general expression of Eq. (24), the contributions from F_+ involve the product of profile functions $\mathscr{L}_g(\omega)$ centered about the values $+\gamma_c T$ and $-\gamma_c T$. The width of $\mathscr{L}_g(\omega)$ is $\sqrt{8}/(n_w\tau_r)$. When this width is much less than $\gamma_c T$, as it is for large n_w, then the overlap of these functions will be negligible, and the only contribution to the spectrum $J_S(\omega)$ will come from the last term. Under these conditions, we obtain the formula

$$J_S(\omega) = \pi(n_w A^2)^2 |\varepsilon_c|^4 F_-(\omega, T)[\mathscr{L}_g(\omega - \gamma_c T)]^2. \tag{31}$$

Because the spectral width of $F_-(\omega,T)$ is usually quite large compared with the width of $\mathscr{L}_g(\omega)$, Eq. (31) expresses a very narrow resonance, in

which position and width depend on laser parameters (through $\mathscr{L}$) and the magnitude is determined (through F_-) by the noise characteristics.

4.2. Modeling seed-laser noise

The function $F_-(\omega,T)$ depends on the fluctuation spectrum. To evaluate this dependence we assume that the time derivative of the seed-laser phase $\varphi_s(t)$ is a zero-mean stochastic process $\xi(t)$ [see Appendix, Eq. (A.4)],

$$\dot{\varphi}(t) = \xi(t). \tag{32}$$

In Appendix A, we discuss using an exponentially correlated (Ornstein–Uhlenbeck) process, with zero mean and exponential correlation

$$\langle \xi \rangle = 0, \qquad \langle \xi(t)\xi(t') \rangle = GD\exp(-G|t-t'|) \tag{33}$$

to carry out the stochastic averaging in expression (23). We use here the results for a limiting case, a delta-correlated process $G \to \infty$, for which simple analytic expressions can be obtained.

As shown in Appendix A, the width of the function $F_-(\omega,T)$ is larger than $1/T$. The spectrum given by Eq. (31) is appreciable only within a narrow interval, of width $\delta\omega \approx \sqrt{8}/(n_w\tau_r)$ near the resonance value $\omega_B = \gamma_c T$. Because the delay is small, $T \ll \tau_r$, the width obeys (for any n_w) the inequality $\delta\omega \ll 1/T$, and we can take $F_-(\omega,T)$ to be $F_-(\gamma_c T,T)$. Moreover, from the conditions $\Delta\tau_r \approx 1$ and $T \ll \tau_r$ we have $\gamma_c T \ll 1/T$, and so we can take $F_-(\omega,T) \simeq F_-(\gamma_c,T) \simeq F_-(0,T)$. Using expression (A.13) we obtain the result

$$F_-(0,T) = (1/D)[1-(1+2DT)\exp(-2DT)]. \tag{34}$$

Thus the expression (31) can be written as

$$J_S(\omega) = J_{res}\exp\left[-(\omega-\gamma_c T)^2(\tau_r n_w/2)^2\right], \tag{35}$$

where

$$J_{res} = \pi(n_w A^2)^2|\varepsilon_c|^4(1/D)[1-(1+2DT)\exp(-2DT)]. \tag{36}$$

These expressions describe a narrow resonance in the spectrum of the beat signal. The maximum of this resonance coincides with the frequency $\omega_B = \gamma_c T$ and the width of this resonance is equal to

$$\Gamma_{res} = 2/(\tau_r n_w). \tag{37}$$

Neither of these parameters depends on the fluctuation properties. The only dependence on the fluctuations appears in the amplitude of the signal, which depends on the intensity of the noise as parameterized by D. For small $DT \ll 1$ the magnitude J_{res} is proportional to DT^2. There is an optimal value of $DT = 0.89664$ for which the amplitude is maximum, with value $J_{res} = 0.5969T\pi[n_w A^2]^2$.

5. Fluctuations of the optical length

Whereas uncontrolled fluctuations of the seed-laser frequency can be useful, any fluctuations of the optical path will degrade the accuracy. In this section we estimate the effect of such fluctuations.

Consider the influence on the resonance profile (31) caused by fluctuations in the optical length of the cavity. We write the optical length as $L(t) = L_0 + \delta L(t)$, where $\delta L(t)$ is a zero-mean fluctuation of the optical length. Taking into account these fluctuations it is easy to show that Eqs. (13), (14) for the field can be rewritten as

$$E(t) = \mathscr{E}_c \sum_{n=0}^{\infty} a_n \exp[-i\Phi_n - i\varphi_s(t-n\tau_r) - i(\omega_s + n\Delta)t]\exp[i\delta\Phi_n(t)], \tag{38}$$

where

$$\delta\Phi_n(t) = -\sum_{l=0}^{n-1}\left[\frac{\omega_s + l\Delta}{c}\right]\delta L(t-l\tau_r) \simeq -\frac{\omega_0}{c}\sum_{l=0}^{n-1}\delta L(t-l\tau_r). \tag{39}$$

For the conditions of the observations of the narrow resonance (31) the correlation function (21) can be written as

$$G(\tau) = |\varepsilon_c|^4 \sum_{n=0}^{\infty}\sum_{l=0}^{\infty}|a_n|^2|a_l|^2\exp[+i(n-l)\Delta T] \times F_-(\tau - l\tau_r + n\tau_r, T)F_3(T,\tau,l,n), \tag{40}$$

where

$$F_3(T,\tau,l,n) \equiv \langle \exp[-i\delta\Phi_n(t) + i\delta\Phi_n(t+T) - i\delta\Phi_l(t+\tau+T) + i\delta\Phi_l(t+\tau)]\rangle. \quad (41)$$

To evaluate the functions $F_3(T,\tau,l,n)$ we assume that the fluctuation $\delta L(t)$ of the optical length is an Ornstein–Uhlenbeck process [39,40] whose parameters we denote by G_L and D_L,

$$\langle \delta L\rangle = 0,$$
$$\left(\frac{\omega_0}{L_0}\right)^2 \langle \delta L(t)\delta L(t')\rangle = G_L D_L \exp(-G_L|t-t'|). \quad (42)$$

We use formula (A.5) to evaluate stochastic averages of exponentiated noise and obtain for $F_3(T,\tau,l,n)$ the result

$$F_3(T,\tau,l,n) = \exp\{-[g_{nn}(0) + g_{ll}(0) - g_{nn}(T) - g_{ll}(T) + g_{nl}(\tau+T) + g_{nl}(\tau-T) - 2g_{nl}(\tau)]\}, \quad (43)$$

where

$$g_{nl}(t) = \sum_{m=1}^{n}\sum_{k=1}^{l} \tau_r^2 G_L D_L \exp[-G_L|t + (m-k)\tau_r|]. \quad (44)$$

We assume that fluctuations of the optical length are relatively slow, $G_L\tau_r \ll 1$. This is always true for fluctuations caused by variation of pump intensity or vibrations. Then we replace the summation over m and k in Eq. (44) by an integration, and for the most interesting case $nG_L\tau_r$, $lG_L\tau_r \gg 1$ write

$$g_{nl}(t) \simeq G_L D_L \int_0^{n\tau_r} dt_1 \int_0^{l\tau_r} dt_2 \exp(-G_L|t+t_1-t_2|) \simeq 2D_L t_< - \frac{D_L}{G_L}[\exp(-G_L|t|) + \exp(-G_L|t+n\tau_r - l\tau_r|)], \quad (45)$$

where $t_<$ is the lesser of $t_1 = n\tau_r$ and $t_2 = l\tau_r - t$. Using Eq. (45) for small $T \ll 1/G_L$ one can obtain the expression

$$F_3(T,\tau,l,n) = \exp\{-\nu[2 - \exp(-G_L|\tau|) - \exp(-G_L|\tau + n\tau_r - l\tau_r|)]\}, \quad (46)$$

where

$$\nu \equiv T^2 D_L G_L. \quad (47)$$

Note that we made no assumptions about the intensity D_L of the fluctuations. Thus the quantity ν can be large, and we cannot generally expand the exponential. For the spectrum $J_S(\omega)$ we obtain the formula

$$J_S(\omega) = \sum_{n,l=0}^{\infty} |a_n|^2|a_l|^2 \int_{-\infty}^{\infty} d\tau\, F_-(\tau,T) \times \exp(-\nu[2 - \exp(-G_L|\tau + (l-n)\tau_r|) - \exp(-G_L|\tau|)]) \times \exp[i\omega\tau + i\omega(l\tau_r - n\tau_r) + i(n-l)\Delta T]. \quad (48)$$

As follows from the above consideration of the delta-correlated fluctuations of the seeding laser the function $F_-(\tau,T)$ can be considered as a very narrow function of τ. Therefore we use the approximation (16) for the amplitudes a_n and write the spectrum $J_S(\omega)$ as

$$J_S(\omega) = J_{res}\frac{1}{\sqrt{\pi}} \int_{-\infty}^{\infty} dx \exp(-x^2) \times \exp\{-\nu[1\exp(-G_L\tau_r n_w|x|)]\} \times \exp[-ixn_w(\omega - \gamma_c T)\tau_r] \quad (49)$$

with J_{res} given by (36).

This is a general result valid for any choice of the noise parameters. For fluctuations originating in various mechanical or technical variations, G_L is about 10^4 to 10^5 s^{-1}. Then for $\tau_r = 1$ ns we have $n_w G_L\tau_r = n_w(10^{-4}-10^{-5})$. Thus there are two different possibilities. The first one is a laser with moderate numbers of the frequency components, $n_w \ll 10^4$, and the second one is a laser with broadband gain (Ti-Sapphire laser) with $n_w \geqslant 10^4$ to 10^5. For given laser properties the two possibilities correspond to correlation times $1/G_L$ much longer than or much shorter than $n_w\tau_r$. We consider these two cases separately below.

5.1. Long correlation time

For the first case, when $G_{L\ nw}\tau_r \ll 1$, one can expand $\exp(-G_L\tau_{r\ nw}|x|)$ as

$$\exp(-G_L\tau_r n_w|x|) = 1 - G_L\tau_r n_w|x| \quad (50)$$

and obtain the resonance shape as a *Voigt profile:*

$$J_S(\omega) = J_{res}\frac{1}{\sqrt{\pi}}\int_{-\infty}^{\infty} dx\left(-x^2 - vG_L\tau_r n_w|x|\right) \times \exp\left[-ixn_w(\omega-\gamma T)\tau_r\right] = J_{res}\frac{2}{\sqrt{\pi}n_w\tau_r}\mathrm{Re}\int_{-\infty}^{\infty} dx\frac{\exp\left(-\left[x\frac{n_w\tau_r}{2}\right]^2\right)}{vG_L + i(\omega-\gamma T - x)}. \quad (51)$$

We now consider two limiting cases of the exponential argument $vG_L\tau_r n_w$.

- For $vG_L\tau_r n_w \ll 1$ the fluctuations of the optical length do not influence the resonance shape. As noted earlier, in this case a narrow resonance exists in the spectrum of the beating signal. The maximum of this resonance coincides with the frequency $\omega_B = \gamma_c T$, and the width is $\Gamma_{res} = 2/(\tau_r n_w)$.
- For $vG_L\tau_r n_w \gg 1$ the spectrum $J_S(\omega)$ is Lorentzian,

$$J_S(\omega) = \tilde{J}_{res}\frac{1}{1+(\omega-\gamma_c T)^2/(vG_L)^2}. \quad (52)$$

The maximum of this resonance again coincides with the frequency $\omega_B = \gamma_c T$ but the width Γ_{res} of this resonances is larger than $2/(\tau_r n_w)$, and is equal to $\Gamma_{res} = vG_L = T^2 D_L G_L^2$. The amplitude $\tilde{J}_{res}$ of the resonance is equal to $\tilde{J}_{res} = J_{res}2/(\sqrt{\pi}vG_L\tau_r n_w)$ and is much smaller than J_{res}.

These formulas show that even with slow fluctuations there will be a limit to the accuracy, i.e., a finite bandwidth of the beat spectrum.

5.2. Short correlation time

Consider now the second case, when $G_L n_w\tau_r \gg 1$. For large detunings $|\omega-\gamma T| \geqslant 1/(n_w\tau_r)$ the main contribution in the integral over x in Eq. (49) and so this integral can be written as

$$J_S(\omega) = J_{res}\frac{\exp(-v)}{\sqrt{\pi}G_L\tau_r n_w}2\mathrm{Re} \times \int_0^{\infty} dy\{\exp[+v\exp(-y)] - 1\} \times \exp\left[-iy\frac{(\omega-\gamma_c T)}{G_L}\right]. \quad (53)$$

This integral describes a resonance which is close to Lorentzian with width $\Gamma_{res} \simeq G_L$. The amplitude of this resonance is equal to

$$J_S(0) = J_{res}\frac{2\exp(-v)}{\sqrt{\pi}G_L\tau_r n_w} \times \int_0^{\infty} dy\{\exp[+v\exp(-y)] - 1\}. \quad (54)$$

This expression has the limiting values

$$J_S(0) = J_{res}\frac{2}{\sqrt{\pi}G_L\tau_r n_w}\begin{cases} v & \text{for } v \ll 1, \\ 1/v & \text{for } v \ll 1. \end{cases} \quad (55)$$

The maximum value of this function of v is $1.312J_{res}/(G_L\tau_r n_w)$, occurring for $v = 1.503$.

For small detunings $|\omega - \gamma T| \leqslant 1/n_w\tau_r$ the main contribution to the integral over x in Eq. (49) comes from large $|x| \geqslant 1$. The result can be written as

$$J_S(\omega) \simeq \exp(-v)J_{res} \times \exp\left[-(\omega-\gamma_c T)^2(\tau_r n_w/2)^2\right] + J_S(0). \quad (56)$$

Thus for relatively fast fluctuations, meaning $n_w G_L\tau_r \gg 1$, and when there is only partial correlation between changes of the phases of the frequency components of the laser spectrum, the beat-frequency spectrum $J_S(\omega)$ is the superposition of a narrow resonance (56) and a wide resonance (53). The ratio of the amplitudes of the narrow and wide resonances is $\sqrt{\pi}\tau_r n_w/(2T_2 D_L) \gg 1$ for small $v = T^2 D_L G_L \ll 1$ and is exponentially small, $\exp(-v)\sqrt{\pi}G_L\tau_r n_w v/2$ for large $v \gg 1$. (Fig. 4) shows the beat signal for various v and G_L.

6. FSF interferometry with an FM seed

Earlier discussion emphasized that some modulation of the seed laser is essential if an interferometer beat signal is to be observed. The needed modulation will automatically occur if the seed laser is noisy. But one may also consider introducing structured modulation, i.e., a frequency-modulated seed laser. Here we analyze this possibility.

Let us consider the case when the seeding laser is frequency modulated. We take the phase of $\varphi_s(t)$ to be, instead of a stochastic quantity, a sinusoid

$$\varphi_s(t) = \varphi_0 + \beta \sin(\Omega_m t), \tag{57}$$

where Ω_m is the modulation frequency, β is the modulation index and φ_0 is the initial phase. Then the FSF laser field (13), (14) reads

$$E(t) = \sum_{n=0}^{\infty} E_n(t) \exp[-\mathrm{i}(\omega_s + n\Delta)t], \tag{58}$$

where the amplitude is now

$$E_n(t) = \varepsilon_c \sum_n a_n \exp[-\mathrm{i}\Phi_n - \mathrm{i}\varphi_0 - \mathrm{i}\beta \sin[\Omega_m(t - n\tau_r)]]. \tag{59}$$

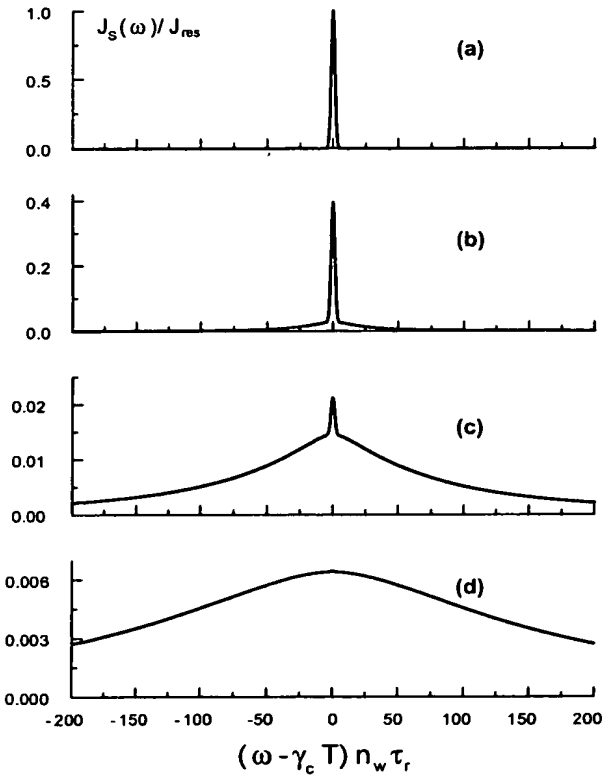

Fig. 4. The evolution of the beat-frequency spectrum $J_S(\omega)$ in the case of short correlation time ($G_L\tau, n_w = 20$) with increasing of the optical length fluctuations intensity: (a) no fluctuations $v = 0$; (b) $v = 1$; (c) $v = 5$ and (d) $v = 10$.

The homodyne beat signal $S(t)$ given by Eq. (18) can be rewritten as

$$S(t) = \exp(\mathrm{i}\Delta\phi)|\varepsilon_c|^2 \sum_{n,l=0}^{\infty} a_n a_l^* \times \exp\{-\mathrm{i}(\Phi_n - \Phi_l) - \mathrm{i}\beta \sin[\Omega_m(t - n\tau_r)] + \mathrm{i}\beta \sin[\Omega_m(t + T - l\tau_r)]\} \exp[-\mathrm{i}(\omega_s + n\Delta)t + \mathrm{i}(\omega_s + l\Delta)(t + T)] + \text{c.c.} \tag{60}$$

We are interested in the part of the signal $S(t)$ that oscillates with the seed modulation frequency Ω_m. More particularly, we consider slow frequency modulation $\Omega_m \simeq \gamma_c T \ll \Delta$. To evaluate such modulation we need only the terms in Eq. (60) for which $l = n$. Then we have the expression

$$S(t) = \exp(\mathrm{i}\Delta\phi)|\varepsilon_c|^2 \sum_{n=0}^{\infty} |a_n|^2 \exp[+\mathrm{i}(\omega_s + n\Delta)T] \times \exp\{+2\mathrm{i}\beta \sin[\Omega_m T/2] \times \cos[\Omega_m(t - n\tau_r + T/2)]\} + \text{c.c.}$$

Using the formula

$$\exp(\mathrm{i}M\cos\Phi) = \sum_{n=-\infty}^{\infty} \mathrm{i}^n J_n(M) \exp(\mathrm{i}n\Phi), \tag{61}$$

where $J_n(x)$ is the nth-order Bessel function, we obtain the result

$$S(t) = \exp(\mathrm{i}\Delta\phi)|\varepsilon_c|^2 \sum_{n=0}^{\infty} |a_n|^2 \times \exp[\mathrm{i}l\Omega_m(t - n\tau_r + T/2)] \times \exp[+\mathrm{i}(\omega_s + n\Delta)T] \times \sum_{l=-\infty}^{\infty} \mathrm{i}^l J_l(2\beta \sin[\Omega_m T/2]) + \text{c.c.} \tag{62}$$

The processing of this signal can proceed in two ways: either by means of a phase sensitive detector, or else with a detector that is insensitive to phase. As we will show next, there are notable advantages for the latter.

6.1. Phase sensitive detectors

Consider phase-sensitive detection of the modulation signal. Typically this produces, as a function of modulation frequency Ω_m and synchronous detector phase Φ_d, a signal

$$S_{\text{phase}}(\Omega_m, \Phi_d) = \frac{\Omega_m}{2\pi} \int_0^{2\pi/\Omega_m} dt\, S(t) \sin(\Omega_m t + \Phi_d). \tag{63}$$

With the same assumption which were made to obtain Eq. (35) the signal of Eq. (62) can be written as

$$\begin{aligned} S_{\text{phase}}(\Omega_m, \Phi_d) = & -n_w A^2 |\varepsilon_c|^2 \sqrt{\frac{\pi}{2}} J_1(2\beta \sin[\Omega_m T/2]) \\ & \times \cos[(-\Omega_m + \gamma_c T)\tau_r n_m + \Omega_m T/2 \\ & - \Phi_d + \omega_s T + \Delta\phi] \\ & \times \exp\left[-\frac{(\Omega_m - \gamma_c T)^2 \tau_r^2 n_w}{8}\right]. \end{aligned} \tag{64}$$

An examination of the argument of the exponential reveals that the signal S_{phase} is a narrow resonance function of the detuning of the modulation frequency Ω_m from the frequency $\gamma_c T$. This signal depends, through the argument of the cosine, on the phase

$$(-\Omega_m + \gamma_c T)\tau_r n_m + \Omega_m T/2 - \Phi_d + \omega_s T + \Delta\phi. \tag{65}$$

This dependence can lead to a resonance shape that differs significantly from a Gaussian form.

6.2. Phase insensitive detection

Phase sensitive detection of the interference beat signal introduces a dependence upon the material phase shift $\Delta\phi$. Thus it will be much more convenient to use amplitude detection. Then the signal is proportional to the square of the amplitude of the variable components,

$$\begin{aligned} S_{\text{ampl}} &= \sqrt{(S_{\Phi_d=0})^2 + (S_{\Phi_d=\pi/2})^2} \\ &= J_1(2\beta \sin[\Omega_m T/2])|\varepsilon_c|^2 n_w A^2 \sqrt{\frac{\pi}{2}} \\ &\quad \times \exp\left[-\frac{(\Omega_m - \gamma T)^2 \tau_r^2 n_w}{8}\right]. \end{aligned} \tag{66}$$

Here there is no dependence upon the material phase shift $\Delta\phi$. Note that this signal can easily be obtained using a standard RF-spectrum analyzer. Regarded as a function of modulation frequency the signal appears as a Gaussian profile. The width of this intensity profile is the same as that of the amplitude profile shown in the beat-frequency spectrum without cavity fluctuations of Fig. 4(a).

To make use of the formula given in Eq. (66) for a determination of h, one would vary the FM frequency Ω_m to find the value $\Omega_{\max}$ for which S_{ampl} is a maximum. The delay time is then

$$T = \Omega_m/\gamma_c. \tag{67}$$

Once an approximate delay time is established, the strength of the peak value can be optimized by adjusting the modulation index . For application to surface profilometry, the reference arm of the interferometer would be adjusted so that the beat frequencies have values within a convenient range, much larger than the width Γ_{res}, and the modulation index β would be adjusted to optimize heights within a range of values.

7. Achievable accuracy

We will show here that the accuracy of interferometry based on the FSF laser can be comparable to the accuracy of conventional interferometry, i.e., a fraction of a wavelength. The analysis starts by expressing the error in step-height measurement δh in terms of beat frequency error $\delta\omega$ as

$$\delta h = \frac{c}{2\gamma_c}\delta\omega = \frac{L}{2\Delta}\delta\omega. \tag{68}$$

We can make this distance error small, for fixed error in beat frequency, by increasing the chirp rate γ_c, by making the cavity circumference L smaller, or by increasing the frequency shift per round trip Δ. Ultimately, however, the achievable error is set by the accuracy with which one can measure the beat frequency. The accuracy of this measurement is determined primarily by the width of the beat-frequency spectrum Γ_{res}. We take the error to be some fraction ϵ of this width:

$$\delta\omega = \epsilon\Gamma_{\text{res}} \tag{69}$$

and write the height error as proportional to a coherence length h_c,

$$\delta h = \epsilon h_c. \tag{70}$$

We can then use the result $\Gamma_{res} = 2/n_w\tau_r$ and $\gamma_c = \Delta/\tau_r$ to write this parameter variously as

$$h_c = \frac{c\Gamma_{res}}{2\gamma_c} = \frac{c}{n_w\Delta} = \frac{c}{\delta\omega_L}, \tag{71}$$

where $\delta\omega_L = n_w\Delta$ is the width of the FSF spectrum. In reference [26] we give several estimates of this width. We show, for example, that $\delta\omega_L$ and n_w are related to Γ_f, the bandwidth of the filtering mechanisms within the FSF cavity, through the approximation

$$\delta\omega_L = n_w\Delta \approx (\Delta\Gamma_f^2)^{1/3}. \tag{72}$$

Thus we can write

$$h_c = \frac{c}{(\Delta\Gamma_f^2)^{1/3}}. \tag{73}$$

For example, with filter bandwidth of 100 nm for light with central wavelength 800 nm (a bandwidth of 47 THz), and a frequency shift per round trip of 200 MHz, this length is 63 μm.

To estimate ϵ we here consider the error present in various realizations of FSF interferometry.

7.1. Phase noisy seed

First we consider the FSF laser to be seeded by a cw laser subject to phase noise. When the resonance width Γ_{res} is sufficiently small, one can consider a direct measurement of the beat frequency using a frequency meter to count cycles within some observation time interval T_0. This time should be significantly longer than the resolving time for the resonance width, $T_0 \gg 1/\Gamma_{res}$. If we consider a measurement time of $T_0 = 10^{-4}$ s, then it is necessary that the resonance width be larger than 10 kHz, meaning a width of a few tens of kHz, in order that $T_0 \gg 1/\Gamma_{res}$. In this case ϵ is roughly

$$\epsilon \approx \frac{1}{\sqrt{\Gamma_{res}T_0}}. \tag{74}$$

This same accuracy is obtainable with other methods. For example in the frequency domain, using a spectrum analyzer that scans the frequency, one can measure the frequency of the peak in the spectral distribution. The result is again Eq. (74).

7.2. Frequency modulated seed

Next we consider using a frequency modulated seed and measuring the modulation frequency Ω_m for which the output signal of Eq. (66) maximizes. There are several possible contributions to the error in measuring the frequency of this peak value.

To use the resonance (66) for the measurement of the delay time T one can additionally slowly modulate the frequency Ω_m. We assume that $\Omega_m(t) = \Omega_m^{(0)} + \delta\Omega_m\cos(2\pi ft)$ where f is a slow modulation frequency and neglect optical length fluctuations. Then for small modulation amplitude $\delta\Omega_m$ and detunings $(\delta\Omega_m, |\Omega_m^{(0)} - \gamma_c T| \ll \Gamma_{res})$ the magnitude of the detected useful signal varies linearly with modulation detuning $\Omega_m^{(0)} - \gamma_c T$,

$$S_{useful} = J_1(2\beta\sin[\Omega_m T/2])|\varepsilon_c|^2 n_w A^2\sqrt{\frac{\pi}{2}} \times \frac{(\Omega_m - \gamma_c T)(\tau_r n_w)^2}{4}\delta\Omega_m. \tag{75}$$

The noise signal S_{noise} can be estimated using (34) for delta-correlated phase fluctuations and small $DT \ll 1$ as

$$S_{noise} = \sqrt{J_S(\omega)}\sqrt{\delta\omega_d} \simeq \sqrt{2\pi}|\varepsilon_c|^2 n_w A^2\sqrt{T^2 D}\sqrt{\delta\omega_d}, \tag{76}$$

where $\delta\omega_d = 1/T_0$ is the filter passband of the detection system. We take the frequency error $\delta\omega$ to be the value of the detuning $\Omega_m - \gamma_c T$ where signal and noise are equal, $S_{noise} = S_{useful}$. This leads to the estimate

$$\delta\omega \approx \frac{2(\Gamma_{res})^2\sqrt{T^2 D}\sqrt{\delta\omega_d}}{J_1(2\beta\sin[\Omega_m T/2])\delta\Omega_m}. \tag{77}$$

For rough estimation one can take $\delta\Omega_m \approx \Gamma_{res}$ and, with appropriate choice of the modulation index β, $J_1(2\beta\sin[\Omega_m T/2]) \simeq 0.5$. Then

$$\delta\omega \approx 4\Gamma_{res}\sqrt{T^2 D\delta\omega_d}, \tag{78}$$

which leads to the result

$$\epsilon \approx 4T\sqrt{D\delta\omega_d} = \frac{1}{\sqrt{T_0\Gamma_{res}}} \times 4T\sqrt{D\Gamma_{res}}, \tag{79}$$

Table 1
Estimates of height errors showing values for three methods of measurement: (1) Phase noisy seed , (2) FM seed, with spectral analysis, (3) quantum noise limit

measurement time [ms]	0.1	1	10	100
$\Gamma_f = 5$ GHz, $h_c = 3$ cm , $n_w = 7$				
h error [nm] noisy seed	5×10^6	1.6×10^6	5×10^5	1.6×10^5
h error [nm] FM seed	8×10^4	2×10^4	8×10^3	2×10^3
h error [nm] quant. lim.	80	25	8	2
$\Gamma_f = 47$ GHz, $h_c = 0.8$ cm, $n_w = 31$				
h error [nm] noisy seed	2.5×10^6	8×10^5	2.5×10^5	8×10^4
h error [nm] FM seed	1.6×10^4	5×10^3	1.6×10^3	5×10^3
h error [nm] quant. lim.	17	5	1.7	0.5
$\Gamma_f = 47$ THz, $h_c = 77$ μm, $n_w = 3 \times 10^3$				
h error [nm] noisy seed	2.5×10^5	8×10^4	2.5×10^4	8×10^3
h error [nm] FM seed	1.6×10^2	51	16	5
h error [nm] quant. lim.	0.2	0.05	0.02	0.005

where D is the bandwidth of the seed laser. For example, with $D = 2\pi \times 1$ MHz and $h = 1$ cm, the ϵ of Eq. (79) is 2×10^{-4} times smaller than Eq. (74).

7.3. Quantum noise

Spontaneous emission in the seed laser itself sets a lower bound on the achievable bandwidth D. As discussed in textbooks on laser theory, this Schawlow–Townes limit can be as small as a few Hz. This bandwidth imposes a fundamental limit on the accuracy of the FM method: when all "technical" noise has been eliminated, there remains an irreducible bandwidth attributable to white noise. As an example, for a linewidth of $D = 2\pi \times 1$ Hz, $T = 0.5$ ns and $\Gamma = 2\pi \times 10$ kHz the factor $4T\sqrt{D\Gamma_{\rm res}}$ is 10^{-6}.

Another ultimate limit on observation comes from shot noise in the detector. We estimate this to be

$$\epsilon \approx \sqrt{\frac{1}{T_0}\left(\frac{\hbar\omega}{\eta P}\right)} = \frac{1}{\sqrt{\Gamma_{\rm res} T_0}} \times \sqrt{\frac{\Gamma_{\rm res}}{R_{\rm phot}}}, \tag{80}$$

where P is the laser power and η is the detector efficiency. $R_{\rm phot}$ is the photon counting rate of the detector (laser power times efficiency divided by photon energy $\hbar\omega$). With reasonable estimates of these parameters (say $P = 1$ W, $\eta = 0.5$) this value of ϵ is 2×10^{-7} times smaller than Eq. (74), and an order of magnitude smaller than the Schawlow-Townes limit mentioned above.

7.4. Examples

Table 1 gives examples of the accuracy possible, using the preceding formulas and the following parameters

$\lambda = 800$ nm	$\Delta = 2\pi \times 200$ MHz
$h = 1$ m	$D = 2\pi \times 1$ MHz
$P = 1$ W	$\eta = 0.5$

The three sections of the table illustrate results for several choices of bandwidth Γ_f, height h and number of discrete components n_w. As can be seen, modulation of the seed offers here a hundredfold improvement in accuracy compared with the reliance on phase noise. The accuracy is still far from the quantum limit.

8. Summary and conclusions

The FSF laser offers useful application for high-accuracy interferometry. It allows determination of distance by measuring frequencies, and is insensitive to material phase shifts that occur upon reflection. As we have shown, it is essential that the laser output have available a range of frequencies that include the beat frequency $\gamma_c T$, for any T of interest. Although the reliance on noise can provide the needed frequencies, we suggest an alternative based on frequency modulation.

The basic principle is that of chirped radar, here implemented with a non-trivial modification in the form of a FSF laser. The greater chirp rate and extreme linearity of chirp make this far superior to conventional methods.

The position error δh can be made small, for fixed error in beat frequency, by increasing the chirp rate γ_c, by making the cavity circumference L smaller, or by making the frequency shift Δ larger.

Our theory provides analytic expressions for the intensity of the beat signal as a function of frequency. For any seed frequency, the beat signal has a spectral distribution sharply peaked about the value $\omega_B = (2\gamma_c/c)h$ and thus a measurement of the position of the spectral peak provides a measurement of h. The theory also provides a connection between the spectral width Γ_{res} and laser parameters, specifically the effective number of discrete frequency components n_w within the output spectrum of the FSF laser (i.e., the output bandwidth divided by the frequency shift Δ). It is this width that ultimately restricts the possible resolution by limiting the accuracy with which the beat frequency can be determined. Under appropriate conditions the error in beat frequency determination can provide subwavelength accuracy comparable to, or exceeding, what is obtained with conventional interferometry.

To achieve the accuracy $\delta h = 100$ nm with a frequency shift of $\Delta = 2\pi \times 100$ MHz one needs $n_w \approx 10^5$. This value is very large, but may be achievable with a Ti-Sapphire laser or fiber laser.

Acknowledgement

We acknowledge support from the Deutsche Forschungsgemeinschaft (436 UKR 113/46/9) and the Stiftung Rheinland-Pfalz für Innovation.

Appendix A. Stochastic averaging

A.1. The noise model

We consider in this appendix the evaluation and behavior of the functions $F_\pm(\omega,T)$, defined as Fourier transforms

$$F_\pm(\omega,T) = \int_{-\infty}^{\infty} d\tau F_\pm(\tau,T)\exp[i\omega\tau] \tag{A.1}$$

of the functions

$$F_\pm(t_1,t_2) = \langle \exp[-i\varphi_s(t) + i\varphi_s(t+t_1) \mp i\varphi_s(t+t_2) \pm i\varphi_s(t+t_2+t_1)]\rangle, \tag{A.2}$$

where $\langle\cdots\rangle$ denotes an averaging over realizations of the stochastic phase $\varphi_s(t)$. These functions incorporate all of the effects of noise upon the interferometer beat spectrum.

We assume that the time derivative of the phase $\varphi_s(t)$ is a stochastic process $\xi(t)$,

$$\dot{\varphi}(t) = \xi(t), \tag{A.3}$$

with zero mean and exponential correlation [$\xi(t)$ is an Ornstein–Uhlenbeck process]

$$\langle\xi\rangle = 0, \qquad \langle\xi(t)\xi(t')\rangle = GD\exp(-G|t-t'|). \tag{A.4}$$

We then evaluate stochastic averages of exponentiated noise, using the formula

$$\langle\exp(i\Phi)\rangle = \exp\left[-\frac{1}{2}\langle\Phi^2\rangle\right]. \tag{A.5}$$

For $F_-(T,\tau)$ one obtains the result

$$\begin{aligned} F_-(t_1,t_2) = \exp\Big(-\frac{1}{2}[&g(t,t) + g(t+t_1,t+t_1) \\ &+ g(t+t_1+t_2,t+t_1+t_2) \\ &+ g(t+t_2,t+t_2) - 2g(t,t+t_1) \\ &+ 2g(t,t+t_2+t_1) - 2g(t,t+t_2) \\ &- 2g(t+t_1,t+t_2+t_1) + 2g(t+t_1,t+t_2) \\ &- 2g(t+t_2+t_1,t+t_2)]\Big), \end{aligned} \tag{A.6}$$

where, with $t_<$ as the lesser of t_1 and t_2,

$$\begin{aligned} g(t_1,t_2) &\equiv \langle\varphi_s(t_1)\varphi_s(t_2)\rangle \\ &= \int_{-\infty}^{t_1} dt' \int_{-\infty}^{t_2} dt''\langle\xi(t')\xi(t'')\rangle \\ &= GD\int_0^{t_1} dt' \int_0^{t_2} dt''\exp(-G|t''-t'|) \\ &= 2Dt_< - \frac{D}{G}[1 - \exp(-Gt_1) - \exp(-Gt_2) \\ &\quad + \exp(-G|t_2-t_1|). \end{aligned} \tag{A.7}$$

The functions $F_{\pm}(t_1,t_2)$ are even function of t_1 and t_2. For positive t_1 and t_2 one obtains the results

$$F_-(t_1,t_2) = \exp\left[-2Dt_< - \frac{D}{G}\{-2 + 2\exp(-Gt_1) + 2\exp(-Gt_2) - \exp(-G|t_2 - t_1|) - \exp(-G[t_2 + t_1])\}\right], \quad (A.8)$$

$$F_+(t_1,t_2) = \exp\left[-2D(2t_1 - t_<) - \frac{D}{G}\{-2 + 2\exp(-Gt_1) - 2\exp(-Gt_2) + \exp(-G|t_2 - t_1|) + \exp(-G[t_2 + t_1])\}\right]. \quad (A.9)$$

These expressions, when used with formulas for $J_S(\omega)$, allow one to calculate the spectrum of beating (24) for arbitrary values of the phase fluctuation parameters G and D, the delay time T and the laser parameters.

A.2. Slow fluctuation

The preceding subsection dealt with an Ornstein–Uhlenbeck process governed by parameters G and D. To get a simpler estimation we consider further two limiting cases: (1) the phase changes slowly, $G \ll D$ and (2) the noise is delta correlated, $G \to \infty$. Bearing in mind the optimal conditions for narrow resonance (24) observation we will deal only with the function $F_-(\tau,T)$. In the first case, of slow phase fluctuations, the expression for F_- becomes

$$F_-(\tau,T) = \begin{cases} \exp\left[-1/3DG^2\tau^2(3T - \tau)\right], & \tau \leqslant T, \\ \exp\left[-1/3DG^2T^2(3\tau - T)\right], & \tau > T. \end{cases} \quad (A.10)$$

For weak fluctuations, $DG^2T^3 \ll 1$, the characteristic width of $F_-(\tau,T)$ as function of τ is $\delta\tau = 1/(DG^2T^2)$. Hence in this case the Fourier component $F_-(\omega,T)$ is a narrow function of ω with characteristic width $\delta\omega = DG^2T^3\frac{1}{T} \ll \frac{1}{T}$. As the fluctuation intensity increases the function $F_-(\tau,T)$ becomes narrower and hence the width of $F_-(\omega,T)$ increases. For $DG^2T^3 \gg 1$ we obtain a Gaussian profile for F_-

$$F_-(\omega,T) = T\frac{\sqrt{\pi}}{\sqrt{DG^2T^3}}\exp\left[-\frac{\omega^2}{4DG^2T}\right]. \quad (A.11)$$

The width of this is $\delta\omega = 2\sqrt{DG^2T^3}\frac{1}{T} \gg \frac{1}{T}$.

A.3. Rapid fluctuations

Here we assume the noise fluctuates rapidly, and consider the limit $G \to \infty$ when the correlation time is infinitesimal, i.e., the noise is delta correlated. Then the expression for F_- becomes

$$F_-(t_1,t_2) = \exp\left[-2Dt_<\right]. \quad (A.12)$$

When $\omega \neq 0$ we obtain for the spectral function $F_-(\omega\ ,T)$ the formula

$$F_-(\omega,T) = 2\mathrm{Re}\left[\frac{1 - \exp(-2DT + i\omega T)}{2D - i\omega} - \exp(-2DT)\frac{1 - \exp(i\omega T)}{-i\omega}\right]. \quad (A.13)$$

For small $DT \ll 1$ this function has the width $\delta\omega \simeq \frac{1}{T}$. With increasing $DT \gg 1$ the width of $F_-(\omega,T)$ increases. The function is Lorentzian

$$F_-(\omega,T) = \frac{4D}{4D^2 + \omega^2} \quad (A.14)$$

with width $\delta\omega \simeq D/2$.

References

[1] K. Takada, IEEE Photon. Technol. Lett. 49 (1992).
[2] R. Passy, N. Gisin, J.P. von der Weid, H.H. Gilgen, J. Lightwave Technol. 12 (1994) 1622.
[3] R. Passy, N. Gisin, J.P. von der Weid, IEEE Photon. Technol. Lett. 7 (1995) 667.
[4] B. Golubovic, B.E. Bouma, G.J. Tearney, J.G. Fujimoto, Opt. Lett. 22 (1997) 1704.
[5] C.-C. Wang, S.B. Trivendi, F. Jin, J. Khurgin, D. Temple, U. Hommerich, E. Gad, F.-S. Choa, Y.-S. Wu, A. Corder, J. Lightwave Technol. 19 (2001) 666.
[6] R. Schneider, P. Thuermel, M. Stockmann, Opt. Eng. 40 (2001) 33.
[7] K. Nakamura, T. Miyahara, M. Yoshida, T. Hara, H. Ito, IEEE Photon. Technol. Lett. 10 (1998) 1772.
[8] K. Nakamura, T. Hara, M. Yoshida, T. Miyahara, H. Ito, IEEE J. Quantum Electron. 36 (2000) 305.
[9] F. Kowalski, J.A. Squier, J.T. Pinckney, Appl. Phys. Lett. 50 (1987) 711.
[10] F.W. Kowalski, S.J. Shattil, P.D. Hale, Appl. Phys. Lett. 53 (1988) 734.

[11] F.V. Kowalski, P.D. Hale, S.J. Shattil, Opt. Lett. 13 (1988) 622.
[12] P.D. Hale, F.V. Kowalski, IEEE J. Quantum Electron. 26 (1990) 1845.
[13] F.V. Kowalski, S. Balle, I.C.M. Littler, K. Bergmann, Opt. Eng. 33 (1994) 1146.
[14] G. Bonnet, S. Balle, T. Kraft, K. Bergmann, Opt. Commun. 123 (1996) 790.
[15] K. Nakamura, F. Abe, K. Kasahara, T. Hara, M. Sato, H. Ito, IEEE J. Quant. Elect. 33 (1997) 103.
[16] K. Kasahara, K. Nakamura, M. Sato, H. Ito, IEEE J. Quant. Elect. 34 (1998) 190.
[17] J.M. Sousa, O.G. Okhotnikov, Opt. Commun. 183 (2000) 227.
[18] M.W. Phillips, G.Y. Liang, J.R.M. Barr, Opt. Commun. 100 (1993) 473.
[19] I.R. Perry, R.L. Wang, J.R.M. Barr, Opt. Commun. 109 (1994) 187.
[20] K. Nakamura, T. Miyahara, H. Ito, Appl. Phys. Lett. 72 (1998) 2631.
[21] A. Yoshizawa, H. Tsuchida, Opt. Commun. 155 (1998) 51.
[22] K.A. Shore, D.M. Kane, IEEE J. Quant. Elect. 35 (1999) 1053.
[23] H. Sabert, E. Brinkmeyer, J. Lightwave Technol. 12 (1994) 1360.
[24] S. Balle, K. Bergmann, Opt. Commun. 116 (1995) 136.
[25] F.V. Kowalski, K. Nakamura, H. Ito, Opt. Commun. 147 (1998) 103.
[26] L. Yatsenko, B.W. Shore, K. Bergmann, Opt. Commun. 236 (2004) 183.
[27] L.P. Yatsenko, M. Loeffler, B.W. Shore, K. Bergmann, Appl. Opt. 43 (2004) 3241.
[28] P. deGroot, A. Dergevorkian, T. Erikson, R. Pavlat, Appl. Opt. 37 (1998) 5116;
P. de Groot, Appl. Opt. 37 (1998) 6654.
[29] A. Biernat, G. Kompa, J. Opt. 29 (1998) 225;
M.-C. Amann, T. Bosch, M. Lescure, R. Myllyl, M. Rioux, Opt. Eng. 40 (2001) 10.
[30] I.C.M. Littler, H.M. Keller, U. Gaubatz, K. Bergmann, Z. Phys. D 18 (1991) 307.
[31] I.C.M. Littler, S. Balle, K. Bergmann, J. Opt. Soc. Am. B 8 (1991) 1412.
[32] I.C.M. Littler, K. Bergmann, R. Roy, Opt. Comm. 87 (1992) 53.
[33] I.C.M. Littler, P. Jung, K. Bergmann, Opt. Commun. 87 (1992) 61.
[34] I.C.M. Littler, S. Balle, K. Bergmann, Opt. Commun. 88 (1992) 514.
[35] I.C.M. Littler, K. Bergmann, Opt. Commun. 88 (1992) 523.
[36] S. Balle, I.C.M. Littler, K. Bergmann, F.V. Kowalski, Opt. Commun. 102 (1993) 166.
[37] D.T. Mugglin, A.D. Streater, S. Balle, K. Bergmann, Opt. Commun. 104 (1993) 165.
[38] M. Stellpflug, G. Bonnet, B.W. Shore, K. Bergmann, Opt. Express. 11 (2003) 2060.
[39] N.G. VanKampen, Stochastic Processes in Physics and Chemistry, North-Holland, NY, 1981.
[40] C.W. Gardiner, Handbook of Stochastic Methods, Springer, NY, 1985.

Available online at www.sciencedirect.com
ScienceDirect
Optics Communications 266 (2006) 266–273
OPTICS COMMUNICATIONS
www.elsevier.com/locate/optcom

High accuracy ranging with Yb^{3+}-doped fiber-ring frequency-shifted feedback laser with phase-modulated seed

V.V. Ogurtsov [a], L.P. Yatsenko [a], V.M. Khodakovskyy [a], B.W. Shore [b,*], G. Bonnet [b], K. Bergmann [b]

[a] *Institute of Physics, Ukrainian Academy of Sciences Prospect Nauki 46, Kiev-39 03650, Ukraine*
[b] *Technical University of Kaiserslautern, 67653 Kaiserslautern, Germany*

Received 25 October 2005; received in revised form 13 January 2006; accepted 26 April 2006

Abstract

This paper demonstrates that a frequency-shifted feedback laser, when seeded by a phase-modulated narrow-band radiation field, is a powerful tool for distance measurements to accuracy better than 10 μm and resolution better than 100 μm, for distances of a few meters. In such measurements the unknown distance forms one arm of a Michelson interferometer, in which the intensity of the output signal is modulated at the phase-modulation frequency of the seed. The amplitude of the output-signal modulation exhibits a resonance for every distinct signal delay, i.e. for each distinct distance within the laser spot on the target. The use of a phase-modulated input seed allows one to use a very narrow-bandwidth filter when measuring the return signal. The results reported in this paper are in excellent agreement with previous theoretical predictions [L. Yatsenko et al., Opt. Commun. 242 (2004) 581] for the resolution limit and high signal-to-noise ratio for this new technique.

PACS: 42.55.–f; 42.60.Da; 42.55.Ah

Keywords: Lasers; Laser ranging; Frequency-shifted feedback

1. Introduction

Laser based techniques – variants of radio-frequency RADAR – find increasing use for a variety of ranging applications, including measurements of distances with accuracy approaching or less than optical wavelengths. Such distances may be meters or kilometers, as is the case with LIDAR, or millimeters or centimeters, as is the case with typical workbench interferometers.

We here describe, and demonstrate, a new technique for accurate distance measurements using a frequency-shifted feedback (FSF) laser seeded by a phase-modulated (PM) laser. As we will note, FSF lasers differ significantly from ordinary lasers, and PM seeding has particular advantages when the laser is used for ranging.

In all FSF lasers, a feedback mechanism introduces a fixed frequency shift Δ_{AOM} with each passage of a wave packet around the laser cavity (during the round-trip time τ_r). After its first demonstration by Kowalski et al. [1], FSF lasers were further studied and developed by Bergmann and co-workers [2]. Later Nakamura et al. further studied such systems and demonstrated the use of FSF lasers for ranging [3,4]. They pointed out that the output of a frequency-shifted feedback (FSF) laser can be regarded as a succession of chirped pulses that can be used to measure distances, in a manner akin to chirped RADAR. In such operation one measures a frequency offset proportional to the time delay $\tau = 2h/c$ between a probe and a reference pulse, and from this one evaluates the incremental distance h.

* Corresponding author.
E-mail address: bwshore@alum.mit.edu (B.W. Shore).

0030-4018/$ - see front matter © 2006 Elsevier B.V. All rights reserved.
doi:10.1016/j.optcom.2006.04.070

In a previous article we provided a theoretical description of ranging measurements using a PM-seeded FSF laser [5]. The present article provides an experimental demonstration of that work. We show, in particular, that the operation of the FSF laser with PM-seeded radiation offers significant advantages over previous approaches to ranging with a FSF laser. The PM-seeding technique encodes the signal into a narrow bandwidth. As we demonstrate, this enhances the signal-to-noise ratio while maintaining the high resolution associated with the large bandwidth of the FSF radiation.

2. Laser ranging techniques

Laser-based techniques are widely used for distance measurement; for a detailed critical review of the usual techniques for distance measurement see [6]. In this section, we briefly discuss the more popular methods. These fall into three main categories: triangulation, time-of-flight and interferometry.

An *optical triangulation* system [7] uses a laser as one corner of a triangle and a camera (or other recording device) as the second one. The distance to the object can be determined using simple trigonometry, if one knows the distance between the laser and the camera and the triangle angles. The technique is applicable for distances of a few millimeters to tens of meters. The accuracy decreases with range, and for commercial devices can be about 0.01% of the range.

A *time-of-flight* (TOF) system [8] measures the time t between a pulse emission and the return of the pulse reflected from the object. The distance h is half of the product of this time and the velocity of light, $h = tc/2$. The precision of such range measurements depends mainly on noise-generated timing jitter, walk (timing error created by variations in the time-pickoff circuit), nonlinearity and drift. By carefully designing the system to minimize systematic errors, and by averaging successive measurements, one can achieve a precision of a few millimeters, although the accuracy of commercial devices is a few centimeters. A TOF system has the advantage of a weak dependence of the accuracy on distance. Furthermore, the technique does not need highly-reflective "cooperative" targets, such as mirrors.

Conventional *interferometers* (e.g. [9]) use fixed-frequency continuous-wave light. Distances are evaluated by measuring (via superposition of the test beam with a reference beam) the phase $\phi = 2\omega h/c$ induced by propagation of the test beam through an incremental distance h to a reflecting (mirror) surface. Interferometric measurements provide only values of relative distances: they give the distance that the mirror has moved from its initial position, rather than an absolute positional measurement. Furthermore, distances obtained using a single-wavelength interferometer have an ambiguity of half a wavelength. Most interferometric systems use mirrors as reflectors and frequency-stabilized lasers. The accuracy of the interferometric measurement can be very high (much better than 1 nm), but to reach this high precision it is essential to minimize changes in the index of refraction of the air that occur as a result of changes in air pressure and temperature.

3. Chirped-pulse interferometry

For measurements of absolute distances without the interference phase ambiguity, chirped-pulse interferometry (or the technique of frequency-modulated continuous-wave laser radar) is often used [6]. The operation of chirped-pulse interferometry can be understood by considering a laser whose frequency ω varies linearly with time (a linearly chirped frequency) according to the formula:

$$\omega = \omega_0 + \gamma_c t, \tag{1}$$

where γ_c is the chirp rate. The chirped radiation passes into a Michelson interferometer having one fixed (reference) arm and one variable-length (measurement) arm, as indicated schematically in Fig. 1. A beamsplitter (BS) provides the beams for each arm. After reflection from mirrors, these beams are brought into coincidence on a photodetector. When the measurement arm differs in length from the reference arm by h the beam in the latter arm incurs a delay $T = 2h/c$. As a result, its frequency is shifted by $\Delta\omega = \gamma_c T = 2h\gamma_c/c$ relative to the frequency of the reference beam. The two overlapping beams produce an amplitude-modulated field on the detector, with the beat frequency $\omega_B = \Delta\omega$. A measurement of this beat frequency provides a measurement of the distance, evaluated from the formula:

$$h = c\omega_B/2\gamma_c. \tag{2}$$

Single-frequency laser diodes are usually used as the light sources in chirped-pulse interferometry because one can easily modulate their frequency by modulating the diode current. The maximum measurable distance of a fre-

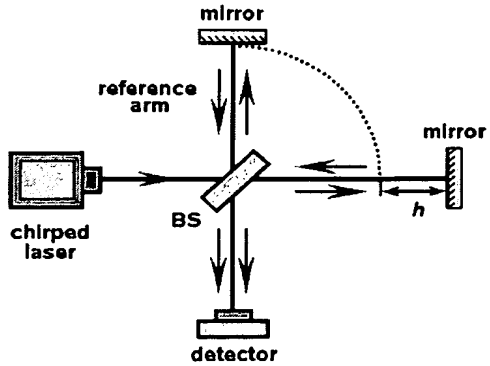

Fig. 1. Schematic diagram of a Michelson interferometer. Chirped-pulse laser light passes through a beam splitter (BS), and then along two arms, one of which contains the unknown height to be measured. Mirrors (or a reflecting surface) and the beam splitter bring these beams into coincidence on a photodiode detector. The height h is found relative to the reference arm length, as shown by dotted partial circumference.

quency-modulated CW laser diode system is ultimately limited by the coherence length of the laser diode, which typically is of the order of several tens of meters.

In chirped-pulse interferometry the measurement accuracy is inversely proportional to the tuning range of the laser frequency. As an example, using continuously tunable laser diodes with a tuning range of 500 GHz, a spectral width of 25 MHz and a repetition time 10 μs (a chirp rate $\gamma_c = 5 \times 10^{16}$), one can expect accuracy of 2.7 μm for 1 cm distance and 43 μms for 1 m [10]. The large modulation bandwidth of laser diodes makes them suitable for accurate and fast measurement of short distances with this technique.

Practical realization of the potential advantages of chirped-pulse interferometry is hindered by the following problems. To achieve high accuracy the frequency sweep must be linear. A sweep nonlinearity will cause the beat frequency to change during the sweep and will thereby decrease the measurement accuracy. This effect is particularly troublesome for measurements of large distances. Furthermore, if there is no prior knowledge of the range, the detection system for a single-mode sweep requires a large bandwidth. For large distances, one needs to measure very high beat frequencies, unless one is able to adjust the length of the reference arm. All these problems can be solved. For example, some elegant methods have been suggested to minimize the errors due to sweep nonlinearity [11]. Nevertheless, the most attractive feature of the frequency-modulated CW laser diode system, namely its simplicity, disappears.

These general principles of chirped-pulse ranging apply also when the laser is a FSF laser. However, there are significant differences, as we shall note.

4. The FSF laser as an interferometer source

A FSF laser differs from an ordinary laser by the presence of an element that shifts the optical frequency (by a discrete amount) on every round trip of a wavepacket within the cavity. In our case, the frequency-shifting element is an acousto-optic modulator (AOM), wherein acoustic waves create a travelling grating. The arrangement is such that the first-order diffracted light (altered in frequency) continues within the cavity, while the zero-order emerges as the output. This construction eliminates the usual cavity interference that, by repeated passages of a wavepacket, builds up discrete fixed-frequency modes. As a result, a FSF has no longitudinal mode structure. The output radiation from a FSF laser has been discussed extensively [2,12]. It can be interpreted as a succession of frequency chirped components, a "moving comb" of frequencies, each of which is linearly chirped in accord with Eq. (1) [13]. Experiments have demonstrated that, as one might anticipate from such radiation, it is possible to use this output to conduct distance measurements [3,4].

Fig. 2 illustrates this comb-like behavior. Within the gain profile this comb has a large number of "teeth", each

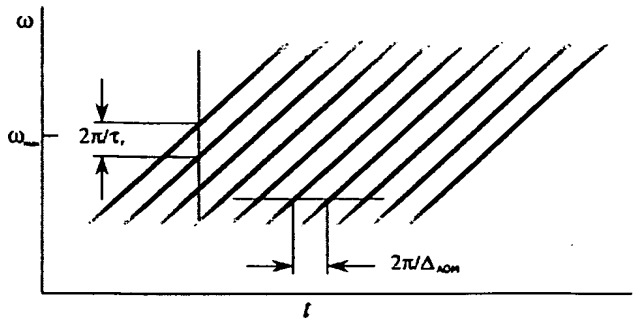

Fig. 2. Schematic diagram of the "moving comb" in the frequency-time space. The frequency distance between "teeth" – the free spectral range (FSR) of the FSF laser – is $2\pi/\tau_r$. The time separation is $2\pi/\Delta_{AOM}$. Every "tooth" has a Gaussian envelope.

with a time varying amplitude $B_n(t)$. The result is the electric field

$$E_{MC}(t) = \mathscr{E}_0 \sum_{n=-\infty}^{+\infty} B_n(t) \exp[-ip_n(t)], \tag{3}$$

where $p_n(t)$ is the phase of the nth component ("tooth"). The frequency of this component, ω_n, undergoes a linear chirp

$$\omega_n(t) \equiv \frac{d}{dt} p_n(t) = \omega_{max} + \frac{\Delta_{AOM}}{\tau_r}(t - n\tau_s), \tag{4}$$

where Δ_{AOM} is the acousto-optic modulator frequency, τ_r is the round-trip time, $\tau_s = 2\pi/\Delta_{AOM}$ is the time separation between teeth and ω_{max} is the frequency of the FSF laser spectrum maximum. The chirp rate is $\gamma_c = \Delta_{AOM}/\tau_r$.

As in any laser, light in a FSF laser passes through a gain medium, where amplification occurs. Any spontaneous emission from the excitation responsible for the gain will, through multiple passes (at successively shifted frequencies), contribute to the circulating field and hence to the output. For better control of the output one can inject a predetermined field into the cavity using a seed laser. This has been our approach.

According to Eq. (4), in the moving-comb model the output from an FSF laser is a set of frequencies (comb teeth), separated by the cavity axial mode interval $\Delta_c = 2\pi/\tau_r$, which are moving with the rate γ_c

$$\omega_n(t) = \omega_{max} + \gamma_c t - n\Delta_c. \tag{5}$$

These frequencies are uniformly chirped, at rate γ_c, so in an interferometer a time delay T produces a number of beating signals between different teeth of the reference and reflected fields. In the absence of fluctuations the phases of all these beat signals are such that they sum to zero. However, fluctuations break this balance, and one can therefore observe a resonant increase in the spectral density of the RF spectrum near these beat frequencies. Although such signals are weak and noisy, nevertheless, they have been successfully used for distance measurements of up to 18 km [4].

With the phase-modulation technique described in this paper, the maximum amplitude modulation of the FSF laser output takes place when the modulation frequency coincides with one of these beat frequencies. The simplest beats, those of lowest frequency, are those that occur between teeth having the same n. Such beats occur, at frequency $\omega_B = \gamma_c T$, when the delay T is less than the time separation between adjacent teeth, $\tau_s = 2\pi/\Delta_{AOM}$, so that the beat signal is less than the cavity frequency Δ_c. However, other beats occur, between tooth n and a tooth $n + \delta n$, with integer δn, at the beat frequency

$$\omega_B(\delta n) = \delta n \Delta_c + \gamma_c T. \tag{6}$$

The existence of this family of beat frequencies allows us to choose one that falls within a frequency range for which electronic signal processing is convenient. It is only necessary that we determine δn in order to deduce the delay T. This we can do by observing the effect of a slight alteration of the cavity frequency from Δ_c to $\Delta_c + \delta_c$, as produced by a change of the cavity optical length. This changes the observed beat frequency by

$$\delta\omega_B(\delta n) = \delta n \times \delta_c \tag{7}$$

(with the neglect of the small change in chirp rate). From knowledge of δ_c and a measurement of $\delta\omega_B(\delta n)$ we can deduce δn.

Using this technique it is possible to measure large distances without changing the reference arm or measuring very high-frequency beats. By making frequent measurements of δn it is possible to track a moving target. The very regular progression of chirped frequencies in the moving comb model provides an ideal linearity of sweep.

The following sections describe the realization of this new technique for ranging with a PM-seeded FSF laser. The technique allows a dramatic enhancement of the signal-to-noise ratio (up to three orders) while preserving all the attractive features of the FSF laser expected from the moving comb model.

5. Seeded FSF laser

The output of any FSF laser can be used for optical ranging, whether the laser field grows from spontaneous emission within the cavity or from a fixed-frequency external-seed laser. The present FSF laser differs from those of previous demonstrations by using a seed laser whose phase $\Phi(t) = \omega_s t + \varphi_s(t)$ is modulated sinusoidally,

$$\varphi_s(t) = \varphi_0 + \beta \sin(\Omega t) \tag{8}$$

as was suggested in [5]. Here, ω_s is the seed laser frequency, Ω is the modulation frequency, β is the modulation index and φ_0 is the initial phase.

Such a *phase-modulated* seed generates a specific FSF-laser output, consisting of a set of discrete optical components with the frequencies $\omega_s + n\Delta_{AOM}$ $(n = 0, 1, 2, \ldots)$. The phases of the components have a time-independent contribution that is quadratic in n and a time-delayed contribution from the phase-modulated seed laser phase $\varphi_s(t - n\tau_r)$. The amplitudes of the components are proportional to a Gaussian function of n, $\exp[-(n - n_m)^2/n_w^2]$, where n_w is the effective number of optical components within the Gaussian profile of the laser spectrum and n_m is the central position of the profile. These two characterizing parameters are large, $n_w \gg 1$ and $n_m \gg 1$, and can be evaluated from measurable laser characteristics (for details see Eqs. (13)–(17) in [5]). When this output is used as input to a Michelson interferometer whose arms differ in length by h, there occurs in the output from the interferometer an *amplitude modulation* with the frequency Ω. The amplitude S_{AM} of this modulation is

$$S_{AM} = S_0 J_1(2\beta \sin[\Omega T/2]) \exp\left[-(\Omega - \gamma_c T)^2 \tau_r^2 n_w^2/8\right], \tag{9}$$

where $J_1(x)$ is the Bessel function of order 1 and S_0 is a normalization factor that incorporates the laser output power. This signal has a Gaussian profile that reaches a maximum when the modulation frequency Ω is equal to

$$\Omega_M \equiv \gamma_c T = \gamma_c 2h/c. \tag{10}$$

Thus, by measuring the modulation frequency for which the interferometer output maximizes we measure h. The constant of proportionality between the distance h and resonance-peak frequency Ω_M is $c/2\gamma_c$. For our setup this had the value $= c/2\gamma_c = 0.02$ mm/kHz.

The accuracy with which one can determine the resonance maximum, and hence the accuracy δh with which one can measure h, is set by the width of this resonance,

$$\Delta\Omega = \frac{2\sqrt{2}}{\tau_r n_w} \tag{11}$$

and can be written as

$$\delta h = \epsilon \Delta\Omega \frac{c}{2\gamma_c}. \tag{12}$$

Here, the small parameter $\epsilon \ll 1$ depends on the signal-to-noise ratio and, as shown in [5], its value can be smaller than 10^{-3}. It is worth noting that for such accuracy it is important to account for a shift of the resonance (9) due to the influence of the frequency dependent Bessel function. For a small modulation index $\beta \ll 1$ this shift can be estimated as

$$\delta\Omega = \cot\left[\frac{\Omega_M T}{2}\right] \frac{\Delta\Omega T}{4} \Delta\Omega. \tag{13}$$

Using values typical for our setup, $T = 2.5$ ns, $\Omega_M = 2\pi \cdot 12.5$ MHz and $\Delta\Omega = 5$ kHz we obtain the estimate $\delta\Omega \simeq 0.8 \times 10^{-3} \Delta\Omega$.

In the present work we scanned the frequency of phase modulation and measured the signal S_{AM} as filtered by a narrow bandpass RF filter set to match the phase modulation frequency Ω. From the envelope of filtered signals we evaluated the frequency of maximum signal, and from this, using Eq. (10), we obtained the distance increment h.

(4)

6. Experimental setup

To demonstrate this technique of PM-seeded FSF for optical ranging we used the setup sketched in Fig. 3. The FSF laser portion consists of an optical fiber incorporating a gain section, closed into a ring configuration by means of mirrors and the first-order diffraction output of an AOM modulator. This is seeded by a PM laser, and its output feeds a Michelson interferometer.

The FSF laser has been described in [15]. Briefly, its parameters are as follows:

- $\Delta_{AOM}/2\pi = 80.3$ MHz, the frequency of the AOM,
- $\tau_r = 10.7$ ns, the round trip time,
- $\gamma_c/2\pi = \Delta_{AOM}/2\pi\tau_r = 7.5 \times 10^{15}$ Hz/s, the chirp rate.

The spectrum of our FSF typically is approximately a Gaussian, with width (FWHM) around 300 GHz, but under appropriate conditions this width can be extended to 3000 GHz (its shape is then no longer Gaussian). The spectral width also can be decreased to 60 GHz by inserting a Fabry–Perot etalon (FPE) with FSR 1000 GHz into the cavity. The FSF laser can operate in the wavelength region 1030–1075 nm. For the distance measurements shown in this work we used the wavelengths 1040 nm (with 300 GHz and 60 GHz bandwidths) and 1055 nm (for 1000–3000 GHz bandwidths).

The seed laser is a single-frequency external cavity diode laser constructed on the Littman–Metcalf scheme, as described in [14]. The phase modulation of the seed laser is produced by an electro-optic modulator (EOM) driven by a FM-generator that sweeps the frequency linearly. This generator is synchronized with the radio-frequency spectrum analyzer (RSA) that contains a RF-filter. This system allows us to detect envelopes of the amplitude modulation and thereby measure distances.

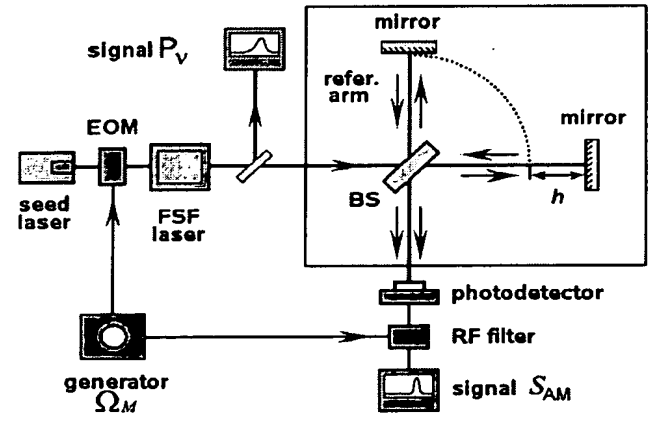

Fig. 3. Schematic diagram of the layout used for distance measurements using a PM-seeded FSF laser. A rectangle encloses the interferometer portion of the apparatus. A signal generator drives both an electro-optic modulator (EOM), which modulates the phase of a seed laser, and adjusts the frequency of an RF filter which precedes the beat signal detector. P_v is the optical spectrum of the FSF laser, S_{AM} is the amplitude modulation signal.

7. Example of optical spectra

When the seed laser power is low, spontaneous emission dominates the FSF-laser field. When the seed power is very high its influence dominates and distorts the shape of the spectrum and, in turn, the envelope of S_{AM} This change in optical spectrum is evident in Fig. 4, which presents typical spectra of the FSF laser used in the present work, with and without an external seed laser. The frequency and the power (near 100 μW) of the seed laser have been chosen to maximize the amplitude modulation signal S_{AM}. The spectrum without a seed is close to a Gaussian in shape, but the seeded spectrum has marked asymmetry induced by the seed laser.

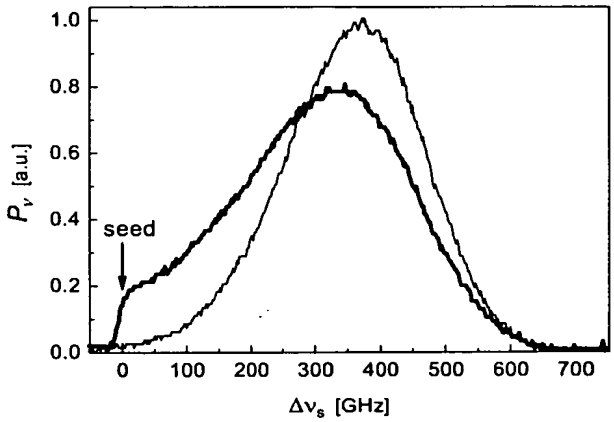

Fig. 4. Output spectral power P_v (arbitrary units) versus frequency offset $\Delta\nu_s$ from the seed frequency, with external seed (thick line) and without seed (thin line).

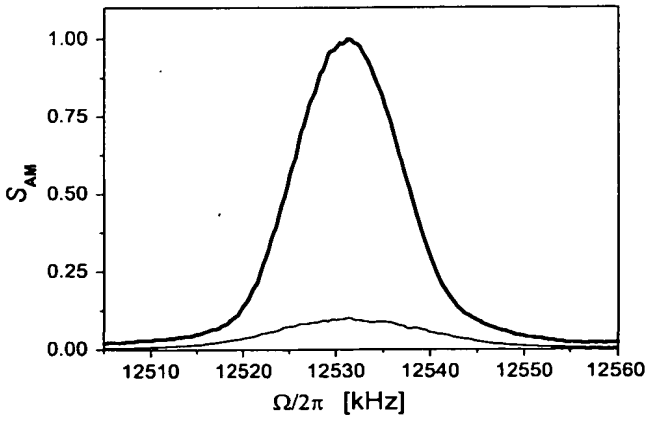

Fig. 5. Amplitude modulation signal S_{AM} versus modulation frequency $\Omega/2\pi$ for signals obtained with external seed (thick line, single scan) and without seed (thin line, averaged over 50 scans).

The use of a external PM seed allows one to limit the detector signal to the PM frequency, thereby eliminating noise from other frequencies. This is possible because the spectral width of the amplitude modulation signal is very small (in our experiments it is less than the apparatus resolution of 50 Hz). This property allows us to use a narrow RF-filter for detecting the desired signal. The benefit of this filtering is seen in Fig. 5, which compares the signal S_{AM} of an unseeded FSF laser and one seeded by a PM signal. The signals have nearly the same width $\Delta\Omega$, but whereas the first signal is weak and noisy (only after averaging 50 scans does it appear close to Gaussian), the second one has a larger amplitude and does not require averaging.

8. Bandwidth–resolution relationship

In keeping with all Fourier-transform frequency-time pairings, one expects an inverse relationship between the bandwidth of the FSF laser and the resolution with which one can measure delay time and distances [13]. Fig. 6 illustrates this relationship by presenting three examples of the spectrum of the seeded FSF laser, each with a different width, together with the corresponding signals of amplitude modulation. The upper plots are for the FSF laser with FPE 1000 GHz inside the cavity. The middle ones are for the usual FSF laser operating near the wavelength corresponding to the maximum of the Yb^{3+} gain profile. The lower ones are for the FSF laser operating near the wavelength corresponding to the local minimum of the Yb^{3+} gain profile, where joint action of AOM dispersion and gain frequency dependence results in nearly flat effective gain and consequent larger spectral width. Theory predicts [13] that the inverse of the width $\Delta\Omega$ of the signal profile S_{AM} should be directly proportional to the bandwidth Γ of the FSF laser. We found this dependence, shown in Fig. 7, fits a straight line even if the spectrum is not Gaussian (as in the lower left hand frame of Fig. 6). This linearity demonstrates that the FSF laser maintains

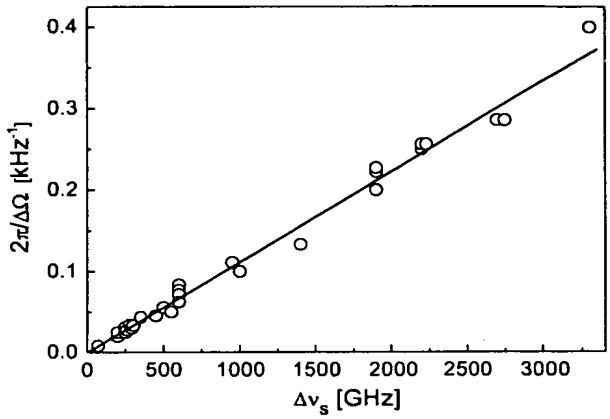

Fig. 7. Dependence of the inverse width $2\pi/\Delta\Omega$ of the amplitude modulation signal upon the FSF-laser spectral width. Circles are experimental points, straight line is a linear fit.

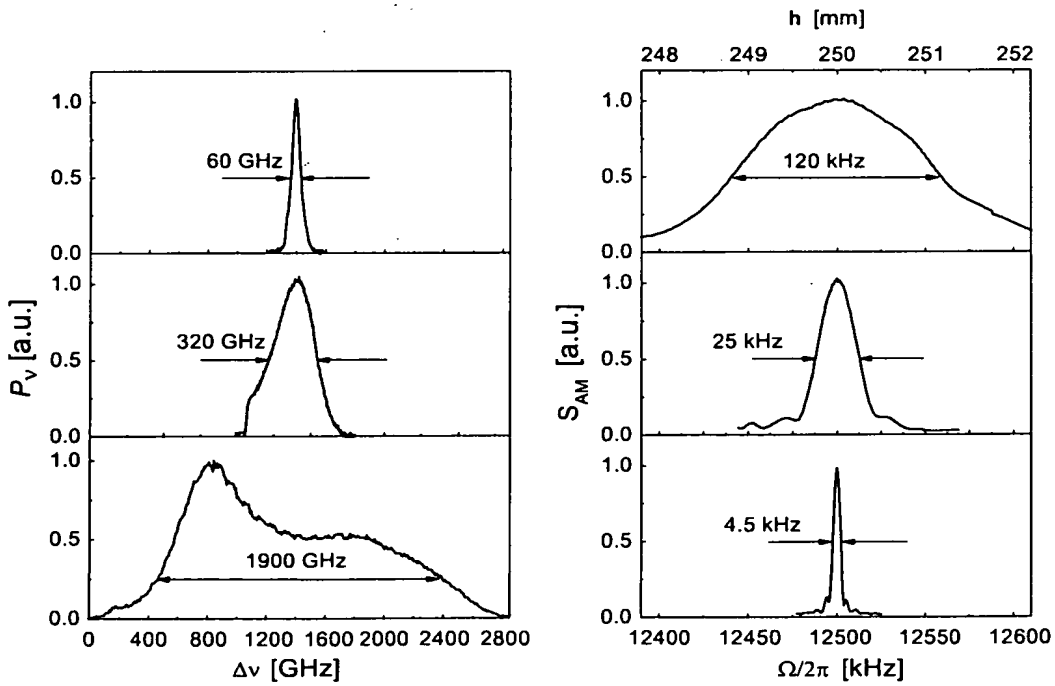

Fig. 6. Left hand: output power spectrum P_ν versus relative frequency $\Delta\nu$ for three values of the FSF-laser bandwidth Γ. Right hand: signal S_{AM} versus modulation frequency $\Omega/2\pi$ for each of these bandwidths.

(4)

coherence of the acousto-optic modes across the entire spectrum of the FSF laser.

9. Demonstration of spatial resolution

The optical ranging technique relies on the observation of a return signal reflected from a target. In our basic experiments we use a smooth flat reflecting surface, oriented to reflect the light directly back into the interferometer. More generally, the target may have a distribution of surface heights within the laser-beam spot, producing multiple reflections; each height provides a different delay time and a different resonance peak in the signal S_{AM}. If these peaks are sufficiently well separated to be resolved they can be identified as originating at distinct heights. The relative magnitude of a signal provides a measure of the relative area, within the laser spot, at the corresponding height.

To demonstrate the resolution available with our system we fabricated samples that provided two distinct heights. These samples were flat rectangular reflectors whose surfaces were interrupted by a single step. As the laser beam moves across such a surface it encounters first one height, then two heights, and then one height again, as illustrated in Fig. 8. In accordance with theory, the relative *positions* of the peaks remains fixed (these depend only on the fixed height of the step on the sample), while the *heights* of the peaks vary in accordance with the relative portion of the beam spot that is occupied by the corresponding height.

We used samples having two height steps: one of 1.0 mm and 0.1 mm. The height difference of 1 mm is readily resolved even with a laser whose spectral width is 1 nm (near 300 GHz). Fig. 9 shows how the amplitude modulation signal S_{AM} changes as the laser beam moves across the 1 mm step sample past the border between the two facets. Relatively low peaks at the positions **b**, **c** and **d** in comparison with **a** and **e** can be explained by the fact that sample facets are not absolutely parallel and so there are slightly different optimal adjustments for every facet.

The step height of 0.1 mm on the second sample was resolved only by the FSF laser with spectral width of about 7 nm (near 2000 GHz). We measured the step height to be 110 μm, with an accuracy of better than 10 μm (see Fig. 10).

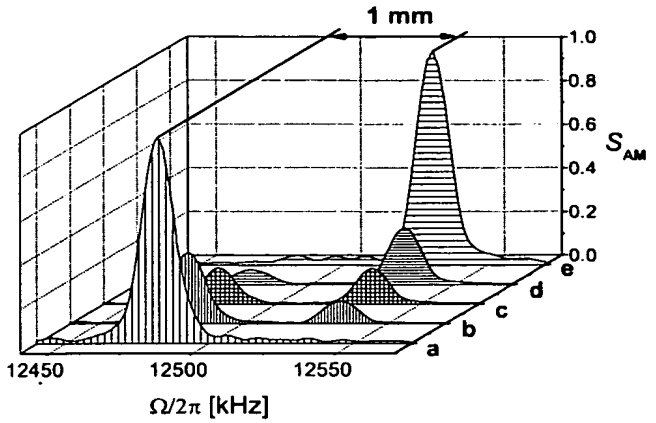

Fig. 9. Signals S_{AM} versus modulation frequency $\Omega/2\pi$ for the sample with step $\delta h = 1$ mm for several positions of the laser beam, as shown in Fig. 8.

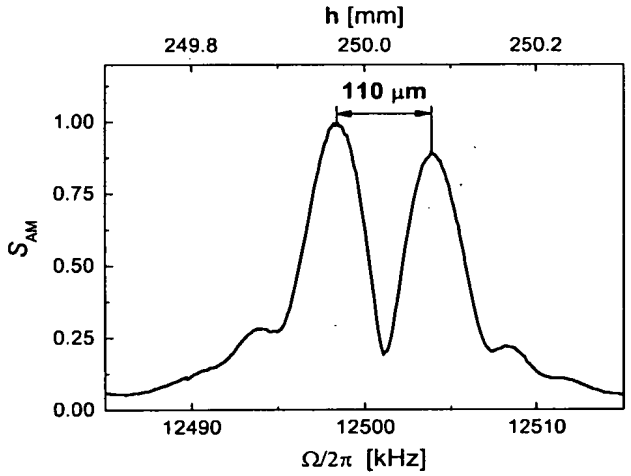

Fig. 10. Signal S_{AM} versus modulation frequency $\Omega/2\pi$ for the sample with step $\delta h = 110$ μm. The upper border shows the distances corresponding to frequencies, according to Eq. (10).

10. Conclusions, outlook and summary

We have demonstrated that a FSF laser, when seeded by a PM signal, is a powerful tool for distance measurements,

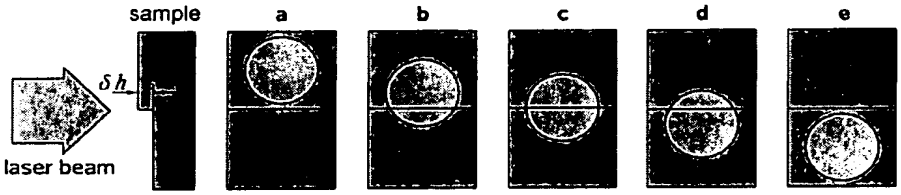

Fig. 8. Sample for the demonstration of spatial resolution: two reflecting facets differing in height by δh. Successive frames show positions used in making observations.

at least in range of a few meters, to an accuracy better than 10 μm and resolution better than 100 μm.

In such measurements the unknown distance forms one arm of a Michelson interferometer, in which the output signal is modulated at the PM frequency of the seed; this output signal exhibits a resonance for every distinct signal delay, i.e. for each distinct distance within the laser spot on the target. The use of a phase-modulated input seed allows one to use a very narrow bandwidth filter when measuring the return signal. The results reported here are in excellent agreement with previous theoretical predictions of a high signal-to-noise ratio and resolution limit for this new technique [5].

Our current resolution is about 30 wavelengths, based on the criterion of resolving two resonances with minimal full width at half maximum equal 2.5 kHz (see Fig. 7). This is smaller than what is achievable with frequency-modulated continuous-wave optical radar [6] but it is larger than the expected limit for frequency-ranging techniques (about one wavelength). Our resolution was limited by the width of the FSF laser spectrum. This limit can be improved by using lasers with broad, almost flat effective gain (defined as the difference between frequency dependent gain and losses). Our current accuracy is at least 5 μm (assuming that the maximum can be determined within 10% of the width). Further improvements in bandwidth and signal-to-noise ratio should enable us to reach accuracy of 1 μm.

The high accuracy of the present technique makes possible submicron resolution of surface structures whose shape is known, so that results can be fitted to theoretical profiles. To achieve such high resolution the spectrum of the FSF laser must be a (broad) Gaussian, to avoid signal oscillations that originate from the Fourier transform of other, truncated spectral distributions.

The present limitation on the distance range of measurements with a FSF laser, seeded by a PM signal, is the coherence length of the seed laser. This value has to be determined using the seed laser spectrum width without slow (on milliseconds scale) drifts. For our laser this coherence length is larger than 1 km.

Acknowledgements

We acknowledge support by the Stiftung Rheinland-Pfalz für Innovation. LPY acknowledges support by the Deutsche Forschungsgemeinschaft (436-UKR-113/16). B.W.S. acknowledges support from the Max Planck Forschungspreis 2003. We thank R. Haberland for fabricating the samples used in this work.

References

[1] F. Kowalski, J.A. Squier, J.T. Pinckney, Appl. Phys. Lett. 50 (1987) 711;
F.V. Kowalski, P.D. Hale, S.J. Shattil, Opt. Lett. 13 (1988) 622;
F.V. Kowalski, S.J. Shattil, P.D. Hale, Appl. Phys. Lett. 53 (1988) 734.

[2] I.C.M. Littler, S. Balle, K. Bergmann, J. Opt. Soc. Am. B 8 (1991) 1412;
I.C.M. Littler, S. Balle, K. Bergmann, Opt. Commun. 88 (1992) 514;
I.C.M. Littler, J.H. Eschner, Opt. Commun. 87 (1992) 44;
S. Balle, I.C.M. Littler, K. Bergmann, F.V. Kowalski, Opt. Commun. 102 (1993) 166;
J. Martin, Y. Zhao, S. Balle, K. Bergmann, M.P. Fewell, Opt. Commun. 112 (1994) 109;
F.V. Kowalski, S. Balle, I.C.M. Littler, K. Bergmann, Opt. Eng. 33 (1994) 1146;
S. Balle, K. Bergmann, Opt. Commun. 116 (1995) 136;
G. Bonnet, S. Balle, T. Kraft, K. Bergmann, Opt. Commun. 123 (1996) 790;
M. Stellpflug, G. Bonnet, B.W. Shore, K. Bergmann, Opt. Express 11 (2003) 2060.

[3] K. Nakamura, T. Miyahara, M. Yoshida, T. Hara, H. Ito, IEEE Photonic. Technol. Lett. 10 (1998) 1772.

[4] K. Nakamura, T. Hara, M. Yoshida, T. Miyahara, H. Ito, IEEE J. Quantum Electron. 36 (2000) 305.

[5] L.P. Yatsenko, B.W. Shore, K. Bergmann, Opt. Commun. 242 (2004) 581.

[6] M.-C. Amann, T. Bosch, M. Lescure, R. Myllylä, M. Rioux, Opt. Eng. 40 (2001) 1019.

[7] M. Rioux, G. Bechthold, D. Taylor, M. Duggan, Opt. Eng. 26 (1987) 1245;
R. Baribeau, M. Rioux, Appl. Opt. 30 (1991) 2873.

[8] R. Myllylä, J. Marszalec, J. Kostamovaara, A. Mäntyniemi, G.-J. Ulbrich, J. Opt. 29 (1998) 188193;
A. Kilpelä, R. Pennala, J. Kostamovaara, Rev. Sci. Instr. 72 (2001) 2197.

[9] C. Yang, A. Wax, M.S. Hahn, K. Badizadegan, R.R. Dasari, M.S. Feld, Opt. Lett. 26 (2001) 1271.

[10] A. Dieckmann, M.-C. Amann, in: O.D.D. Soares (Ed.), Trends in Optical Fibre Metrology and Standards, Kluwer Academic Publishers, Dordrecht, 1995, p. 791.

[11] A. Dieckmann, M.-C. Amann, Opt. Eng. 34 (1995) 896;
K. Iiyama, L-T. Wang, K. Hayashi, J. Lightwave Technol. 14 (1996) 173178.

[12] J.M. Sousa, O.G. Okhotnikov, Opt. Commun. 183 (2000) 227;
F.V. Kowalski, C. Ndiaye, K. Nakamura, H. Ito, Opt. Commun. 231 (2004) 149164.

[13] I.R. Perry, R.L. Wang, J.R.M. Barr, Opt. Commun. 109 (1994) 187;
K. Kasahara, K. Nakamura, M. Sato, H. Ito, Opt. Rev. 4 (1997) 180;
K. Nakamura, F. Abe, K. Kasahara, T. Hara, M. Sato, H. Ito, IEEE J. Quantum Electron. 33 (1997) 103;
K. Nakamura, F.V. Kowalski, H. Ito, Opt. Lett. 22 (1997) 889;
A. Yoshizawa, H. Tsuchida, Opt. Commun. 155 (1998) 51;
F.V. Kowalski, K. Nakamura, H. Ito, Opt. Commun. 147 (1998) 103.

[13] L. Yatsenko, B.W. Shore, K. Bergmann, Opt. Commun. 236 (2004) 183.

[14] M. Littman, H. Metcalf, Appl. Opt. 17 (1978) 2224.

[15] V.V. Ogurtsov, L.P. Yatsenko, V.M. Khodakovskyy, B.W. Shore, G. Bonnet, K. Bergmann. Opt. Commun. (2006) in press.

Available online at www.sciencedirect.com
ScienceDirect
Optics Communications 266 (2006) 627–637
OPTICS COMMUNICATIONS
www.elsevier.com/locate/optcom

(3)

Experimental characterization of an Yb^{3+}-doped fiber ring laser with frequency-shifted feedback

V.V. Ogurtsov [a], L.P. Yatsenko [a], V.M. Khodakovskyy [a], B.W. Shore [b,*], G. Bonnet [b], K. Bergmann [b]

[a] *Institute of Physics, Ukrainian Academy of Sciences, Prospect Nauki 46, Kiev-39, 03650, Ukraine*
[b] *Universität Kaiserslautern, 67653 Kaiserslautern, Germany*

Received 25 October 2005; received in revised form 8 May 2006; accepted 10 May 2006

Abstract

We present experimental characteristics of an Yb^{3+}-doped fiber ring laser operating with frequency-shifted feedback (FSF) through an acousto-optic modulator (AOM) and seeded by both a stationary continuous-wave (CW) laser and spontaneous emission. We show the spectrum and output characteristics for operations with several effective gain bandwidths, as established by Fabry–Perot etalons inside the cavity. Observation using a high finesse Fabry–Perot interferometer shows that, as expected from earlier work, although the spectrum of the FSF laser without seeding is continuous, when seeded by a CW-laser the spectrum consists of a comb of discrete modes, each offset from the seed by an integer number of AOM frequency shifts. The experimental results are in excellent quantitative agreement with the theory developed earlier [L. Yatsenko, B.W. Shore, K. Bergmann, Opt. Commun. 236 (2004) 183].

PACS: 42.55.–f; 42.60.Da; 42.55.Ah

Keywords: Optics; Lasers; Frequency-shifted feedback

1. Introduction

In conventional lasers, the light makes multiple passes through a gain medium inside a cavity. The cavity length defines discrete allowed longitudinal modes for which constructive interference supports gain [1]. By contrast, frequency-shifted feedback (FSF) lasers have within their cavity some element that introduces a frequency shift during each successive pass. In such a laser no single frequency has any special advantage for gain, and growth (lasing) can occur from any initial seed frequency. Consequently, the output spectrum from an FSF laser can cover a much broader range of frequencies than do conventional lasers, see e.g. [2].

The first FSF laser system was suggested in 1965 by Froster et al. [3], who demonstrated modelocking operation of a He–Ne laser coupled to an external linear cavity by means of an acousto-optic Bragg diffraction cell driven at half of the laser-mode separation frequency. After interaction with the cavity, the frequency-shifted radiation locked all the longitudinal oscillating modes. A modern concept of a FSF laser, with an acousto-optic cell inside the cavity, was suggested in 1970, when Streifer et al. [4] proposed a new scheme using a dye laser electronically tuned by an acousto-optic filter. After these pioneering works, the idea of a FSF laser was picked up and extended by many authors, who suggested and investigated numerous FSF-laser systems, such as: a dye laser that was electronically tunable over 78 nm [5]; diode lasers with an external cavity;

* Corresponding author.
E-mail address: bwshore@alum.mit.edu (B.W. Shore).

0030-4018/$ - see front matter © 2006 Published by Elsevier B.V.
doi:10.1016/j.optcom.2006.05.026

a diode laser with frequency-shifted feedback that generated output over a large frequency range [6,7]; and bulk solid-state FSF lasers such as Ti:sapphire [8–10], Nd:YVO_4 [11] and many others.

The reason for this interest is easily understood, for FSF lasers have many peculiar spectral features: the spectrum is modeless, nearly Gaussian in shape (shifted away from the minimum of losses), with a very weak dependence upon pump and seed power. The output exhibits a chirped structure, which can cover a large, continuous range of frequencies. These features under the many applications of FSF lasers, such as optical frequency domain ranging [12,13], optical pumping [14,15], velocity control and cooling of atomic beams [16], and measuring the separation of widely spaced optical frequencies to an accuracy of ±5 kHz [29].

One of the most intriguing application of FSF lasers is to distance measurement. As has been discussed by Kasahara et al. [11], the FSF-laser output consists of periodically generated chirped-frequency components whose chirp rate is faster than 10^{17} Hz/s. Phase relationships are maintained among various discrete frequency components. This structure allows one to overcome the conventional limits on operating range and spatial resolution and has thereby enabled distance measurements of 3.7 km with a resolution of 9.4 mm [12] and 18.5 km with a resolution of 20 mm [13].

A new stage in the study of FSF lasers began with the appearance of fiber lasers. These have a number of advantages, such as compactness, great range of cavity length, simplicity of exploitation, and great amplification per round trip. As with the usual FSF laser, a fiber FSF laser can operate in different regimes. The Kerr-type nonlinearity in an amplifying fibre may initiate the spontaneous formation of short pulses [17,18]. These pulses can be controlled by properly designing the gain-bandwidth of the fibers [19,20]. Fiber FSF lasers can also demonstrate continuous-wave, modeless radiation, that can be tuned over a broad range [21], and to broadband multiwavelength operation; for example, the appearance of 34 lasing wavelengths within a bandwidth of 28 nm [22]. Injection of a narrow-bandwidth seeding laser into the cavity will generate a discrete comb of optical frequencies, separated by the frequency Δ associated with the total round trip time [23].

Fiber FSF lasers have already found many applications, such as measurements of group velocity [24] and polarization-mode dispersion [25] in fibers. They are also useful for optical reflectometry. The first works in that direction have already been reported: Yoshida et al. [26] described a FSF laser using erbium-doped fiber as a gain medium that allowed distance measurements with a spatial resolution of 1.5 mm. Ogurtsov et al. [27] have improved this method and have demonstrated a ytterbium-doped fiber FSF laser that is able to measure meter-long distances with an accuracy of 10 μm. Such results support the conclusion that fiber FSF lasers offer opportunities for new devices that will enable distance measurements to be made rapidly and with high accuracy over a large range of distances.

Early publications dealing with FSF-laser operation concentrated on characterizing the output under various conditions of operation [17,7,30]. As that work made clear, a FSF laser can exhibit a variety of output scenarios, from steady to pulsed, depending on controllable parameters such as the pump power and the frequency shift.

Although FSF lasers have been discussed for many years, and many interesting properties have been recognized [32,8], only recently has a theory provided a complete description of the phase and intensity of the output of a FSF laser, as seeded both by spontaneous emission within the gain medium and by a monochromatic continuous-wave (CW) laser injected from outside the cavity [33]. There the spectrum of an externally seeded FSF laser is predicted to have some remarkable properties. The present paper provides experimental verification of this theory.

We begin, in Section 2, with a description of our apparatus, which includes an Yb^{3+}-doped fiber ring FSF laser with associated pump laser, a seeding laser and diagnostic devices with their parameters. Section 3 presents several characteristics of the FSF laser without any elements that deliberately limit the bandwidth. Because the loss profile is not known, these results could not be compared directly with the theory. However, data taken after inserting a well-characterized Fabry–Perot etalon (FPE) into the cavity provided a clear demonstration of the theory. Section 4 describes measurements on such a system, with and without an external seeding laser. To investigate the detailed structure of the FSF-laser spectrum, we inserted into the cavity a narrow bandwidth filter, consisting of four FPEs. The data show that without external seeding the spectrum of the FSF is continuous, but that with such seeding it consists of a comb of discrete frequencies, differing by the frequency of the acousto-optic modulator (AOM), as predicted by theory [33].

2. Apparatus

The experimental arrangement comprises four interconnected parts: (a) the FSF ring laser itself; (b) the pump laser that produces the gain in the active fiber; (c) the CW seed laser; and (d) output diagnostics. Fig. 1 shows these four parts and their individual components, each numbered for reference.

2.1. The FSF laser

The FSF laser itself consists of several elements, labeled in Fig. 1. Gain occurs in an ytterbium-doped fiber (2) [Jena 325sA4 IPHT] with length 0.45 m; the Yb^{3+} fiber is fusion spliced onto a passive fiber (1) with length 1.15 m. Light from the fiber passes through a dichroic mirror (4), a turning mirror (5), and an output mirror (8), whose partial transparency (about 5%) diverts some of the light to the diagnostics section. Following this mirror, most light continues within the FSF, passing into an AOM (9). The first-order diffracted light from the AOM, shifted in frequency

(3)

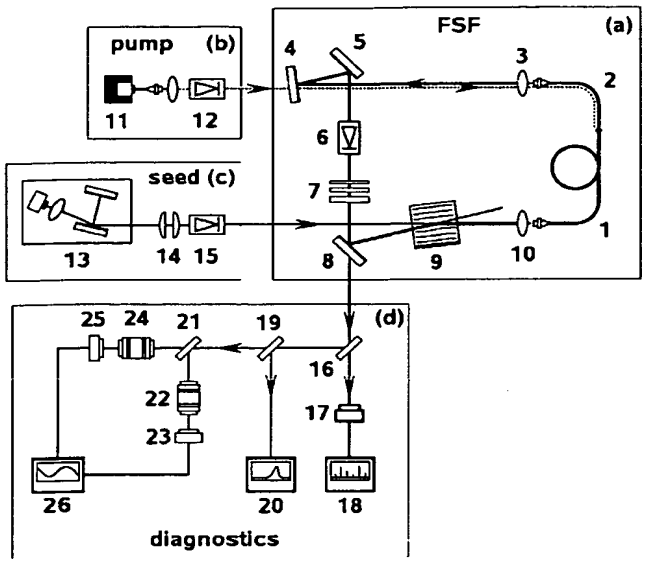

Fig. 1. Layout of our apparatus, showing (a) the FSF ring laser, (b) the pump laser, (c) the seed laser, and (d) the apparatus for diagnostics. Heavy lines, with arrowheads, show the closed path of FSF laser light. Dotted lines, with arrowheads, show the pump light path. Thin lines with arrowheads show seed and diagnostics light paths.

by $\nu_{AOM} = 80$ MHz, then returns to the fiber (1) for subsequent round trips. Aspherical lenses (3) and (10), with focal lengths 4.5 mm, collimate the light and couple the laser radiation into the fiber.

In such an arrangement, after each round trip the frequency of the intracavity radiation decreases by ν_{AOM}. The maximum efficiency of the AOM is about 87%, so some 13% of the intracavity power is lost with each pass. A set of FPEs (7) are usually inserted to decrease the spectral width of the FSF-laser and to provide reproducible and measurable loss characteristics.

As indicated in Fig. 1, the light in the ring laser circulates in a counterclockwise direction. An optical diode (6) inside the cavity diminishes the clockwise wave. The optical length of the ring FSF laser is 3.1 m, and its free spectral range (FSR) is about 96 MHz.

2.2. The pump laser

Excitation and consequent gain in the Yb^{3+}-doped fiber is produced by pump radiation of wavelength 980 nm from a fiber-pigtailed diode laser (11) [Multiplex, Inc. MTX9P], which enters the FSF ring path through a dichroic mirror (4) and thereafter couples into the Yb^{3+}-doped fiber by a lens (3). The maximum output power of this pump laser is 200 mW. An optical diode (12) reduces the influence of back reflection of the laser radiation on the pump laser.

2.3. The seed laser

The external seed radiation for the present work comes from a single-frequency external-cavity diode laser (13), constructed according to the Littman–Metcalf scheme [34]. It consists of a laser diode, an aspheric lens, a diffraction grating and a mirror. The spectral width of the laser radiation is less than 1 MHz. The seed-laser radiation passes through a cylindrical-lens telescope (14) and an optical diode (15) and enters the FSF laser cavity through the zeroth order of the AOM (9). The maximum power of the seed-laser radiation on the face of the AOM was about 1 mW. Only 2–3% of that was injected into the FSF laser fiber. As result, the injected seed power is much smaller than the intracavity laser power in the operation regime, and the seed laser can be considered as weak.

2.4. The diagnostics

Output from the FSF laser emerges through the dichroic mirror (8). It passes, through beamsplitters (16), (19) and (21), into several monitoring devices. A spectrometer (20), with a resolution of 50 GHz, monitors the optical spectrum of the FSF laser. Spectral characteristics requiring higher resolution are measured with the aid of two scanning Fabry–Perot interferometers (22) and (24), two photodiodes (23) and (25) and a digital oscilloscope (26). The first interferometer has a FSR of 800 GHz and a finesse of about 80, while the second one has a FSR of 7.9 GHz and a finesse of about 400. The time dependence of the FSF-laser output is monitored with a fast InGaAs photodiode (17) whose bandwidth is 5 GHz. The radio-frequency spectrum of the FSF-laser intensity is recorded by a radio-frequency spectrum analyzer (18), which is sensitive over a range from 9 kHz to 2.6 GHz.

3. Characteristics of the unfiltered FSF laser

Two measurable basic properties hold particular interest when characterizing the operation of the FSF laser. One is the output power, P_{out}, integrated over all frequencies, and the other is the spectral distribution of this output power. Both of these properties are affected by the power of the pump laser, by the gain (and loss) bandwidth within the FSF-laser cavity, and by the presence of an external seed laser (supplementing or competing with the ever-present spontaneous emission seed). Each of these factors is controllable; displays of the resulting FSF attributes – and comparison of these with theory – provide useful indicators of the FSF-laser operation.

3.1. Output power of the unfiltered FSF laser

A traditional diagnostic tool for characterizing laser operation is measurement of the total output power of a laser as the pump power is varied. Fig. 2 illustrates this dependence of output on pump input for the simplest configuration of the fiber FSF ring laser. For these results there was no external seed laser (only spontaneous emission within the range of frequencies where gain occurs), and no FPEs (element (7) in Fig. 1) to limit the gain bandwidth

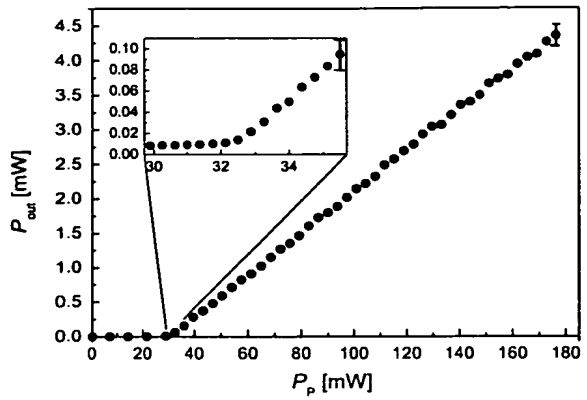

Fig. 2. Output power of unseeded FSF laser versus pump power for operation without intracavity FPEs. The inset shows details of the threshold. Representative error bars are shown on a single element of each plot.

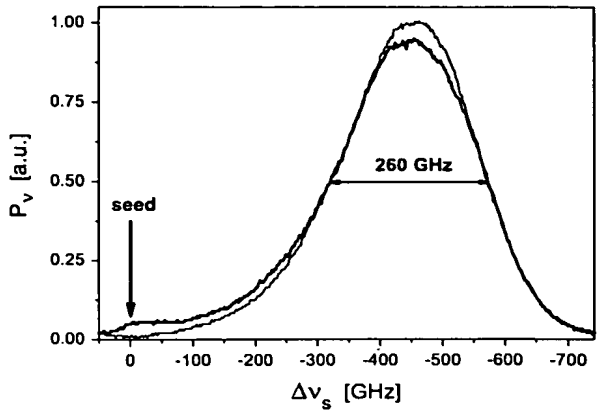

Fig. 3. Spectrum of the FSF laser with (thick line) and without (thin line) seed laser. The arrow marks the frequency of the external seed laser. The difference frequency $\Delta\nu_s$ expresses the offset from the seed laser frequency. The pump power is 90 mW, the seed laser power is 60 μW. There are no selective elements in the cavity (no FPEs).

within the ring cavity. To eliminate additional frequency-dependent losses caused by polarization effects in the fiber, we adjusted a polarization controller created by fiber coils to obtain a smooth laser spectrum. The results shown here do not depend on whether there is an injected seed.

This curve is a typical laser input–output curve [1]. It has a threshold for laser operation at about 32 mW; for higher pump powers the FSF laser output is a linear function of the pump power. The inset in Fig. 2 enlarges the threshold region of the figure. A clear threshold exists for this laser, in contrast to the reported behavior of a Ti:Sapph FSF laser with an intracavity filter [28], which showed a smooth onset of lasing rather than a well-defined threshold.

When no intracavity filter is present, the FSF fiber laser generates only CW radiation for pump powers up to the maximum available, 200 mW.This is the preferred operating regime for practical applications of FSF lasers to frequency ranging [27]. However, if some frequency selectivity of the cavity is introduced, an oscillatory regime exists that is typical for FSF lasers [8]: for low pump powers there occur low frequency (about 50 kHz) pulsations of the output power (with 100% modulation). These oscillatory regimes have been described in detail for a Ti:sapphire laser [28].

3.2. Spectrum of the unfiltered FSF laser

To obtain the spectral distribution of the FSF laser output, we used a scanning Fabry–Perot interferometer (FPI) (item (22) and (24) of Fig. 1). Fig. 3 shows the results obtained when the FPI had a FSR of 800 GHz and a finesse of 80. The figure shows typical results for the operation of the FSF laser without external seeding or with a weak seed laser that cannot significantly distort the spectrum of the FSF laser. When the FSF laser is not externally seeded, the observed spectral bandwidth of the FSF laser is 260 GHz (full-width at half-maximum, FWHM). When the external seed is weak, the spectrum is slightly broader and somewhat shifted towards the seed laser frequency. The width of the spectrum, Γ, is much smaller than the effective gain bandwidth determined jointly by the Yb^{3+}-doped fiber gain line and by dispersion of the AOM. We estimate the effective gain bandwidth to be about 10^4 GHz.

As will be noted in the following sections, the spectral narrowing and the asymmetric spectral profile are characteristic of FSF lasers, and are in accord with recent theory [33].

3.3. Dependence of the spectral width of the unfiltered FSF laser on pump power

When the FSF ring laser operates without any bandwidth-narrowing filters (the FPE (7) of Fig. 1), the spectral width is relatively insensitive to the pump power. Fig. 4 shows the dependence of the width Γ and the asymmetry

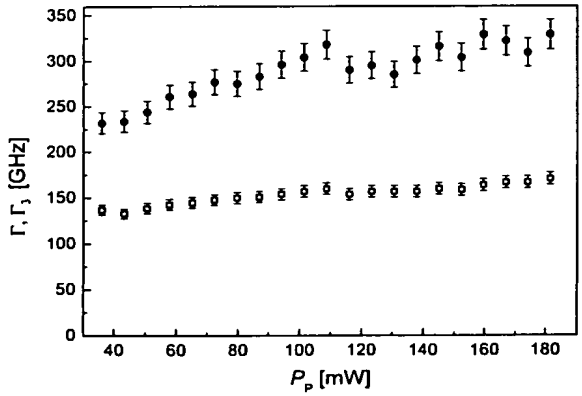

Fig. 4. Width Γ (□) and asymmetry parameter Γ_3 (●) of unfiltered FSF laser spectrum [FWHM] versus pump power.

parameter Γ_3 on the pump power. These parameters were obtained by fitting the experimental spectrum to the asymmetric Gaussian

$$P_\nu(\Delta\nu) = P_0 \exp\left[-\frac{(\Delta\nu - \Delta\nu_0)^2}{\Gamma^2} - \frac{(\Delta\nu - \Delta\nu_0)^3}{\Gamma_3^3}\right]. \quad (1)$$

The spectral width increases only slightly as the pump power increases from threshold (32 mW) to 160 mW.

4. Characteristics of the filtered FSF laser

The operation of a seeded FSF laser can be understood as follows. The intracavity field consists of many components equidistantly separated in frequency. The first one is the CW field of the seed-laser radiation coupled into the cavity. The frequency of the seed laser is normally set very close to the minimum of the frequency-dependent intracavity losses. The frequency of each subsequent component is larger by the AOM frequency. The amplitude of the component is a result of equilibrium between four competing processes:

(1) income from the adjacent component that has been frequency shifted by the AOM,
(2) gain, saturated by the total intensity of all spectral components,
(3) frequency dependent losses, (those present intrinsically and those added deliberately as spectral filters), and
(4) loss due to AOM frequency shifting to the next component.

The self-consistent theory of the dynamics of the FSF laser [33] predicts the formation of a stationary spectrum in which the total intensity does not fully saturate the gain. Thus, starting from the initial seed frequency, the amplitude of each component increases as long as the gain is larger than the losses. At some frequency the gain will no longer suffice to overcome the losses. Beyond this frequency the component amplitudes will decrease. Thus, the output spectrum will exhibit a maximum.

A similar picture applies when spontaneous emission provides the only seed. We can then imagine that the field in the cavity results from incoherent seed sources with different frequencies continuously distributed near the maximum of the effective gain profile (the difference between gain and frequency-dependent losses). In this case the spectrum is predicted [33] to be continuous with a shape similar to that observed with a seed laser.

The position of the spectral maximum, and the width of the output spectrum, are both predictable if one knows the spectral characteristics of the gain and loss mechanisms affecting the FSF laser. These are difficult to measure accurately – indeed, they vary irregularly and uncontrollably – but they can be controlled and accurately measured by introducing well-characterized spectral filters. Towards that end, we investigated a FSF-laser cavity containing a relatively broadband filter, created from FPEs (element (7) of Fig. 1). The effective FSR was 1 THz. The following paragraphs describe the observed properties of that system.

4.1. Loss profile and output spectrum of the filtered FSF laser

4.1.1. Broadly filtered FSF laser

Fig. 5a shows the measured relative transmission profile (dots) of the FSF cavity when a broadband FPE was present to act as a filter. The full line is a Gaussian fit to these values; this is an excellent approximation.

Fig. 5b shows the measured output spectrum of the FSF laser in more detail, as recorded using a scanning FPI with FSR of 800 GHz and finesse of 80. The vertical dashed line marks the maximum of the output spectrum. Physical intuition, validated by theory [33], predict that this maximum should occur where the saturated gain equals the losses from a cavity round trip [33]. This behavior allows us to find the full width of the frequency interval in which the saturated gain exceeds losses. We measured this width to be 180 GHz. It is significant that Fig. 5, which is entirely experimental, is basically the same as Fig. 2 from the theory paper [33]. As predicted by theory [33], the experimental spectrum is close

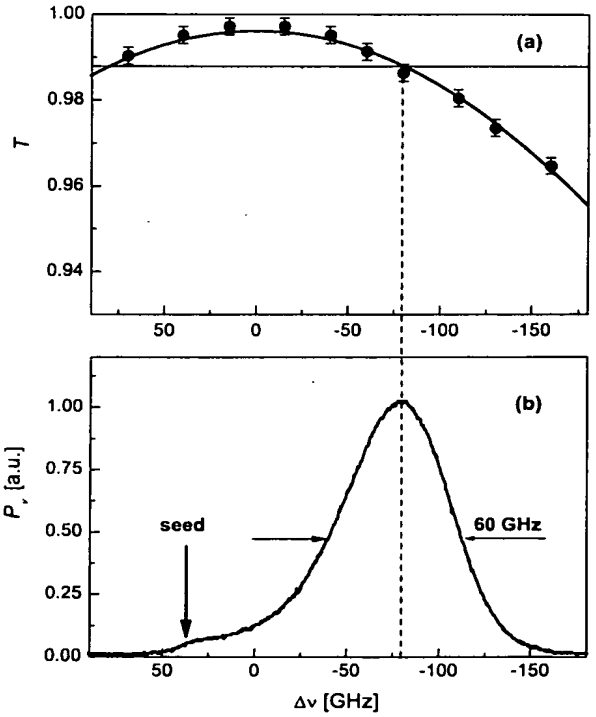

Fig. 5. (a) Transmission profile of broad filter, and (b) spectrum of seeded FSF laser with this filter inside the cavity. The detuning $\Delta\nu$ is defined as the difference between the observation frequency and the frequency of maximum filter transmission.

to a Gaussian near the maximum, but shows asymmetry in the wings of the profile. As also predicted, its maximum coincides with the zero of the effective gain.

4.1.2. Spectra of a narrowly filtered FSF laser with and without a seed laser

The only difference between the experimental results shown in Fig. 5 and the theory presented in Fig. 2 of Ref. [33] is that the experimental spectrum does not reveal the discrete structure of the output spectrum of a seeded FSF laser. This is predicted to consist of a multitude of discrete components, each separated by the frequency increment $\nu_{AOM} \equiv \Delta/2\pi = 80$ MHz of the AOM. To resolve these components it is necessary to limit the bandwidth of the cavity by inserting a very narrow bandwidth filter. Such filtering leads to a laser spectral width smaller than the FSR of 7.9 GHz for the available FPI. We accomplished this filtering by inserting into the cavity four FPEs, with FSR 1000, 200, 50 and 15 GHz. The resulting spectral output has a bandwidth of 2.8 GHz, in contrast to the 60 GHz bandwidth shown in Fig. 5.

The lower frame of Fig. 6 shows the output spectrum of the narrow-band FSF laser, as recorded using a scanning FPI with a FSR of 7.9 GHz and a finesse of 400. Arrows mark the spectral bandwidth (FWHM) of 2.8 GHz. The individual discrete spectral components expected from theory are clearly visible. For comparison, a solid line shows the spectrum observed when there is no external seed laser; as expected, the latter is a continuum, with a bandwidth of 2.7 GHZ.

The upper frame of Fig. 6 provides an expanded view of the individual spectral components. Vertical lines, rising from the lower border, mark increments of the AOM frequency. Fiducial marks along the top border occur at the spacing expected for longitudinal modes in a cavity whose length equals that of the FSF laser. The observed spectral components do not have the frequency spacing of longitudinal modes; they occur at multiples of the AOM frequency, as predicted.

It is worth noting that the experimental evidence of a discrete stationary spectrum, comprising a set of frequencies separated by the AOM frequency, does not conflict with the well-documented moving-comb model of a FSF laser [11]. In the moving-comb model the output of a FSF laser is a set of discrete frequencies ("teeth"), whose separation is the cavity axial mode interval $\Delta_{ax} = 2\pi\nu_{LM}$, and which shift steadily in frequency at the rate $\gamma_c = \Delta/\tau_r$ where τ_r is the round-trip time. In [33] we proved that, in a FSF laser without fluctuations, both models are equivalent. This becomes immediately obvious if one notices that the moving comb model [11] describes a process that is periodic in time, with the period $2\pi/\Delta = 1/\nu_{AOM}$. This means that the process can be considered as a discrete Fourier series with the frequency difference Δ between components, as fixed by the AOM. Although the FSF laser, when seeded by CW radiation, is periodic, it will not be periodic when the field grows from a short pulse.

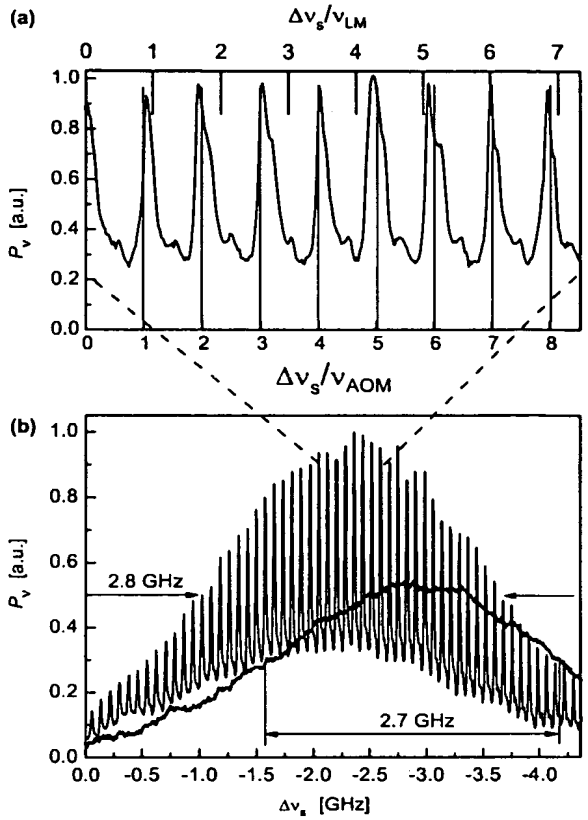

Fig. 6. Spectrum of the FSF laser observed through a narrow bandwidth filter: the power spectral density P_ν (arbitrary units) versus $\Delta\nu_s$, the frequency offset from the frequency of seed laser. (a) expanded view of (b), with $\Delta\nu_s$ in units of the AOM frequency. Thin lines are with external seed laser, thick lines are without seed laser.

To display a moving comb of frequencies one needs a spectral recording device with bandwidth $\delta\omega$ smaller than the cavity axial mode interval Δ_{ax} (to resolve adjacent components). The signal integration time $1/\delta\omega$ has to be shorter than the time interval $1/\Delta$ between the occurrence of teeth near the observation frequency. Thus, the bandwidth $\delta\omega$ must satisfy the condition $\Delta < \delta\omega < \Delta_{ax}$. Because in our experiment we have the condition $\Delta > \Delta_{ax}$, we do not see any comb-like structure. In [31] the moving comb has been observed for a very small FSF frequency (1 MHz or less) realized by shifting 80 MHz up by one AOM and 79 MHz down by a second AOM.

These restrictions on the bandwidth requirements are relevant for displaying a moving comb from which one could directly measure the changing positions of frequency components, i.e. the chirp. Alternatively, one can use a Michelson interferometer and interpret the results to infer a chirped frequency of a moving comb with fluctuating parameters, as was done by Kasahara et al. [11]. We discuss this further in a forthcoming paper submitted to Optics Communications.

(3)

Because the output bandwidth is important for applications, it is useful to estimate the frequency range over which a seeded comb can extend. For a broadly filtered (and especially for an unfiltered) FSF laser, direct observation of a stationary comb is impossible with our scanning FPI for any total laser output bandwidth that is larger than the FSR of the FPI. Nevertheless, we have observed [27] that, when using a technique requiring coherence between comb components, the distance resolution is directly proportional to the bandwidth Γ of the FSF laser (see Fig. 7 in [27]). This observed linearity demonstrates that the FSF laser maintains coherence of the acousto-optic modes across the entire spectrum of the FSF laser, right up to the spectrum width of about 3500 GHz. This corresponds to about 80,000 frequency components (comb teeth).

4.2. Output power of the spectrally filtered FSF laser

Fig. 7a shows that the output power from the FSF laser depends upon the pump power when a broadband FPE is inserted into the ring cavity but no external seed laser is present. In contrast to the behavior of the unfiltered FSF laser (see Fig. 2), the output of the FSF laser with the FPE spectral filter in place exhibits a regime of CW operation (labeled C, this exists for $P_O < P_{out} < P_U$ as the pump power increases), a regime of low-frequency oscillation (labeled O, this exists for $P_{out} < P_O$ as the pump power increases and for $P_{out} < P_D$ as the pump power decreases), and a third regime, one characterized by modelocking (labeled M, this exists for $P_{out} > P_U$ as the pump power increases and for $P_{out} > P_D$ as the pump power decreases). Unlike the unfiltered laser, for which a CW regime exists for all available pump power (up to 200 mW), the FSF laser exhibits mode locking when a broadband intracavity FPE filter is in place and the pump power is high. (When the filter bandwidth is narrow, no FSF modelocking regime exists.) The transition to mode locking is apparent in the output when viewed by the radio-frequency (RF) analyzer. Fig. 8 shows the RF analyzer signal near the axial mode frequency of the ring cavity (about 95.88 MHz). In the CW regime of FSF laser operation, there is no axial mode beating. However, near the frequency corresponding to an axial-mode difference there occurs a resonance increase in the spectral density of laser output power fluctuations. This resonance arises because any fluctuation in the laser intracavity power persists much longer than a round-trip time, thereby contributing periodically to the output power fluctuations. The width of the resonance is determined by the fluctuation life-time. This picture changes completely in the mode-locking regime: the amplitude of the signal grows by more than two orders of magnitude and the beating signal is almost monochromatic (the width of the spectrum in Fig. 8(b) is determined by the apparatus function). The narrowing of the RF spectrum is clear evidence that, in the modelocking regime, there exist frequency components separated by the axial mode frequency. We observe a signal arising from the beating between these phase-synchronized components. The time duration of the pulses generated in the modelocking regime is determined, as usual for fluctuation-free pulses, by the total laser spectral bandwidth. It is about 10 ps.

Unlike behavior reported with a Ti:Saph FSF laser [8], the fiber FSF exhibits no discontinuity in the spectrally integrated total power at the onset of modelocking. For an unseeded laser, the interval of pump powers where the CW regime exists is quite narrow (from $P_O \simeq 42$ mW to $P_U \simeq 49$ mW). The modelocking behavior shows a pronounced hysteresis, evident in Fig. 7. As the pump power increases, mode locking begins when the pump power is P_U, but when the power is decreasing the modelocking ceases when the pump power is P_D. For pump power less than P_D the CW regime does not exist at all.

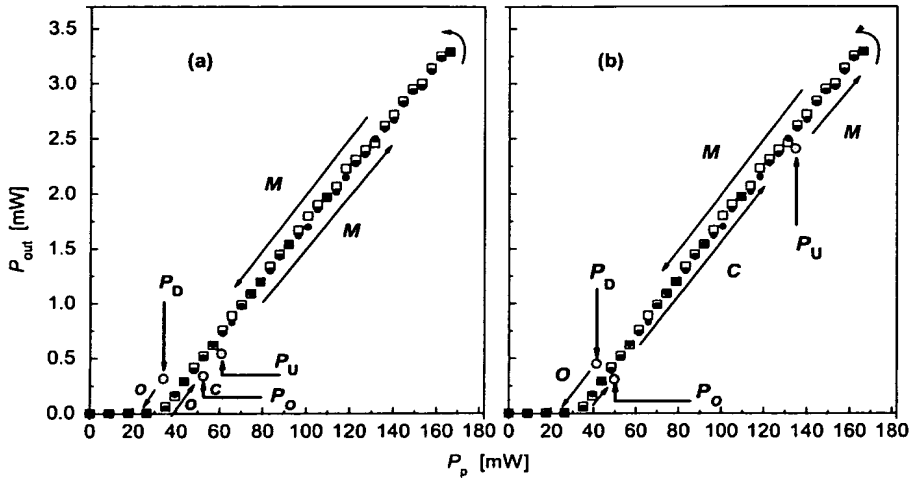

Fig. 7. Output power P_{out} of the FSF laser versus pump power P_P when (a) the cavity includes a broadband filter and no seed laser, and (b) with external seed-laser.

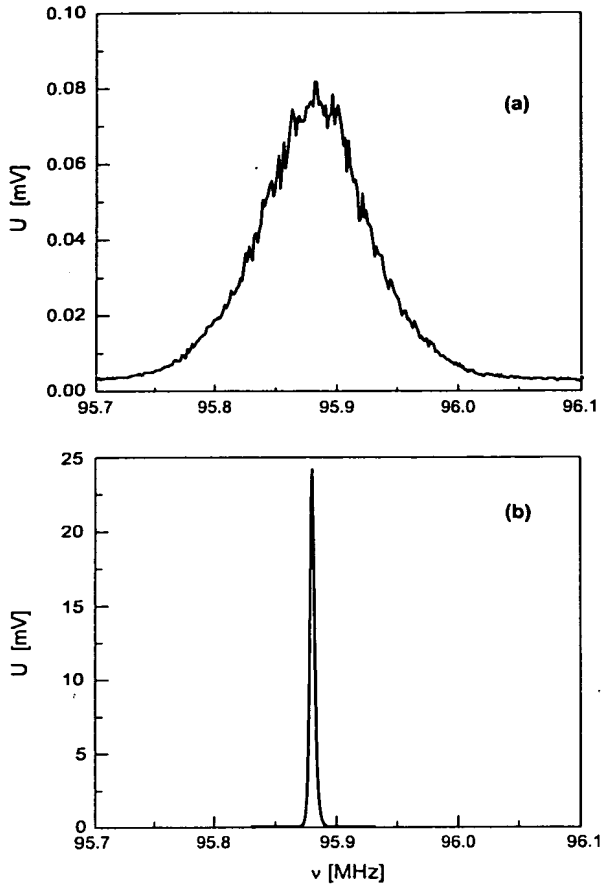

Fig. 8. Radio frequency analyzer signal near the axial mode difference frequency of the ring cavity (about 95.88 MHz). Frame (a) is for the CW regime, and frame (b) is for the self mode-locking regime.

4.3. Seeded self mode-locking

4.3.1. Dependence on the seed-laser frequency

The operation of the filtered FSF laser depicted in Fig. 7a relies on signal growth from spontaneous emission. The use of an external seed laser provides better control over the output characteristics, evidenced in the values of P_U and P_D where self modelocking begins and ends. The seed laser increases thresholds of the beginning and the end of the mode-locking interval, thereby enlarging the regime of "useful" CW operation (see Fig. 7).

Fig. 9 shows the pump powers P_U and P_D corresponding to the beginning and ending of self modelocking as a function of the detuning of the seed laser frequency from the frequency where the cavity loss is minimum (the central frequency of the inserted FPE). The thresholds P_U and P_D are reproducible, as indicated by the size of the error bars in the figure.

For reference, the figure also indicates, by arrows, the threshold for laser operation and the values obtained when there is no seed. The influence of the seed laser is most pronounced when its frequency is 30 GHz higher than the frequency of minimum loss.

4.3.2. Dependence on the seed-laser power

As the seed power increases, the hysteresis changes and the pump powers P_U and P_D, for which self modelocking begins and ends, each increase. Fig. 10 shows the dependence of P_U and P_D upon the seed laser power. Horizontal arrows mark the values observed when there is no seed. Thus, the seed laser suppresses self modelocking. This shows that the self modelocking regime is qualitatively different than pulsed operation of a seeded FSF laser considered in [33].

4.3.3. Spectra of the FSF laser in the self-modelocked regime

Fig. 11 illustrates the behavior of self mode-locking in the fiber FSF laser. A large shift and distortion of the spec-

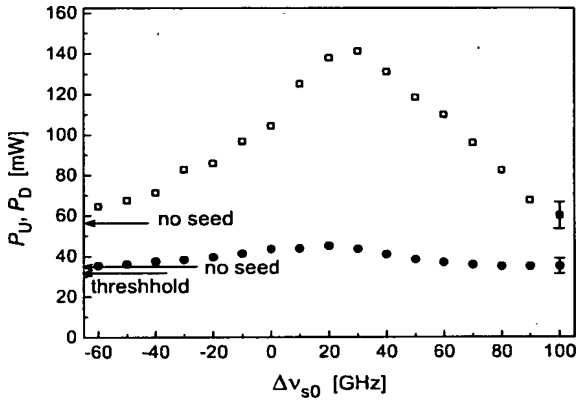

Fig. 9. Pump powers P_U and P_D corresponding to beginning (□) and ending (●) of self modelocking versus detuning $\Delta\nu_{s0}$ of the seed laser frequency from the cavity loss minimum. Arrows mark the laser operation threshold and the values obtained when there is no seeding.

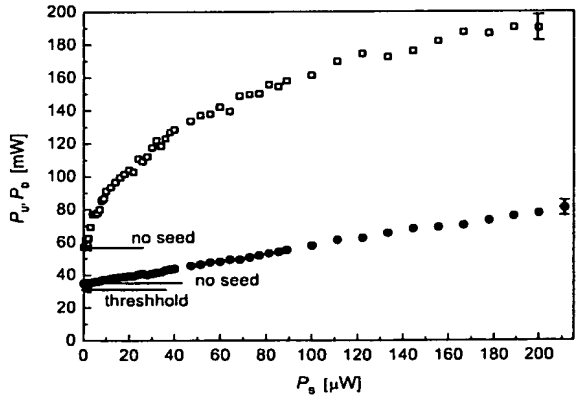

Fig. 10. Pump powers P_U and P_D corresponding to the beginning (□) and ending (●) of self mode-locking versus power of the seed laser. Arrows mark the thresholds without external seed and the laser operation threshold.

trum are observed when mode-locking occurs. This contrasts with the mode-locking behavior in a Ti:Saph FSF laser [8]. There the spectrum in the mode-locking regime underwent only a small frequency shift while maintaining the same shape. The spectrum in Fig. 11 shows that two regimes (CW and mode-locking) seem to coexist in our laser, localized in different spectral areas. Mode-locking exists near the minimum of intracavity losses, whereas the spectrum of the CW regime is shifted to lower frequencies according to the sign of the AOM shift. Observations of the spectral changes occurring when the external seed laser is turned on (intermediate line on Fig. 11) confirm this interpretation. The laser power is redistributed in such a way that the CW-regime spectrum increases and mode-locking diminishes significantly. This behavior confirms the conclusion that the seed laser suppresses self mode-locking by promoting a redistribution of laser power from mode-locking to CW spectral regions.

4.4. Comparison with theory

Our earlier work [33] presented a theoretical description of the spectral characteristics of the FSF laser seeded both by spontaneous emission and a monochromatic external seed laser. That theory predicts that, apart from a small asymmetry, the FSF laser spectrum is accurately approximated by a Gaussian,

$$P_\nu(\Delta\nu) = P_0 \exp\left(-\left[\frac{(\Delta\nu-\omega_0)^2}{\Gamma^2}\right]\right), \tag{2}$$

where $\Delta\nu$ is the detuning of the observation frequency from the minimum of the filter losses. This Gaussian form describes both the continuous spectrum of the laser seeded by spontaneous emission and the envelope of the comb

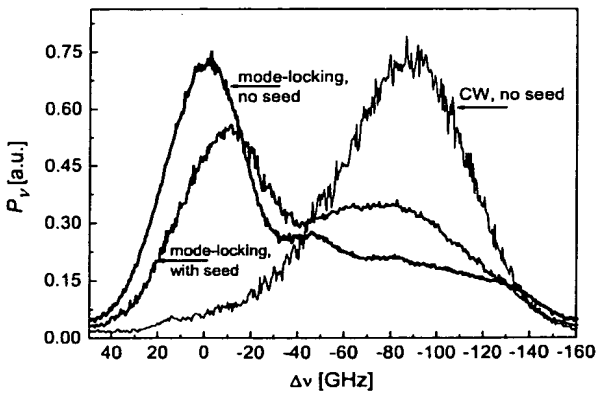

Fig. 11. Spectrum of the FSF laser when the broadband filter is inserted into the cavity: the thin line is valid for CW operation (regime (C)) without an external seed laser; the intermediate line is the self mode-locking (regime (M)) with a seed laser; the thick line is the self mode-locking (regime (M)) without a seed laser. The detuning $\Delta\nu$ is the difference between the observation frequency and the frequency of maximum filter transmission.

of discrete components for a FSF laser seeded by a monochromatic laser. Our previous work [33] presented simple formulas for the spectral width Γ and the shift ω_0 of the spectral maximum from the minimum of filter losses. For a FSF laser without external seed, the relevant formulas are

$$\Gamma = \frac{\gamma}{\sqrt{\sigma}}, \tag{3}$$

$$\omega_0 = \sigma\gamma, \tag{4}$$

where

$$\gamma = [\Delta\Gamma_f^2]^{1/3} \tag{5}$$

and

$$\sigma = \left(\frac{3}{4}\ln\frac{1}{\beta_{sp}}\right)^{1/3}. \tag{6}$$

The parameters characterizing the spectrum depend mainly on the precisely known AOM frequency and on the filter width, parameterized as Γ_f. As mentioned above, quantitative comparison of experimental results with theory prediction requires the use of well-characterized spectral intracavity filters. With such a filter emplaced, the parameter Γ_f is obtained by fitting the measured variation of filter transmission versus frequency to the theoretical curve.

The parameter σ, determined by the small parameter $\beta_{sp} \ll 1$, characterizes spontaneous emission. In principle β_{sp} can be estimated from characteristics of the fiber and the laser cavity. However, it is more convenient to derive the parameter σ from Eqs. (3) and (4) as

$$\sigma = \left(\frac{\omega_0}{\Gamma}\right)^{2/3}, \tag{7}$$

thereby allowing estimation from experimental data for the width and shift of the laser spectrum.

Figs. 12 and 13 show measured values of the width Γ and frequency of spectral maximum ω_0 versus pump power. Filled and empty points refer to laser operation with and without an external seed laser. Different combinations of intracavity etalon filters were used: (1) one etalon (FSR 1000 GHz), (2) two etalons (FSR 1000 and 200 GHz) and (3) three etalons (1000, 200 and 50 GHz). The measurement errors are less than the symbol sizes. Table 1 gives the values of Γ_f obtained, as described before, by fitting the measured variation of filter transmission versus frequency to the theoretical Gaussian profile The table also collects calculated and measured parameters for laser operation without an external seed laser. Using the mean value of the parameter $\sigma = 1.98$, we calculated the shift ω_0 and width Γ. To take into account the apparatus width of the FPEs (5 GHz for cases 1 and 2, and 0.5 GHz for case 3), we evaluated a convolution of a Gaussian spectrum with the apparatus function and fitted it to a Gaussian with a width Γ_{calc}. The straight lines in Figs. 12 and 13 mark the theoretical values of Γ_{calc} and $\omega_{0,calc}$.

Table 1 and Figs. 12 and 13 show excellent quantitative agreement between theory and experiment when there is no

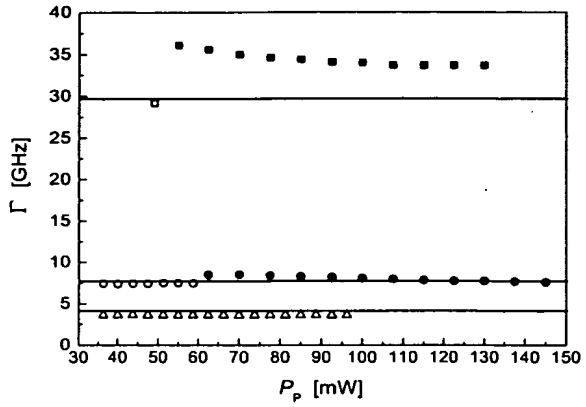

Fig. 12. The spectral width of the FSF laser Γ versus pump power P_P for different combinations of intracavity etalon filters: one etalon (FSR 1000 GHz, square points), two etalons (FSR 1000 and 200 GHz, round points) and three etalons (1000, 200 and 50 GHz, triangular points). Solid points: external seed is present; open points: no external seed. The straight lines show the calculated values of Γ_{calc}.

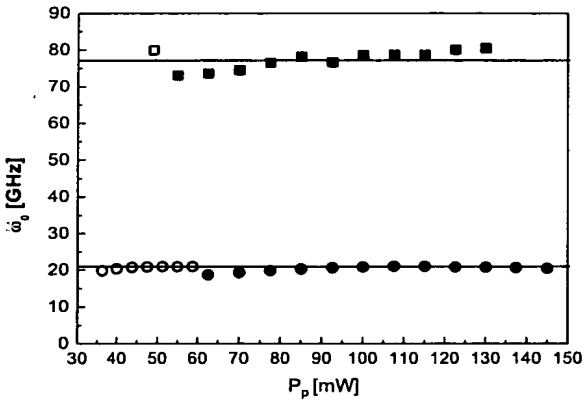

Fig. 13. The shift ω_0 of the spectral maximum of the FSF laser with respect to the minimum of the overall losses versus pump power P_P for one etalon (FSR 1000 GHz, square points) and two etalons (FSR 1000 and 200 GHz, round points). Solid points: external seed is present; open points: no external seed. The straight lines show the calculated $\omega_{0,calc}$.

Table 1
Experimental and theoretical parameters

Case	1	2	3
FSR	1000 GHz	200 GHz	50 GHz
Γ_f	867 GHz	120 GHz	41 GHz
γ	39.2 GHz	10.5 GHz	5.1 GHz
σ	1.97	1.99	–
Γ_{calc}	29.9 GHz	7.64 GHz	3.82 GHz
Γ_{meas}	29 GHz	7.5 GHz	3.6 GHz
$\omega_{0,calc}$	77.2 GHz	20.8 GHz	10.1 GHz
$\omega_{0,meas}$	80 GHz	21 GHz	–

external seeding. When an external seed is present, there is competition between spontaneous emission and seeding that leads to a slight, but still observable, dependence of Γ and ω_0 upon pump power.

5. Summary and conclusions

This paper presents detailed properties of a FSF laser constructed in a ring configuration, using an Yb^{3+}-doped fiber as the gain medium and an acousto-optic modulator as the frequency shifter.

The results demonstrate the absence of longitudinal modes for the FSF laser when it operates without any external seed. When a monochromatic seed is present, the output spectrum exhibits the predicted discrete frequencies built by successive AOM increments upon the seed frequency. The envelope of these frequency components follows the predicted analytic form, rising to a maximum at the predicted frequency. The peak frequency and the width of the spectrum are essentially independent of pump power, as theory predicts.

Examples of the spectra and output power characteristics with different intracavity selective filters have been presented here. These demonstrate that, by increasing the power of the seed laser, it is possible to increase the threshold power where mode-locking begins. Such an increase enlarges the CW-regime of the output radiation – the "useful" regime for application to distance measurements.

By using an intracavity filter with known loss characteristics, we have been able to calculate important laser parameters. Using only a single parameter, obtained by fitting observations, we are able to predict all other parameters in excellent agreement with experiment.The results are in perfect agreement with our earlier theory [33]. This detailed agreement with experiment gives us confidence that, within its expected domain of applicability, the theory provides a satisfactory basis for predicting FSF-laser properties. Recent work provides a detailed description of an application of this FSF laser to distance measurements [27].

Acknowledgements

We acknowledge support by the Stiftung Rehinland-Pfalz für Innovation. L.P.Y. acknowledges support by the Deutsche Forschungsgemeinschaft (436-UKR-113/16). B.W.S. and L.P.Y. acknowledge support from the Max Planck Forschungspreis 2003.

References

[1] A.E. Siegman, Lasers, Univ. Sci. Books, Mill Valley, CA, 1986; P. Milonni, J.H. Eberly, Lasers, Wiley, New York, 1988.
[2] F.V. Kowalski, S.J. Shattil, P.D. Hale, Appl. Phys. Lett. 53 (1988) 734;
K. Nakamura, K. Kasahara, M. Sato, H. Ito, Opt. Commun. 121 (1995) 137;
K. Nakamura, F. Abe, K. Kasahara, T. Hara, M. Sato, H. Ito, IEEE J. Quant. Electron. 33 (1997) 103;
I.C.M. Littler, S. Balle, K. Bergmann, Opt. Commun. 88 (1992) 514; I.C.M. Littler, S. Balle, K. Bergmann, J. Opt. Soc. Am. B 8 (1991) 1412.
[3] L.C. Foster, M.D. Ewy, C.B. Crumly, Appl. Phys. Lett. 6 (1965) 6.
[4] W. Streifer, J.R. Whinnery, Appl. Phys. Lett. 17 (1970) 335.
[5] D.J. Taylor, S.E. Harris, S.T.K. Nieh, T.W. Hansch, Appl. Phys. Lett. 19 (1971) 269.

(3)

[6] A.P. Willis, A.I. Ferguson, D.M. Kane, Opt. Commun. 116 (1995) 87.
[7] K.A. Shore, D.M. Kane, IEEE J. Quant. Electron. 35 (1999) 1053.
[8] G. Bonnet, S. Balle, Th. Kraft, K. Bergmann, Opt. Commun. 123 (1996) 790.
[9] J. Geng, S. Wada, Y. Urata, H. Tashiro, Opt. Lett. 24 (1999) 676.
[10] J. Geng, S. Wada, N. Saito, H. Tashiro, Opt. Lett. 24 (1999) 1635.
[11] K. Kasahara, K. Nakamura, M. Sato, H. Ito, IEEE J. Quant. Electron. 34 (1998) 190.
[12] K. Nakamura, T. Miyahara, M. Yoshida, T. Hara, H. Ito, IEEE Photon. Techn. Lett. 10 (1998) 1772.
[13] K. Nakamura, T. Hara, M. Yoshida, T. Miyahara, H. Ito, IEEE J. Quant. Electron. 36 (2000) 305.
[14] M.J. Lim, C.I. Sukenik, T.H. Stievater, P.H. Bucksbaum, R.S. Conti, Opt. Commun. 147 (1998) 99.
[15] M. Cashen, V. Bretin, H. Metcalf, J. Opt. Soc. Am. B 17 (2000) 530.
[16] I.C.M. Littler, H.M. Keller, U. Gaubatz, K. Bergmannn, Z. Phys. D 18 (1991) 307.
[17] H. Sabert, E. Brinkmeyer, Electron. Lett. 29 (1993) 2122.
[18] H. Sabert, E. Brinkmeyer, J. Lightwave Technol. 12 (1994) 1360.
[19] O.G. Okhotnikov, Electron. Lett. 34 (1998) 1493.
[20] J.M. Sousa, O.G. Okhotnikov, Opt. Commun. 183 (2000) 227.
[21] S.H. Yun, D.J. Richardson, D.O. Culverhouse, B.Y. Kim, IEEE J. Sel. Top. Quant. Electron. 3 (1997) 1087.
[22] S.K. Kim, M.J. Chu, J.H. Lee, Opt. Commun. 190 (2001) 291.
[23] I.R. Perry, R.L. Wang, J.R.M. Barr, Opt. Commun. 109 (1994) 187.
[24] M. Yoshida, K. Nakamura, H. Ito, IEEE Photon. Techn. Lett. 13 (2001) 227.
[25] M. Yoshida, T. Miyamoto, N. Zou, K. Nakamura, H. Ito, Opt. Exp. 9 (2001) 207.
[26] M. Yoshida, K. Nakamura, H. Ito, Rev. Laser Eng. 27 (1999) 490.
[27] V.V. Ogurtsov, L.P. Yatsenko, V.M. Khodakovskyy, B.W. Shore, G. Bonnet, K. Bergmann, Opt. Commun., in press, doi:10.1016/j.optcom.2006.04.070.
[28] M. Stellpflug, G. Bonnet, B.W. Shore, K. Bergmann, Opt. Exp. 11 (2003) 2060.
[29] J.R.M. Barr, G.Y. Liang, M.W. Phillips, Opt. Lett. 18 (1993) 1010.
[30] F. Kowalski, J.A. Squier, J.T. Pinckney, Appl. Phys. Lett. 50 (1987) 711;
F.V. Kowalski, P.D. Hale, S.J. Shattil, Opt. Lett. 13 (1988) 622;
P.D. Hale, F.V. Kowalski, IEEE J. Quant. Electron. 26 (1990) 1845;
P.I. Richter, T.W. Hänsch, Opt. Commun. 85 (1991) 414;
M.W. Phillips, G.Y. Liang, J.R.M. Barr, Opt. Commun. 100 (1993) 473;
J. Martin, Y. Zhao, S. Balle, K. Bergmann, M.P. Fewell, Opt. Commun. 112 (1994) 109.
[31] S. Balle, I.C.M. Littler, K. Bergmann, F.V. Kowalski, Opt. Commun. 102 (1993) 166.
[32] C.C. Cutler, IEEE J. Quant. Electron. 28 (1992) 60;
I.C.M. Littler, J.H. Eschner, Opt. Commun. 87 (1992) 44;
S. Balle, K. Bergmann, Opt. Commun. 116 (1995) 136;
K. Kasahara, K. Nakamura, M. Sato, H. Ito, Opt. Rev. 4 (1997) 180.
[33] L. Yatsenko, B.W. Shore, K. Bergmann, Opt. Commun. 236 (2004) 183.
[34] M.G. Littman, H.J. Metcalf, Appl. Opt. 17 (1978) 2224.

Available online at www.sciencedirect.com
ScienceDirect
Optics Communications 281 (2008) 1679–1685
OPTICS COMMUNICATIONS
www.elsevier.com/locate/optcom

An all-fiber frequency-shifted feedback laser for optical ranging; signal variation with distance

V.V. Ogurtsov [a], V.M. Khodakovskyy [a], L.P. Yatsenko [a], B.W. Shore [b,*], G. Bonnet [b], K. Bergmann [b]

[a] *Institute of Physics, Ukrainian Academy of Sciences, Prospect Nauki 46, Kiev-39, 03650, Ukraine*
[b] *Technische Universität Kaiserslautern, 67653 Kaiserslautern, Germany*

Received 14 November 2007; accepted 17 November 2007

Abstract

A recent paper [L.P. Yatsenko et al., Opt. Commun. 242 (2004) 581] provided a first-principles prediction for the optical ranging signals obtained when using a frequency-shifted feedback (FSF) laser system, seeded by a phase-modulated laser. Such a system has many useful advantages over other alternative FSF laser techniques. We report here experimental verification of that theory, specifically the variation of the amplitude modulation signal with both distance and modulation index of the seed laser. We describe the operation of an all-fiber FSF laser that uses an Er^{3+}-doped active fiber as the gain medium. To improve the signal and minimize the noise we seed the FSF laser with a phase-modulated (PM) laser; the measurement of distance derives from a measurement of amplitude modulation within a narrow frequency interval. We demonstrate that the resulting system is capable of fast and precise measurements. With the bandwidth limitations of our current system we achieved an accuracy better than 0.1 mm. Although measurements based on interferometry offer the potential for much greater accuracy under carefully controlled conditions, the present method does not suffer from the presence of a material-dependent phase shift at the surface of the measured object.

PACS: 42.55.–f; 42.60.Da; 42.55.Ah

Keywords: Lasers; Laser ranging; Frequency-shifted feedback

1. Introduction

A frequency-shifted feedback (FSF) laser is a special type of laser with a frequency shifter inside the cavity (it can be an acousto-optic modulator (AOM), a moving diffractive grating, etc.) [1–9]. The presence of such an element that shifts radiation frequency by a fixed value during each cavity round trip provides FSF lasers with several unusual properties not found with ordinary lasers. Most notably, the spectrum of a FSF laser has no well-defined longitudinal modes because the frequency shifter destroys the constructive interference inside the cavity. This makes a FSF laser a potential source of wideband continuous radiation, a property that has already found many applications [10–14]. Another important feature of a FSF laser is that, because of periodic frequency shifting on each round trip, the output radiation can be regarded as frequency swept (chirped) [6,15]. After passing through a Michelson interferometer any chirped laser will produce an amplitude modulation at a frequency proportional to the difference in length of the two interferometer arms. This makes the FSF laser a promising tool for optical ranging of distances up to several kilometers [16,17].

As describe earlier [24], optical ranging with a FSF laser can be greatly improved by using an external phase-modulated monochromatic laser to seed the FSF laser, thereby

* Corresponding author. Tel.: +1 925 455 0627.
E-mail address: bwshore@alum.mit.edu (B.W. Shore).

0030-4018/$ - see front matter © 2007 Elsevier B.V. All rights reserved.
doi:10.1016/j.optcom.2007.11.074

improving the signal detection and lessening the noise. This method was demonstrated experimentally [18] with an accuracy better than 10 μm.

Ranging devices based on all-fiber FSF lasers hold promise for practical application because of their robust and compact construction. The use of an Er^{3+}-doped active fiber as a gain medium offers particular advantages because their central wavelength, 1.55 μm, is used in telecommunication and therefore there are many readily available inexpensive fiber elements and devices for that wavelength. Another advantage of erbium lasers, very important for any industrial application, is their safety for eyes.

Our technique, like those based on interferometry, has at first glance an intrinsic ambiguity regarding the deduction of a length from a time or frequency: the measurements only give a result modulo an increment. Interferometric methods commonly use the technique of an effective wavelength, based on the use of two wavelengths or a phase modulation, to resolve the ambiguity. We have noted appropriate approaches to overcome this problem.

The present paper describes the experimental characteristics of an all-fiber FSF laser with Er^{3+}-doped active fiber as the gain medium. It is seeded by a phase-modulated (PM) laser for precise measurements of distances. Using this laser we are able to confirm the recent first-principles derivation [24] of the dependence of signal strength upon distance; the predicted Bessel function behavior is clearly seen.

2. Er^{3+}-doped fiber FSF laser

As shown in Fig. 1, the all-fiber FSF laser consists of a fiber cavity (optical length 19.2 m), into which is inserted an Er^{3+}-doped active fiber (5 m long) pumped by a diode laser of wavelength 980 nm) through a wavelength division multiplexer (WDM). The frequency-shifting element is an acousto-optic modulator (AOM) that upshifts the intracavity radiation by 80 MHz with each round trip. Output and seed insertion occurs through two 10% couplers. We use two couplers instead of one to avoid placing 90% of the

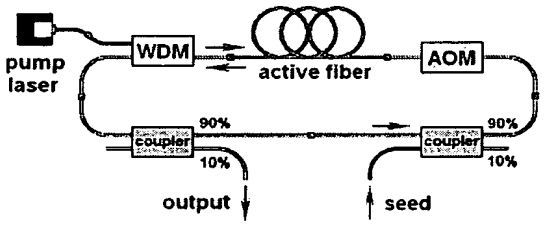

Fig. 1. Layout of the all-fiber FSF laser. Light from a pump laser enters the fiber circuit through a WDM (top left) and provides gain in an Er^{3+}-doped active fiber (shown as loops). Within the circuit the FSF light travels counterclockwise, starting from an external seed laser (lower right) entering the circuit through a coupler that transmits 10% of this light. An AOM induces a frequency upshift of 80 MHz prior to amplification in the active fiber. A second coupler diverts 10% of the light into output for observation.

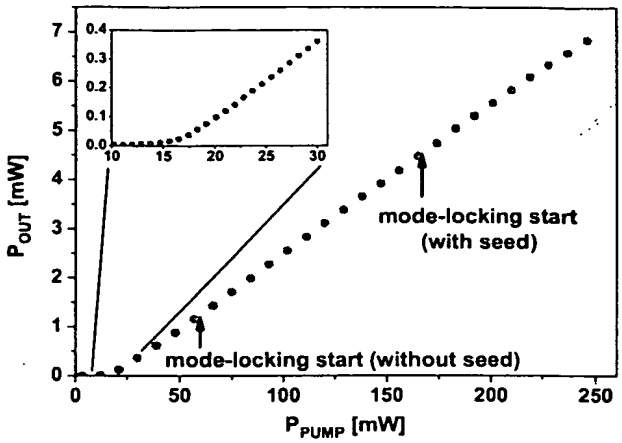

Fig. 2. Power characteristics of the all-fiber FSF laser with and without the seed laser: output power P_{out}, in mW, as a function of pump power P_{pump}, also in mW. The insert shows the threshold region. The output exhibits mode-locking, with consequent formation of pulse trains, when the pump power is sufficiently large. The arrows show the beginning of the mode-locking regime with and without external seed: the presence of the seed increases the power at which mode-locking starts. The useful regime for ranging is to the left of these arrows.

seed laser power into the output radiation [19]. All fiber components are joined by a fusion splice.

The output characteristics of our FSF laser are typical (see Fig. 2): the output power increases linearly with the pump power above a threshold of about 15 mW pump. A common feature of FSF lasers [5,19] is that for sufficiently high pump power a self mode-locking regime usually exists. Such pulse-train output is not suitable for optical ranging. In our laser, in the absence of the seed laser, mode-locking appears at quite low pump power (about 60 mW). Injection of an external CW seed greatly increases the threshold pump power for self mode-locking from about 60 mW to about 170 mW, thereby extending the CW-regime that is suitable for distance measurements [19].

The spectrum of this laser with and without external monochromatic seed is a slightly asymmetric Gaussian (Fig. 3) with FWHM 150–160 GHz. The FSF laser spectrum without a seed laser is continuous whereas with a seed it consists of equidistant components (unresolved in Fig. 3) separated by the AOM frequency [15,19,20].

3. Ranging with a FSF laser seeded by a phase-modulated external laser

The output radiation from a FSF laser can be described by a so-called "moving comb" model [15,16,20–23]. In this model a FSF laser, characterized by a round-trip time τ_r and an AOM frequency Δ, has an output spectrum comprising a very large number (103 or more) of equidistant frequencies (comb teeth), separated by the cavity axial mode interval $\Delta_c = 2\pi/\tau_r$, and moving with the rate $\gamma \equiv \Delta/\tau_r$,

$$\omega_n(t) = \omega_{max} + \gamma t - n\Delta_c. \quad (1)$$

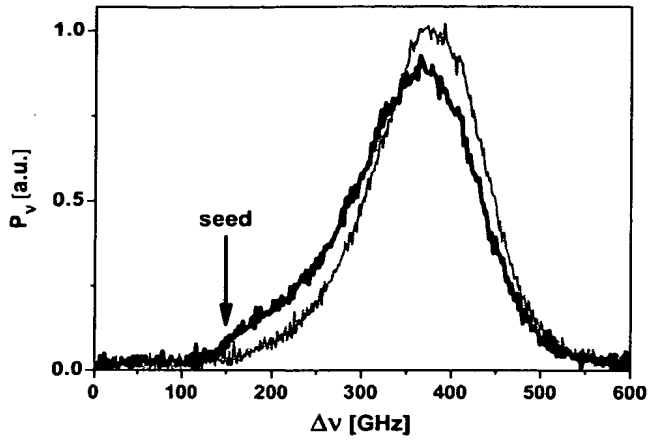

Fig. 3. Spectrum of the all-fiber FSF laser with (thick black line) and without (thin red line) the external seed laser. The arrow marks the frequency of the seed laser. The presence of the seed introduces some distortion of the spectrum, but it remains reasonably well-described by a Gaussian. (For interpretation of the references to color in this figure legend, the reader is referred to the web version of this article.)

Here, as in previous work, the constant ω_{max} is the frequency at which the time varying component has maximum amplitude. Fig. 4aa portrays, at a fixed time t, this frequency comb. Such a field, when delayed by time increment T, will again appear as a frequency comb, but offset (at time t) by a frequency increment γT (see Fig. 4b).

For application to ranging these two fields are those of the two arms of a Michelson interferometer whose arms differ in length by L. The resulting time delay $T = 2L/c$ produces a set of difference frequencies, from combinations

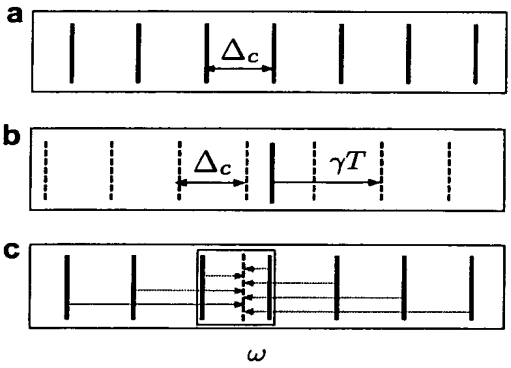

Fig. 4. (a) A portion of the sequence of equidistant discrete FSF-output frequencies (solid vertical lines) at a fixed time t, separated by the cavity-mode spacing Δ_c. (b) The output frequencies (dashed vertical lines) after the field undergoes a delay in time, as would occur with a reflected field. Shown is one possible value of γT that would produce this sequence, along with a single unshifted component (solid line); other possibilities differ by $n\Delta_c$, with integer n. (c) Arrows mark some of the frequency differences that are beat-frequency signals, observable as resonances. Those pointing to the right contribute to the "direct" resonances, those to the left contribute to the "reverse" resonances. The central rectangle encloses a frequency interval of size Δ_c used for measurement.

of different teeth of the reference and reflected fields. Fig. 4c shows some of these frequencies. Two classes occur, distinguished in the figure by arrows pointing to the right and arrows pointing to the left. These frequency differences are observed as beat signals at the frequencies

$$\omega_B^+(q) = q\Delta_c + \gamma T \tag{2}$$

and

$$\omega_B^-(p) = p\Delta_c - \gamma T \tag{3}$$

with integer $q, p = 0, \pm 1, \pm 2, \ldots$

At each frequency $\omega_B^{\pm}(n)$ the beating signal is a sum of many contributions from paired teeth of the reference and reflected fields (each with the same frequency difference $\omega_B^{\pm}(n)$). A very important feature of a FSF laser is that in the absence of fluctuations, e.g. those caused by spontaneous emission, the phases of all these contributions are balanced in such a way that their *sum is equal to zero*. However, unavoidable fluctuations break this balance, and one can therefore observe a resonant increase in the spectral density of the RF spectrum of the Michelson interferometer output intensity fluctuations near these beat frequencies. Such signals have been used for distance measurements in [16,17]. Recently we have proposed [24] and experimentally demonstrated with a Yb^{3+}-doped fiber-ring FSF laser [18] another approach to distance measurements, based on the use of a phase-modulated laser as an external seed. When the output of such a laser passes through a Michelson interferometer, the phase modulation induces amplitude modulation. The variation of the magnitude of the amplitude modulation as a function of the modulation frequency Ω reveals very sharp resonances. This occurs whenever Ω coincides with the beat frequencies given by Eq. (2) or (3).

From a measurement of the frequency associated with the maxima of the amplitude modulation signal we can deduce the delay T and hence the distance L. Because the monochromatic amplitude modulation of the FSF laser output can be measured with a very narrow-bandwidth filter, the technique allows a significant decrease in the noise and a corresponding improvement in the signal-to-noise ratio.

Fig. 5 shows the various resonance frequencies $\omega_B^+(q)$ and $\omega_B^-(p)$ for given delay time T, and hence for distance $L = cT/2$. The locus of values appear as lines marked by integers p and q. For best results the modulation frequency should be chosen within a region convenient for measurements. The most natural choice is a modulation frequency which is smaller than the free spectral range of the cavity, Δ_c (or the cavity mode spacing)

$$0 < \Omega < \Delta_c, \tag{4}$$

shown hatched in Fig. 5. In this region, where $L \neq k\pi c/\Delta$, $(k = 0, 1, 2, \ldots)$, there exist, for a given γT, two resonance frequencies, $\Omega = \Omega_D$ and $\Omega = \Omega_R$, corresponding to specific values of integers p and q. With increasing distance L the "direct" resonance frequency Ω_D increases and the

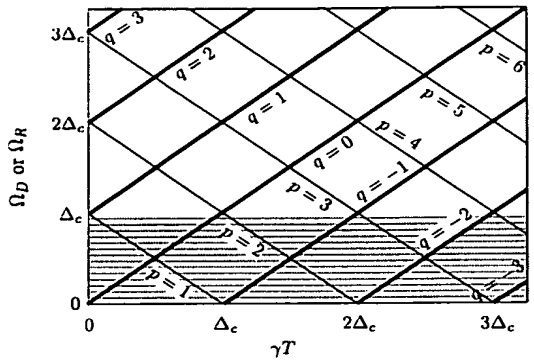

Fig. 5. Possible frequencies of amplitude modulation resonances, Ω_D or Ω_R, as functions of $\gamma T \equiv (2\Delta/c\tau_r)L$. Thick lines, labelled by q, mark values for Ω_D, Eq. (5). Thin lines, labelled by p, mark values for Ω_R, Eq. (6). The shaded portion marks the region $0 < \Omega < \Delta_c$ used for frequency modulation.

"reverse" frequency Ω_R decreases. The relevant connection with distance comes from Eq. (2) or (3), namely

$$\Omega_D = q\Delta_c + (2\Delta/c\tau_r)L \tag{5}$$

and

$$\Omega_R = p\Delta_c - (2\Delta/c\tau_r)L. \tag{6}$$

As with any interferometry, there is an ambiguity in the present technique. Distances which differ by an integer number of intervals $L_\Delta = \pi c/\Delta$ give the same resonance frequencies in the interval $0 < \Omega < \Delta_c$. This ambiguity is resolvable by measuring changes $\delta\Omega_D$ or $\delta\Omega_R$ produced by changing the AOM frequency from Δ to $\Delta + \delta\Delta$ [16,17]. The required theoretical relationship is obtained from Eqs. (5) and (6) for constant Δ_c, and with variable Δ. As long as the change $\delta\Delta$ of the AOM frequency is small enough that integers q and p do not change we obtain the distance L from the formula

$$L = \frac{c\tau_r}{2}\frac{\delta\Omega_D}{\delta\Delta} = -\frac{c\tau_r}{2}\frac{\delta\Omega_R}{\delta\Delta}. \tag{7}$$

4. Variation of amplitude modulation signal with distance

For practical applications it is important to know the degree of amplitude modulation at resonance. To derive it consider, following [24], the FSF laser seeded by a CW laser whose phase $\Phi(t) = \omega_s t + \varphi_s(t)$ is modulated sinusoidally,

$$\varphi_s(t) = \varphi_0 + \beta\sin(\Omega t). \tag{8}$$

Here ω_s is the seed laser frequency, β is the modulation index and φ_0 is the initial phase. To obtain the amplitude modulation signal we model the FSF-laser output as a discrete spectrum. In [15] we have shown that this model is equivalent to the moving comb model. In this model the FSF-laser output consists of a set of discrete optical components with the frequencies $\omega_s + n\Delta$ ($n = 0, 1, 2, \ldots$). The phases of the components have a time-independent contribution that is quadratic in n and a time-delayed contribution from the phase-modulated seed laser phase $\varphi_s(t - n\tau_r)$. The amplitudes of the components are proportional to a Gaussian function of n,

$$a_n = a_{max}\exp\left[-(n - n_{max})^2/n_w^2\right], \tag{9}$$

where n_w is the effective number of optical components within the Gaussian profile of the laser spectrum, n_{max} identifies the component closest to the maximum of the spectral profile and a_{max} is the amplitude of the central component. The parameters n_w and n_{max} are large, $n_w \gg 1$ and $n_{max} \gg 1$, and can be evaluated from measurable laser characteristics (for details see Eqs. (13)–(17) in [15]).

When this output enters a Michelson interferometer whose arms differ in length by L, the interference term in the interferometer output intensity is a sum of independent contributions $\delta P_{int}^{(n)}$ from each nth frequency component. Every contribution is proportional to a cosines of the phase difference between reference and reflected components

$$\phi_n = (\omega_s + n\Delta)T + \varphi_s(t + T - n\tau_r) - \varphi_s(t - n\tau_r) \tag{10}$$

and to the square of the component amplitude:

$$\delta P_{int}^{(n)} \propto a_n 2\cos\phi_n. \tag{11}$$

Because the phase $\varphi_s(t)$ of the seed laser is modulated, the difference phase ϕ_n will also be modulated, with a time-dependent part

$$\delta\phi_n(t) = 2\beta\sin[\Omega T/2]\cos[\Omega t + \Omega T/2 - n\Omega\tau_r], \tag{12}$$

as follows from Eq. (8) and the use of a trigonometric identity. Thus the contribution of each individual component has an amplitude modulation with the period $2\pi/\Omega$. Making use of a Jacobi–Anger expansion [25]

$$\exp[iZ\cos(\theta)] = \sum_{l=-\infty}^{\infty} i^l J_l(Z)\exp[il\theta] \tag{13}$$

one can consider this periodic modulation as a sum of the harmonic components with the frequencies $l\Omega$ ($l = 1, 2, \ldots$) and with the amplitudes proportional to the Bessel function $J_l(Z)$ of integer order l and of argument $Z = 2\beta\sin(\Omega T/2)$. The amplitude $S_n(\Omega, T)$ of the harmonic of present interest, the first harmonic, varies with time delay $T = 2L/c$ and with frequency Ω in accordance with the formula,

$$S_n(\Omega, T) = s_0 J_1(2\beta\sin[\Omega T/2])a_n 2, \tag{14}$$

where $J_1(Z)$ is the Bessel function of order 1 and s_0 is a normalization factor that incorporates the laser output power. For particular combinations of the modulation index β, the modulation frequency Ω and the time delay T, the amplitude modulation with frequency Ω may actually be suppressed for each elementary interference term. This will occur when

$$2\beta\sin[\Omega T/2] = j_{1,k}, \tag{15}$$

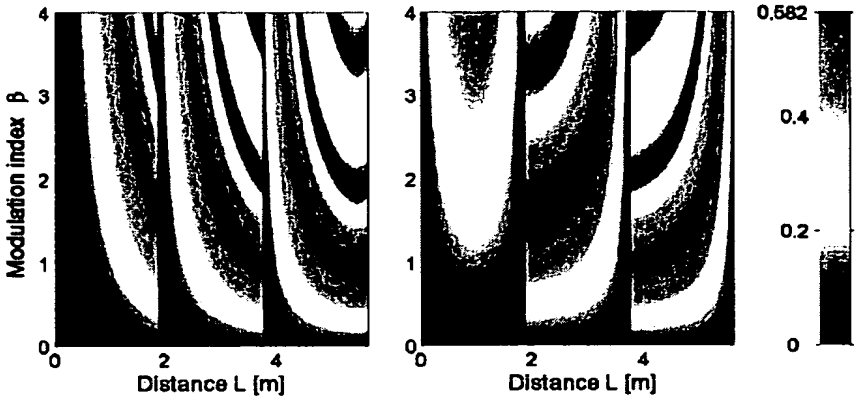

Fig. 6. Density plot of the calculated amplitude-modulation signal S_A as a function of distance L and the modulation index β. The left frame corresponds to the "direct" signal, the right frame corresponds to the "reverse" one. The basic length scale of the figure is $L_0 = \pi c/\Delta = 1.875$ m for our AOM frequency of $\Delta = 80$ MHz.

where $j_{1,k} = 0, 3.8317, 7.0156, \ldots$ are the kth zeros of the Bessel function of order 1.

If the condition (15) is not fulfilled it is easy to see from (10) and (12) that there are two sets of elementary contributions to the signal of the amplitude modulation with depending on n phases: a "direct" signal with phase $\psi_n^{(+)} = n(\Omega\tau_r + \Delta T)$ and a "reverse" signal having phase $\psi_n^{(-)} = n(\Omega\tau_r - \Delta T)$.

The sum of these contributions, weighted by the smoothly varying squared amplitude a_n^2 will be zero for all Ω except for very narrow intervals near the frequencies Ω_p providing that

$$\Omega_p\tau_r \pm \Delta T = 2\pi p \tag{16}$$

with $p = 0, \pm 1, \pm 2 \ldots$ Note that the frequencies Ω_p determined by this condition coincide with the beating frequencies of Eqs. (2) and (3) obtained from the moving comb model.

Regarded as a function of modulation frequency Ω, the amplitude modulation signal has a Gaussian profile: it has the width $\Delta\Omega = 2\sqrt{2}/(\tau_r n_w)$ and reaches a maximum

$$S_A(\Omega, T) = S_0 J_1(2\beta \sin[\Omega T/2]) \tag{17}$$

with $S_0 = n_w s_0 \sqrt{\pi/2}$, when the modulation frequency Ω has the value determined by Eq. (16). Thus by measuring the modulation frequency for which the amplitude modulation of the interferometer output maximizes, and knowing the chirp rate γ, we obtain the interferometer-arm difference L.

Fig. 6 shows a density plot of the amplitude modulation signal S_A, calculated from Eq. (17), as a function of the distance L and the modulation index β for the "direct" and "reverse" signal. The basic scale length of the interferometer-arm difference L_0 for this plot is determined by the condition $\gamma T \equiv \Delta T/\tau_r = \Delta_c$. Using the relationships $T = 2L/c$ and $\Delta_c = 2\pi/\tau_r$ we obtain $L = \pi c/\Delta$. Thus, the scale length in Fig. 6 is determined by the AOM frequency Δ. Our AOM frequency is 80 MHz, leading to the distance scale of $L_0 = \pi c/\Delta = 1.875$ m, apparent in the figure.

The Bessel function in the expression (17) for the signal produces a strong variation of the signal S_A with distance L and modulation index β. Fig. 6 illustrates this rather complicated behavior. The regions of minimal signal (dark blue[1] regions in Fig. 6) pose challenges for detection. However, these can be circumvented by proper selection of the modulation index β at each distance L.

The preceding analysis assumed a monochromatic seed. In reality the seed laser has a finite spectral width, set by the finite coherence length of the seed laser. This will decrease the signal (17) in a manner that can be approximately described by a damping factor $\exp(-L/L_{coh})$, where L_{coh} is the coherence length of the seed laser:

$$S_A = S_0 J_1(2\beta \sin[\Omega L/c]) \exp(-L/L_{coh}). \tag{18}$$

The inclusion of a finite bandwidth of the seed laser does not alter the Bessel-function variation of the signal amplitude with distance L.

5. Experimental results and comparison with theory

Fig. 7 shows the experimental setup we used for the distance measurements. It consists of an all-fiber FSF laser seeded by a phase-modulated external monochromatic diode laser. The output power of the FSF laser passes through a Michelson interferometer with one fixed and one movable arm. The distance difference between them can be changed from 15 cm to 5 m. After emerging from the Michelson interferometer the laser light impinges on a photodetector with bandwidth 50 MHz connected to a lock-in amplifier. The latter is driven by the same generator that operates the electro-optic modulator. Thus the lock-in amplifier detects resonances of the amplitude modulation S_{AM} that correspond to various distances L. We observed the spectrum of the FSF laser using a Fabry–Perot interferometer (FPI) with the free spectral range of 650 GHz, see Fig. 7.

[1] For interpretation of color in Fig. 6, the reader is referred to the web version of this article.

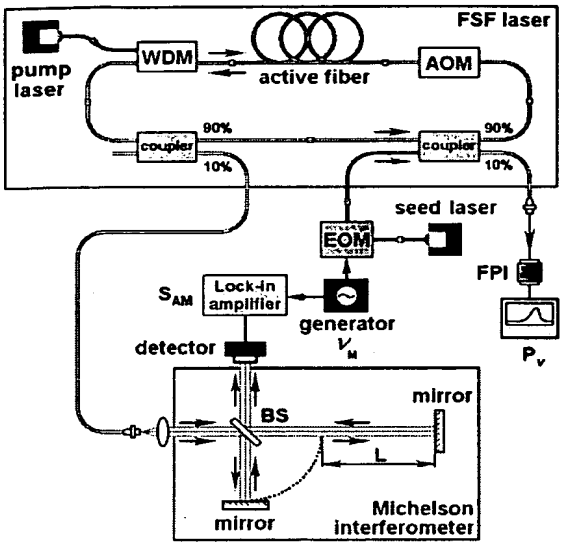

Fig. 7. Experimental setup for distance measurements. The upper rectangle encloses the FSF laser of Fig. 1. The seed laser is modulated by an EOM. The output coupler feeds 10% to the Michelson interferometer (rectangular box at bottom of the figure), one arm of which includes the length L to be measured. The output from a beam splitter (BS) in the interferometer is detected as an amplitude modulation signal S_A with a lock-in amplifier matched to the frequency of the EOM. The seed input coupler also provides output analyzed by a Fabry–Perot interfermometer (FPI).

Fig. 8 shows a typical example of a narrow "direct" resonance in the magnitude S_A as a function of the modulation frequency Ω. Because in this case the distance L is smaller than $\pi c/\Delta$ the frequency of the resonance maximum is directly proportional to L. For our laser system the proportionality constant is 8.316 kHz/mm. The FWHM of the resonance is about 7 kHz. Thus, the resolution available with our system is better than 1 mm and the accuracy is better than 0.1 mm (assuming that the frequency position of the resonance maximum can be determined within 10% of its width).

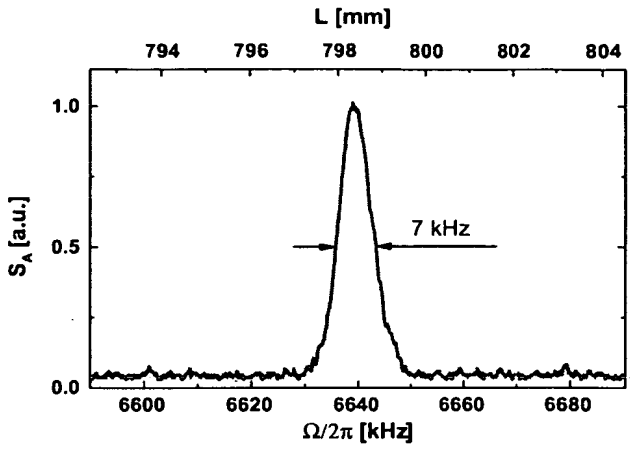

Fig. 8. Amplitude modulation signal S_A versus modulation frequency Ω.

As was mentioned above, the amplitude modulation signal S_A has a complicated dependance upon the distance L and the index of modulation β, described by formula (18). Fig. 9a and b compare the experimental results with the theoretical calculation made for our laser system. The experimental results are in excellent agreement with the theory.

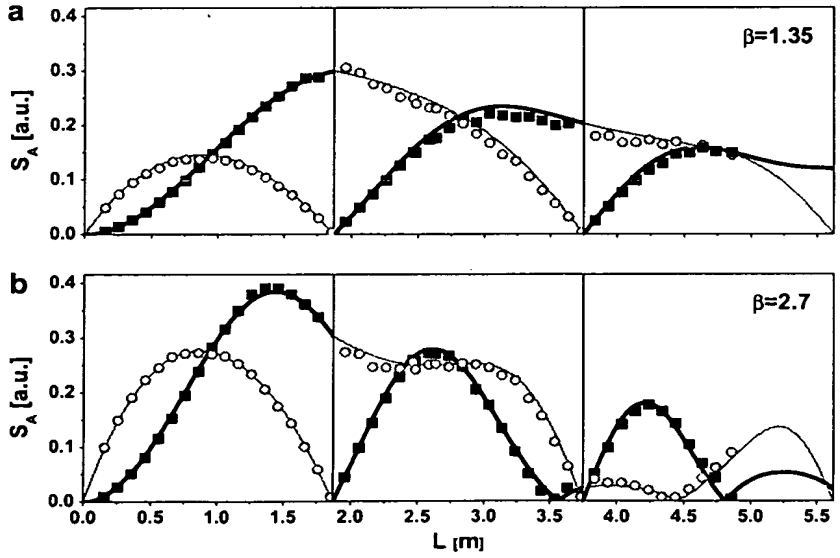

Fig. 9. Dependance of the amplitude modulation signal size upon the distance for a modulation index $\beta = 1.35$ (frame a) and $\beta = 2.7$ (frame b). Dots are experimental results and lines are theoretical simulation. Black squares and thick lines refer to the "direct" maxima (D, see Fig. 5), red circles and thin lines refer to "reverse" maxima (R).

Fig. 9 shows that there are two minima of the "direct" signal for $\beta = 2.7$, at the distances 3.6 and 4.8 m. These do not exist for $\beta = 1.35$. This means that for any distance L there is an optimal modulation index β such that it is possible to avoid signal minima. Thus the useful range of our method is limited only by the coherence length of the seed laser (this was 3.6 m in our work), which is set by the bandwidth of the seed, and the collection efficiency of the reflected light. For our setup this latter restriction is several tens of meters.

6. Summary and conclusions

This paper describes an all-fiber FSF laser with Er^{3+}-doped fiber as the gain medium and an acousto-optic modulator as the frequency shifter. The spectral and power characteristics are presented for cases with and without an external seed laser; these are typical of FSF lasers.

We have used our system, a FSF laser with an external PM seed laser, to measure distances with a Michelson interferometer scheme. We display examples of the amplitude-modulation signal for distances ranging from 15 cm to 5 m. Our results are in very good quantitative agreement with numerical simulations which take the finite bandwidth of the seed laser into account. We thereby verify the theory first presented in [24]. Notably, the signal exhibits pronounced minima at particular distances, set by the zeros of a Bessel function. These "blind" zones can be avoided by changing the modulation index of the PM seed laser and/or the AOM frequency.

The all-fiber FSF laser seeded by an external PM laser is a powerful noise-immune tool for distance measurements over a range of distances up to tens of meters. The bandwidth limitation of our present apparatus allows an accuracy better than 0.1 mm and resolution better than 1 mm.

Dual wavelength interferometric measurements offer the opportunity to determine lengths to within a small fraction of a wavelength, as numerous publications have attested [26–29]. Such high accuracy is only possible under carefully controlled conditions. However, measurements of distances to arbitrary objects require detailed information about the surface, because there occurs a material-dependent phase shift that affects any measurement based on phases, such as interferometry [30]. Techniques based on the use of a FSF laser, being essentially measurements of time rather than phase, do not suffer from this problem.

Acknowledgments

We acknowledge support by the Stiftung Rheinland-Pfalz für Innovation and by CNES, INTAS and NSAU (06-1000024-9075). L.P.Y. acknowledges support by the Deutsche Forschungsgemeinschaft (436-UKR-113/16). B.W.S. acknowledges support from the Max Planck Forschungspreis awarded to K.B. in 2003.

References

[1] L.C. Foster, M.D. Ewy, C.B. Crumly, Appl. Phys. Lett. 6 (1965) 6.
[2] W. Streifer, J.R. Whinnery, Appl. Phys. Lett. 17 (1970) 335.
[3] J. Martin, Y. Zhao, S. Balle, I.C.M. Littler, K. Bergmann, Opt. Commun. 111 (1994) 101.
[4] A.P. Willis, A.I. Ferguson, D.M. Kane, Opt. Commun. 116 (1995) 87.
[5] G. Bonnet, S. Balle, Th. Kraft, K. Bergmann, Opt. Commun. 123 (1996) 790.
[6] K. Kasahara, K. Nakamura, M. Sato, H. Ito, IEEE J. Quantum Electron. 34 (1998) 190.
[7] K.A. Shore, D.M. Kane, IEEE J. Quantum Electron. 35 (1999) 1053.
[8] J. Geng, S. Wada, Y. Urata, H. Tashiro, Opt. Lett. 24 (1999) 676.
[9] J. Geng, S. Wada, Y. Urata, H. Tashiro, Opt. Lett. 24 (1999) 1635.
[10] I.C.M. Littler, H.M. Keller, U. Gaubatz, K. Bergmann, Zs. Phys. D 18 (1991) 307.
[11] D.T. Mugglin, A.D. Streater, S. Balle, K. Bergmann, Opt. Commun. 104 (1993) 165.
[12] J.R.M. Barr, G.Y. Liang, M.W. Phillips, Opt. Lett. 18 (1993) 1010.
[13] M.J. Lim, C.I. Sukenik, T.H. Stievater, P.H. Bucksbaum, R.S. Conti, Opt. Commun. 147 (1998) 99.
[14] M. Cashen, V. Bretin, H. Metcalf, J. Opt. Soc. Am. B 17 (2000) 530.
[15] L.P. Yatsenko, B.W. Shore, K. Bergmann, Opt. Commun. 236 (2004) 183.
[16] K. Nakamura, T. Miyahara, M. Yoshida, T. Hara, H. Ito, Photon. Technol. Lett. 10 (1998) 1772.
[17] K. Nakamura, T. Hara, M. Yoshida, T. Miyahara, H. Ito, IEEE J. Quantum Electron. 36 (2000) 305.
[18] V.V. Ogurtsov, L.P. Yatsenko, V.M. Khodakovskyy, B.W. Shore, G. Bonnet, K. Bergmann, Opt. Commun. 266 (2006) 266.
[19] V.V. Ogurtsov, L.P. Yatsenko, V.M. Khodakovskyy, B.W. Shore, G. Bonnet, K. Bergmann, Opt. Commun. 266 (2006) 627.
[20] I.R. Perry, R.L. Wang, J.R.M. Barr, Opt. Commun. 109 (1994) 187.
[21] M.W. Phillips, G.Y. Liang, J.R.M. Barr, Opt. Commun. 100 (1993) 473.
[22] K. Nakamura, F. Abe, K. Kasahara, T. Hara, M. Sato, H. Ito, IEEE J. Quantum Electron. 33 (1997) 103.
[23] A. Yoshizawa, H. Tsuchida, Opt. Commun. 155 (1998) 51.
[24] L.P. Yatsenko, B.W. Shore, K. Bergmann, Opt. Commun. 242 (2004) 581.
[25] Weisstein, Eric W. Jacobi–Anger Expansion. From MathWorld–A Wolfram Web Resource. <http://mathworld.wolfram.com/Jacobi-AngerExpansion.html>.
[26] F. Bien, M. Camac, H.J. Caulfield, S. Ezekiel, Appl. Opt. 23 (1981) 2982.
[27] P. de Groot, J. McGarvey, Opt. Lett. 17 (1992) 1626.
[28] P. Hariharan, D. Malacara, B.J. Thompson (Eds.), Interference, Interferometry, and Interferometric Metrology, SPIE Optical Engineering Press, Bellingham, WA, 1995.
[29] O.P. Lay, S. Dubovitsky, R.D. Peters, J.P. Burger, S.-W. Ahn, W.H. Steier, H.R. Fetterman, Y. Chang, Opt. Lett. 28 (2003) 890.
[30] L.P. Yatsenko, M. Loeffler, B.W. Shore, K. Bergmann, Appl. Opt. 43 (2004) 3241.

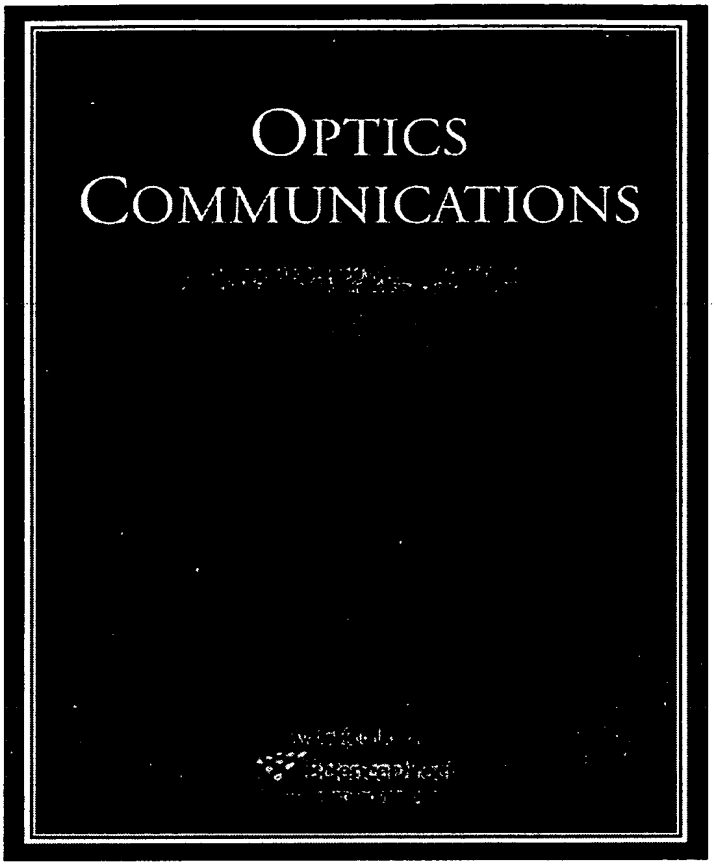

Optics Communications 282 (2009) 300–309

Contents lists available at ScienceDirect

Optics Communications

journal homepage: www.elsevier.com/locate/optcom

Coherence in the output spectrum of frequency shifted feedback lasers

L.P. Yatsenko [a], B.W. Shore [b,*], K. Bergmann [b]

[a] Institute of Physics, National Academy of Sciences of Ukraine Prospect Nauki 46, Kiev-39, 03650, Ukraine
[b] Technical University, Kaiserslautern, 67653 Kaiserslautern, Germany

ARTICLE INFO

Article history:
Received 9 June 2008
Received in revised form 30 August 2008
Accepted 1 October 2008

ABSTRACT

We present a detailed theoretical analysis, using correlation functions, of the coherence properties of the output from a frequency shifted feedback (FSF) laser seeded simultaneously by an external seed laser and by spontaneous emission (SE). We show that the output of a FSF laser is a cyclostationary process, for which the second-order correlation function is not stationary, but periodic. However, a period-averaged correlation function can be used to analyze the optical spectrum. From the fourth-order correlation function of the output of a Michelson interferometer we obtain the essential characteristics of the radio-frequency (RF) spectrum, needed for describing the use of the FSF laser for optical-ranging metrology. We show that, even for a FSF laser seeded by SE, the RF spectrum comprises a sequence of doublets, whose separation gives directly a measure of the length difference between the interferometer arms. This doublet structure is a result of the correlation of interference terms of individual components of the cyclostationary stochastic process. It is not seen in the optical spectrum of the FSF laser but is observable in the RF spectrum. We analyze the competition between SE and continuous wave (CW) seeding to obtain an analytical expression for the ratio of power in the discrete CW signal to the background continuum spectrum from SE. We show that, unlike mode competition in conventional lasers, where there occurs exponential selectivity, here there is a balance between the two fields; the power in the fields is related linearly, rather than exponentially, to the control parameters.

1. Introduction

The remarkable properties of frequency shifted feedback (FSF) lasers have drawn attention as broad-band light sources [1–4] and, more recently, as tools for metrology [5–9]. In essence, an FSF laser comprises a closed optical path, of total optical length L (a linear cavity or a ring), in which light undergoes not only the usual gain of energy from excited states but also, during each cavity round trip, a discrete-frequency shift Δ. This differs from the axial mode spacing of the cavity, the free-spectral range (FSR), which is $2\pi c/L$. The operation of FSF lasers has been considered by several research groups [10–20] and it has been used for a number of practical applications [21–26].

Two complementary viewpoints offer means for understanding the output characteristics, and uses, for an FSF laser. In one, the output field is regarded as a comb of chirped frequencies, separated in frequency at any instant by the free-spectral range $2\pi c/L$ (the *moving-comb model*) [5,6,14–16,27]. The other approach considers the output growing from a discrete-frequency seed as a stationary set of frequencies starting from the seed frequency and separated from each other by Δ [19,20,23,28,29]. Spontaneous emission (SE) provides a continuous distribution of such seed frequencies.

For applications to metrology, specifically the determination of distances by optical ranging, it is important to understand the coherence characteristics of the output from an FSF laser. In the absence of any external seed, this output originates from a distribution of spontaneous-emission (SE) events within the gain medium. These are uncorrelated and intrinsically incoherent. We here examine, by following a sequence of cyclic passages within the FSF cavity, how this radiation acquires coherence properties, as evidenced in correlation functions.

We discuss here the operation of a FSF laser whose field originates either entirely from spontaneous emission or else from the joint action of spontaneous emission and a continuous-wave (CW) monochromatic laser seed. We pay particular attention to the RF spectrum of the output of a Michelson interferometer driven by a FSF laser. As we will note, this signal underlies metrology applications.

Earlier we have presented the basic theory of the operation of a FSF laser [19]. That work treated the SE as a seed field of very large bandwidth. It also described the effect of an external CW laser seed field, one whose phase could be modulated. However, it did not discuss the competition between these two sources. Here we remedy these shortcomings by treating the two sources as coexisting.

* Corresponding author. Address: 618 Escondido Cir., Livermore, CA 94550, USA. Tel.: +1 925 455 0627.
E-mail address: bwshore@alum.mit.edu (B.W. Shore).

0030-4018/$ - see front matter © 2008 Elsevier B.V. All rights reserved.
doi:10.1016/j.optcom.2008.10.002

All applications of FSF lasers to distance measurements (optical ranging) rely on measurements of the RF spectrum of the output of a Michelson interferometer with FSF-laser input. Hitherto there has been no quantitative *ab initio* theory of the properties of this spectrum. Such a description must originate with intensity correlation functions, as presented here. We will show how the frequency-shifting element produces a field which, when passed through a Michelson interferometer, produces spectral signals from which the interferometer-arm distance can be deduced. Specifically, the information is contained in sets of frequency doublets. We present here a first-principles derivation of the "beat frequencies" that have been discussed earlier based on the moving-comb model of FSF operation. We show that such signals occur even when the FSF laser is seeded entirely by spontaneous emission, and that there is no need to invoke a moving comb model to explain this structure. The interferences from such SE sources are not seen in the optical spectrum of the FSF laser; they are observable only in the RF signals from the interferometer.

Our earlier work [19] considered the FSF output field from a specific seed field. We used these results to model the output from an FSF laser seeded either solely by SE or exclusively by an externally controlled laser field. As shown in [7], the latter option offers significant improvement in signal-to-noise ratio over SE seeding. The present paper treats FSF-laser operation when an external seed field is accompanied by the inevitable spontaneous emission that provides an unavoidable stochastic background. In normal laser operation the competition between modes leads to exponential growth of favored modes at the expense of those with less gain. We shall show that in the FSF laser the competition between SE and external seed does not act in this way. Instead, there occurs a balance between the two fields that is related linearly, rather than exponentially, to the control parameters. Although it would be desirable to suppress the amplified spontaneous emission (ASE) component of the FSF-laser output, thereby improving the signal-to-noise ratio, we shall show that this is not possible. This behavior differs, perhaps unexpectedly, from that of a normal laser, where suitable choice of gain characteristics can place all of the output into a favored mode.

2. Basic model

This article draws upon two recent papers [7,19] that present, in some detail, an idealized model for an FSF laser. We here first review the basic principles of that work and then extend it by examining correlation functions, thereby allowing analysis of the coherence and spectral properties of the FSF laser.

2.1. The FSF-laser layout

Fig. 1 presents a schematic drawing of the essentials of a FSF laser in a ring configuration. Light propagates along a closed optical path that passes through a gain medium (G), a frequency shifter [usually accomplished by an acousto-optic modulator, (AOM)] and a filter (F). In G a combination of stimulated emission and spontaneous emission add energy. The AOM adds a fixed increment Δ to each frequency component. A number of elements within the overall optical path have frequency dependent losses that we here represent as a single spectral filter, F. The output emerges through the zero diffraction order of the AOM. The AOM also serves to couple any external seed laser beam into the cavity.

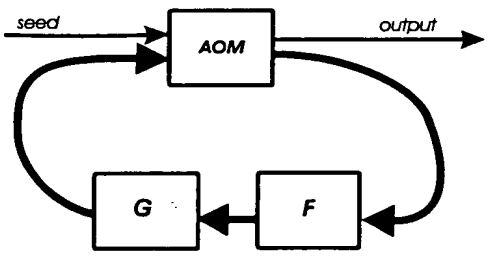

Fig. 1. Symbolic diagram of a ring cavity showing gain G, spectral filter F and frequency-shifter AOM as well as seed and output.

2.2. The field description

The filtering elements (F), which remove energy, and the gain medium (G), which replenishes this energy, together provide an *effective gain* (the growth minus the loss) distributed over a range of frequencies. We take the center of this range to be ω_f, regarding this as a carrier frequency. We consider the propagation of the electric field along a one-dimensional path, coordinate z, within the ring. The round-trip time in the cavity is $\tau_r = L/c$.

We denote by $E(t)$ the complex-valued electric field at position $z = 0$, taken to be the entrance surface of the AOM. We express this field in terms of a complex-valued envelope $\mathscr{E}(t)$ and a carrier:

$$E(t) = \mathscr{E}(t)\exp(-i\omega_f t). \tag{1}$$

The intensity of the FSF laser at $z = 0$, is

$$I(t) = \frac{c}{8\pi}|\mathscr{E}(t)|^2. \tag{2}$$

The AOM diffracts into first order a fraction of the beam intensity, denoted $\mathscr{R}^2$. Typically $\mathscr{R}^2 \approx 0.9$. The frequency of this fraction is shifted, in passing through the AOM, by Δ. This portion continues to circulate within the cavity. The unshifted fraction $(1 - \mathscr{R}^2)$, usually small, remains in zeroth order and forms the output field.

We consider an arbitrary but fixed reference time T and a time window that endures for one round-trip time prior to T. Within this interval, $T - \tau_r < t < T$, we introduce a sliding windowed Fourier transform (SWFT) of the envelope, writing

$$\mathscr{E}(t) = \int_{-\infty}^{\infty} d\varpi \mathscr{E}(\varpi, T)\exp(-i\varpi t), \quad \text{for } T - \tau_r < t < T, \tag{3}$$

where

$$\mathscr{E}(\varpi, T) \equiv \frac{1}{2\pi}\int_{T-\tau_r}^{T} dt \mathscr{E}(t)\exp(+i\varpi t). \tag{4}$$

Here and in the following we denote by $\varpi \equiv \omega - \omega_f$ a frequency offset from the carrier ω_f. The SWFT field $\mathscr{E}(\varpi, T)$ for a fixed reference time T provides the essential tool with which we express the operation of the FSF and the output field [19]. From it we construct the field envelope $\mathscr{E}(t)$ for all time, and deduce the output characteristics of the FSF for any given experimental conditions.

2.3. The field amplitude equations

As in our earlier work [19], we derive the basic equation for the laser field by considering its history during the round trip prior to time T. It began this circuit, starting at time $t = T - \tau_r$, with frequency $\omega = \omega_f + \varpi - \Delta$. It then underwent a frequency shift Δ as it passed through the AOM. It changed amplitude in passing through the filter and gain medium. It also acquired a phase increment $(\omega_f + \varpi)\tau_r$ as it propagated around the loop. To describe these changes it proves useful to introduce a two-dimensional time–frequency space $\vec{X} = (\varpi, T)$ in which to present the equations [19]. Successive circulations around the ring involve a change of the two-dimensional vector $\vec{X}$ by the increment $\vec{X}_0 = (\Delta, \tau_r)$. The field change after one round trip is expressible as

$$\mathscr{E}(\vec{X}) = \mathscr{E}(\vec{X} - \vec{X}_0)\exp\left[G(\vec{X})\right] + \xi(\vec{X}) + \varepsilon(\vec{X}). \tag{5}$$

Here the effect of gain and loss appears through the propagator argument $G(\vec{X})$, described in detail below, and the terms $\xi(\vec{X})$ and $\varepsilon(\vec{X})$ represent, in Fourier space, additions to the field during the time interval τ_r. The first of these, $\xi(\vec{X})$, expresses the field increment supplied by spontaneous emission. It is the SWFT of $\xi_{sp}(t)$, the amplitude of the stochastic field created by spontaneous-emission events,

$$\xi(\vec{X}) \equiv \xi(\varpi, T) = \frac{1}{2\pi}\int_{T-\tau_r}^{T} dt\,\xi_{sp}(t)\exp(+i\varpi t). \tag{6}$$

The second contribution to the field, $\varepsilon(\vec{X})$, describes the external seed field, if present. We take this to have a carrier frequency ω_s offset from the central filter frequency ω_f by ϖ_s,

$$\omega_s = \omega_f + \varpi_s. \tag{7}$$

We are interested in seeding by monochromatic light; we write its SWFT as

$$\varepsilon(\vec{X}) = \frac{\varepsilon_s}{2\pi}\int_{T-\tau_r}^{T} dt\exp[-i\varpi_s t + i\varpi t], \tag{8}$$

where ε_s is the amplitude of the seeding laser field within the cavity.

We write the propagator argument $G(\vec{X})$ as the difference between gain $g(\omega)$ and losses $f(\omega)$, modified by the phase $(\omega_f + \varpi)\tau_r$ acquired during the round trip. We approximate the effect of losses by means of a filter function, taken to be a quadratic centered at $\omega = \omega_f$ with characteristic width Γ_f,

$$f(\omega) = f_m + \frac{1}{2}\left(\frac{\omega-\omega_f}{\Gamma_f}\right)^2. \tag{9}$$

The frequency-independent term f_m describes fixed losses, such as those from mirror reflectivities.

We will regard the spectral filter as having narrower bandwidth than the broader bandwidth of the gain medium; it fixes the range of frequencies we need to consider. In this approximation we neglect the frequency dependence of the gain and approximate it as

$$g(\omega) \equiv g_{sat} = \frac{g_0}{1+\bar{I}/I_{sat}}. \tag{10}$$

Here g_{sat} is the saturated frequency-independent gain, g_0 is the unsaturated gain, $\bar{I}$ is the laser intensity averaged over one round trip and I_{sat} is the saturation intensity. The averaged intensity, and hence the saturated gain, must be evaluated from appropriate equations describing the FSF laser, see Section 5.1 below. Combining these three contributions, we write the propagator argument as

$$G(\vec{X}) \equiv G(\varpi, T) = i(\omega_f+\varpi)\tau_r + g_{sat} - f_m - \frac{1}{2}(\varpi/\Gamma_f)^2. \tag{11}$$

This depends on frequency ω through the detuning $\varpi \equiv \omega - \omega_f$.

The basic parameters under the control of the experimenter are those of the cavity τ_r, Δ, those of the filter ω_f, Γ_f, f_m, those of the gain g_0, I_{sat}, and those of the seed, ε_s, ω_s. The mean intensity $\bar{I}$, and the concomitant saturated gain g_{sat} must be determined such that the equations for the field, with predicted output intensity, are self consistent.

2.4. The output intensity

An important characteristic of the FSF-laser output is the intensity averaged over a round trip,

$$\bar{I}(T) \equiv \frac{1}{\tau_r}\int_{T-\tau_r}^{T} dt I(t). \tag{12}$$

We define the spectral intensity $I(\varpi, T)$ by writing this average as a frequency distribution,

$$\bar{I}(T) = \int_{-\infty}^{\infty} d\varpi I(\varpi, T). \tag{13}$$

Using Eq. (3) we write the intensity as

$$I(t) = \frac{c}{8\pi}\int_{-\infty}^{\infty}\int_{-\infty}^{\infty} d\varpi_1 d\varpi_2 \exp[-i(\varpi_1-\varpi_2)t)] \times \mathscr{E}(\varpi_1, T)\mathscr{E}(\varpi_2, T)^*. \tag{14}$$

From this integral we extract an expression for the spectral intensity of Eq. (13) as

$$I(\varpi, T) = \frac{c}{8\pi}\int_{-\infty}^{\infty} d\varpi' \mathscr{E}(\varpi, T)\mathscr{E}(\varpi+\varpi', T)^* \times \frac{1-\exp[-i\varpi'\tau_r]}{i\varpi'\tau_r}\exp[i\varpi' T]. \tag{15}$$

The fields described here, and the corresponding output intensity, involve uncontrollable events, the stochastic processes that describe spontaneous emission. Observations inevitably introduce averages over stochastic realizations of the average intensity during a round trip. Thus we are interested in stochastic averages $\langle\cdots\rangle$ that give the spectrum

$$J(\varpi) \equiv \langle I(\varpi, T)\rangle, \tag{16}$$

and the mean intensity

$$\bar{J} \equiv \langle \bar{I}(T)\rangle. \tag{17}$$

2.5. The general solution for the output field

The FSF laser based on the growth of spontaneous emission acts as a regenerative amplifier of spontaneous emission, as described by basic Eq. (5). The solution to this equation, as discussed earlier [19], is expressible as the contribution of two parts,

$$\mathscr{E}(\vec{X}) = \mathscr{E}_{sp}(\vec{X}) + \mathscr{E}_{seed}(\vec{X}), \tag{18}$$

a field that grows from the spontaneous emission,

$$\mathscr{E}_{sp}(\vec{X}) = \xi(\vec{X}) + \sum_{n=1}^{\infty}\xi(\vec{X}-n\vec{X}_0)\exp[\lambda_n(\vec{X})], \tag{19}$$

and a field that grows from the external seed,

$$\mathscr{E}_{seed}(\vec{X}) = \varepsilon(\vec{X}) + \sum_{n=1}^{\infty}\varepsilon(\vec{X}-n\vec{X}_0)\exp[\lambda_n(\vec{X})]. \tag{20}$$

Here

$$\lambda_n(\vec{X}) \equiv \sum_{l=0}^{n-1} G(\vec{X}-l\vec{X}_0). \tag{21}$$

These formulas express the field as the most recent added increments from seed and spontaneous emission, together with the succession of fields from earlier passes, each altered by the appropriate propagator $\exp[\lambda_n(\vec{X})]$. Our earlier work considered each of these separately. Here we consider the operation of the laser when both are present.

3. Seeding by spontaneous emission. The optical spectrum

Earlier work on the theory of the FSF laser emphasized the structure of the output fields. To gain a full understanding of the FSF laser it is necessary to evaluate various spectral properties. For the field emerging from the FSF cavity the significant observable is the optical spectrum. When the FSF laser is used for metrology, the significant observable is the RF spectrum from a Michelson interferometer. To quantify either of these it is necessary to have a theoretical description of various correlation

functions. Specifically, we require the second-order correlation functions for the optical spectrum, considered in this section. We require fourth-order functions to describe the RF spectrum, discussed in Section 4.

We begin by considering the FSF laser seeded only by SE. This provides a simple foundation for more elaborate models of FSF-laser operation.

3.1. Passive frequency-independent cavity

To simplify the problem as much as possible, we first consider a passive-cavity model, one in which there is no gain and in which losses are independent of frequency. We assume that the cavity field originates with the intracavity spontaneous emission. The lack of frequency dependence allows usto construct the solution using the fact that after one round trip the field $E(t)$ reproduces, with no distortion, the field at the earlier time $t-\tau_r$. The results of this simplified approach clarify some of the apparent peculiarities of the FSF-laser field.

For our idealized cavity the main losses occur from the small nonideality of the AOM, whose efficiency $\mathscr{R}^2=\exp(-2f_m)<1$ is taken here to be independent of frequency. We assume that the spontaneous emission source in the cavity creates the stochastic electric field with the amplitude $\xi_{sp}(t)$ and the carrier optical frequency ω_{sp}. We take $\xi_{sp}(t)$ to have mean value zero and the correlation behavior

$$\left\langle \xi_{sp}(t)\xi^*_{sp}(t+\tau)\right\rangle = \xi_0^2 F(\tau). \tag{22}$$

To avoid the unphysical occurrence of an infinite energy and infinitely broad spectrum we take the function $F(\tau)$ to be

$$F(\tau)=\frac{\Gamma_{sp}}{2}\exp(-\Gamma_{sp}|\tau|+i[\omega_{sp}-\omega_f]\tau), \tag{23}$$

rather than the usual delta function $F(\tau)=\delta(\tau)$. Here Γ_{sp} and ω_{sp} are, respectively, the spectral width and the central frequency of the spontaneous-emission line, much larger than all others frequencies in the system. (For the moment we disregard gain; the assumption of very large Γ_{sp} is equivalent to our earlier assumption of constant gain within the spectral range of interest.)

Because we assume here that the cavity losses are independent of frequency we can write the amplitude $\mathscr{E}(t)$ of the electric field in the cavity as the sum of the immediate spontaneous-emission contribution $\xi_{sp}(t)$ together with emission that was present at the earlier time $t-\tau_r$ along with similar emissions at a succession of earlier times, each diminished by a diffraction $\mathscr{R}$ but with *unchanged* time dependance,

$$\begin{aligned}\mathscr{E}(t)=\xi_{sp}(t)&+\mathscr{R}\xi_{sp}(t-\tau_r)e^{-i\Delta t}+\mathscr{R}^2\xi_{sp}(t-2\tau_r)e^{-i\Delta(t-\tau_r)t-i\Delta t}\\&+\mathscr{R}^3\xi_{sp}(t-3\tau_r)e^{-i\Delta(t-2\tau_r)t-i\Delta(t-\tau_r)t-i\Delta t}+\cdots\end{aligned} \tag{24}$$

Thus the cavity field is an infinite sum

$$\mathscr{E}(t)=\xi_{sp}(t)+\sum_{n=1}^{\infty}\mathscr{R}^n\xi_{sp}(t-n\tau_r)e^{-in\Delta t+i\Phi_n} \tag{25}$$

where the phase of component n is $\Phi_n=\sum_{l=0}^{n-1}l\Delta\tau_r$.

We infer from Eq. (25) that the spectrum of the field is the sum of spontaneous-emission spectra weighted with $\mathscr{R}^{2n}$ and shifted by $n\Delta$. We verify this by examining the second-order correlation function for the electric field amplitude,

$$G^{(2)}(t,t+\tau)=\langle\mathscr{E}(t)\mathscr{E}^*(t+\tau)\rangle\exp(i\omega_f\tau). \tag{26}$$

The term $\exp(i\omega_f\tau)$ provides a shift to the optical frequency.

It is customary to deal with stationary processes for which correlation functions depend on the time interval τ but not on the time t. For such processes one can evaluate the power spectrum as the Fourier transform of the correlation function; that is the content of the Wiener–Khinchine (WK) theorem. For the system considered here this theorem does not apply. Instead, we use Eq. (25) and the correlation behavior of the spontaneous-emission source, Eq. (22), to obtain the result

$$G^{(2)}(t,t+\tau)=\xi_0^2\sum_{n,k=0}^{\infty}\mathscr{R}^{n+k}F(\tau-[n-k]\tau_r)\times\exp[iS(t,n,k)+i\omega_{sp}\tau] \tag{27}$$

where

$$S(t,n,k)\equiv-(n-k)\Delta t+k\Delta\tau+\Phi_n-\Phi_k. \tag{28}$$

This correlation function $G^{(2)}(t,t+\tau)$ depends explicitly on time t. This means that the electric field in the FSF laser is not a stationary process. However, this time dependence is periodic, with period $2\pi/\Delta$. Thus we have here an example of a stochastic process which is periodically correlated (or *cyclostationary, periodically stationary* [30]). For such a process the spectrum can be defined as the output of a narrow-bandwidth optical filter. The output of such a filter, for such a process, is obtained from the Fourier transform of the period-averaged correlation function [30]. When we average over time the terms of Eq. (27) with $k\neq n$ cancel, leading to the result

$$g^{(2)}(\tau)\equiv\overline{G^{(2)}(t,t+\tau)}=\xi_0^2\sum_{k=0}^{\infty}\mathscr{R}^{2k}F(\tau)e^{ik\Delta\tau+i\omega_{sp}\tau}. \tag{29}$$

The laser spectrum is the Fourier transform of this time-averaged correlation function,

$$J^{(2)}(\omega)=\frac{c}{4\pi}\frac{1}{2\pi}\int_{-\infty}^{\infty}d\tau g^{(2)}(\tau)\exp(-i\omega\tau). \tag{30}$$

This can be considered as an extension of the WK theorem to cyclostationary processes.

Because the correlation function $g^{(2)}(\tau)$ is the sum of independent terms, so too is the spectrum the sum of separate spectra.

$$\mathscr{L}_{spont}(\omega)=\frac{c}{4\pi}\frac{\xi_0^2}{2\pi}\int_{-\infty}^{\infty}d\tau F(\tau)e^{i\omega_{sp}\tau-i\omega\tau}, \tag{31}$$

each offset by an increment Δ and weighted by a power of $\mathscr{R}^2$,

$$J^{(2)}(\omega)=\sum_{k=0}^{\infty}\mathscr{R}^{2k}\mathscr{L}_{spont}(\omega-\omega_{sp}-k\Delta). \tag{32}$$

This result confirms our expectation based upon Eq. (25).

3.2. Frequency-dependent effective gain

We next consider a more realistic model of the FSF laser by including gain and frequency-dependent losses. The field is given by Eq. (19). We assume that the width Γ_{sp} of the spontaneous-emission spectrum is much larger than the width Γ_f of the intracavity filter. Thus, the spontaneous-emission process $\xi_{sp}(t)$ can be considered here as a delta-correlated (Wiener–Levy) stochastic process:

$$\left\langle \xi_{sp}(t_1)\xi^*_{sp}(t_2)\right\rangle=\xi_0^2\delta(t_1-t_2). \tag{33}$$

When we use this property of $\xi_{sp}(t)$ to calculate the field, using Eq. (19) we obtain the correlation function

$$\begin{aligned}G^{(2)}(t,t+\tau)=\frac{\xi_0^2}{(2\pi)}\int_{-\infty}^{\infty}d\varpi\sum_{n=0}^{\infty}&\\\times\exp\left[\sum_{l=0}^{n-1}[g_{sat}-f(\varpi-l\Delta)]+\sum_{l=0}^{n+M-1}[g_{sat}-f(\varpi-l\Delta)]\right]&\\\times\exp\left[+i(\varpi+\omega_f)\delta\tau+iM\Delta t+\frac{i}{2}\Delta M^2\tau_r-\frac{i}{2}\Delta M\tau_r\right].&\end{aligned} \tag{34}$$

We have here defined M and $\delta\tau$ by expressing τ as $\tau = M\tau_r + \delta\tau$ with $-\tau_r/2 < \delta\tau < \tau_r/2$.

As in a passive FSF cavity, the correlation function $G^{(2)}(t, t+\tau)$ given by Eq. (34) depends explicitly on time t. As discussed above, to obtain the spectrum we need the period-averaged correlation function. When we average over time the terms of Eq. (34) with $M \neq 0$ cancel. The resulting average vanishes unless $-\tau_r/2 < \tau < \tau_r/2$, when it gives the result

$$g^{(2)}(\tau) = \frac{\xi_0^2}{(2\pi)} \int_{-\infty}^{\infty} d\varpi \sum_{n=0}^{\infty} \exp[S_n + i(\varpi + \omega_f)\tau]. \tag{35}$$

The amplitude of component n here depends on the exponent

$$S_n \equiv 2\sum_{l=0}^{n-1}[g_{sat} - f(\varpi - l\Delta)]. \tag{36}$$

Because the spectral width of $J(\varpi)$ is much larger than $2\pi/\tau_r$ this averaged correlation function is just the Fourier transform of the spectral density,

$$\frac{c}{8\pi} g^{(2)}(\tau) = \int_{-\infty}^{\infty} d\varpi J^{(2)}(\varpi) \exp[+i(\varpi + \omega_f)\tau], \tag{37}$$

with

$$J^{(2)}(\varpi) = \frac{c}{8\pi} \frac{\xi_0^2}{(2\pi)} \sum_{n=0}^{\infty} \exp(S_n). \tag{38}$$

This result was obtained earlier [19] using the definition (15) of the optical spectral density.

4. Seeding by spontaneous emission. The radio-frequency spectrum

As we have shown above, the FSF laser output is an example of a cyclostationary stochastic process [30]. This property has no substantial consequences for the second-order correlation functions, such as those associated with the optical spectrum, other than the need to average over a period. However, the cyclostationarity has significant consequences in the fourth-order correlation functions. These determine, for example, the RF spectrum of the FSF output intensity. In this section we analyze such signals.

4.1. Passive, frequency-independent cavity

The output intensity of the idealized FSF cavity, seeded only by spontaneous emission, will obviously be noisy. The RF spectrum of the fluctuations of the output intensity is of special interest for applications to metrology, where it is observed the output of a Michelson interferometer. Observations of the RF spectrum were important in the use by Nakamura et al. of a FSF laser, not seeded from an external source, for ranging measurements [5,6]. RF spectral measurements continue to be central to the use of externally seeded FSF lasers for ranging [9].

The RF spectrum derives from the second-order correlation function of the intensity, i.e. the fourth-order correlation function of the electric field of Eq. (25).The intensity is

$$\begin{aligned} I(t) &= \frac{c}{8\pi}\mathscr{E}(t)\mathscr{E}^*(t) \\ &= \frac{c}{8\pi}\sum_{n,k=0}^{\infty} \mathscr{R}^{n+k}\xi_{sp}(t - n\tau_r)\xi_{sp}^*(t - k\tau_r) \times e^{i(n-k)\Delta t - i\Phi_n + i\Phi_k}. \end{aligned} \tag{39}$$

We define the correlation function for this intensity, based on deviation from the mean value $\bar{I}$, as

$$G^{(4)}(t,\tau) = \langle[I(t) - \bar{I}][I(t+\tau) - \bar{I}]\rangle = \langle I(t)I(t+\tau)\rangle - \bar{I}^2. \tag{40}$$

We express the averages as the multiple sums

$$\begin{aligned} \langle I(t)I(t+\tau)\rangle = (c/8\pi)^2 &\sum_{n,k,m,s=0}^{\infty} \mathscr{R}^{n+k}\mathscr{R}^{m+s} \\ &\times \left\langle \xi_{sp}(t - n\tau_r)\xi_{sp}^*(t - k\tau_r)\xi_{sp}(t + \tau - m\tau_r)\xi_{sp}^* \right. \\ &\left. \times (t + \tau - s\tau_r)\right\rangle \times \exp[i(n-k)\Delta t + i(m-s)\Delta(t+\tau) \\ &- i\Phi_n + i\Phi_k - i\Phi_m + i\Phi_s] \end{aligned} \tag{41}$$

and

$$\bar{I}^2 = (c/8\pi)^2\left[\sum_{n,k=0}^{\infty} \mathscr{R}^{n+k}\left\langle \xi_{sp}(t - n\tau_r)\xi_{sp}^*(t - k\tau_r)\right\rangle e^{i(n-k)\Delta t - i\Phi_n + i\Phi_k}\right]^2. \tag{42}$$

To average the product of four random functions we need to invoke additional assumptions about the statistical behavior of the function $\xi_{sp}(t)$. We will assume that this is a Gaussian random process [31]. This assumption allows the factorization

$$\begin{aligned} \left\langle \xi_{sp}(t_1)\xi_{sp}^*(t_2)\xi_{sp}(t_3)\xi_{sp}^*(t_4)\right\rangle &= \left\langle \xi_{sp}(t_1)\xi_{sp}^*(t_2)\right\rangle\left\langle \xi_{sp}(t_3)\xi_{sp}^*(t_4)\right\rangle \\ &+ \left\langle \xi_{sp}(t_1)\xi_{sp}^*(t_4)\right\rangle\left\langle \xi_{sp}(t_3)\xi_{sp}^*(t_2)\right\rangle. \end{aligned} \tag{43}$$

The width of the spontaneous-emission spectral distribution is much larger than all the relevant frequency parameters. Therefore we assume that the τ dependence of the function $F(\tau)$ in Eq. (23) is much more localized than are the variations with τ in Eq. (41). We carry out the ensemble average of the particular products shown above and find that the fourth-order correlation function is independent of time:

$$G^{(4)}(t,\tau) = G^{(4)}(\tau) = G_0 \sum_{M=-\infty}^{\infty} |F(\tau - M\tau_r)|^2 \mathscr{R}^{2|M|} \tag{44}$$

with

$$G_0 = \left(\frac{c}{8\pi}\xi_0^2 \sum_{k=0}^{\infty} \mathscr{R}^{2k}\right)^2. \tag{45}$$

This correlation function does not depend on the frequency shift Δ. Therefore particular characteristics of the FSF behavior is not important; we obtain the same result by considering a cavity that has no frequency shifter. The periodic structure of the correlation functions occur because the field repeats itself after one round trip. The field at any time results builds on superpositions of many contributions, each shifted in time by τ_r and weighted by the reflection coefficient $\mathscr{R}^2$. The interference terms involving different components do not contribute to the mean intensity but they do give important contributions to the correlation function. This correlation function is independent of time and so, by the WK theorem, the RF spectrum $J^{(4)}(\Omega)$ is its Fourier transform,

$$J^{(4)}(\Omega) = \frac{1}{2\pi}\int_{-\infty}^{\infty} d\tau G^{(4)}(\tau)\exp(-i\Omega\tau). \tag{46}$$

Thus the spectrum of output intensity fluctuations is the infinite sum

$$J^{(4)}(\Omega) = \frac{G_0}{2\pi}\int_{-\infty}^{\infty} d\tau \exp(-i\Omega\tau)\sum_{M=-\infty}^{\infty} |F(\tau - M\tau_r)|^2 \mathscr{R}^{2|M|}. \tag{47}$$

We write this as the product of a scaling factor G_0 and two frequency-dependent functions,

$$J^{(4)}(\Omega) = G_0 L_{sp}(\Omega)\mathscr{L}(\Omega). \tag{48}$$

Here the smooth envelope

$$L_{sp}(\Omega) = \frac{1}{2\pi}\int_{-\infty}^{\infty} d\tau |F(\tau)|^2 \exp(-i\Omega\tau) = \frac{1}{2\pi}\frac{\Gamma_{sp}/4}{1 + (\Omega/4\Gamma_{sp})^2} \tag{49}$$

incorporates the broad but finite width of the spontaneous-emission spectrum. For the RF spectrum it suffices to use the approximation $L_{sp}(\Omega) \approx L_{sp}(0) = \Gamma_{sp}/8\pi$. The sum over M in the spectrum (47) produces the factor

$$\mathscr{L}(\Omega) \equiv \sum_{M=-\infty}^{\infty} \mathscr{R}^{2|M|} \exp(-i\Omega M\tau_r) = \frac{1-\mathscr{R}^4}{1-2\mathscr{R}^2\cos\Omega\tau_r+\mathscr{R}^4}. \quad (50)$$

This is a periodic function of Ω with a period $2\pi/\tau_r$. For a high quality cavity, one with $1-\mathscr{R}^2 \ll 1$, this function describes a set of narrow lines, each centered near a value $\Omega_q = 2\pi q/\tau_r$ for some positive integer q. The line profile $\mathscr{L}(\Omega-\Omega_q)$ of each individual component is a Lorentzian

$$\mathscr{L}(x) = \frac{1}{(1-\mathscr{R})[1+(x/\Gamma_c)^2]}, \quad (51)$$

where $\Gamma_c = 2(1-\mathscr{R})/\tau_r$.

Thus the RF spectrum of the passive cavity output comprises a sequence of equidistant spectral features, each with the same narrow profile $\mathscr{L}(x)$, and each centered at an integer multiple of the cavity axial-mode frequency-difference $2\pi/\tau_r$. The width of each peak is determined by the lifetime of a photon in the cavity. The amplitudes of the peaks differ very little. The origin of this spectrum regularity is a periodic repetition of any initial fluctuation of the spontaneous emission source. Note, as remarked above, that the FSF behavior of the cavity has no effect on these properties of the RF spectrum.

Frames (a) and (d) of Fig. 2 illustrate the properties of the correlation function $G_1(\tau)$ of Eq. (44) and the spectrum $S(\Omega)$ of Eq. (47). For this figure the various times have been chosen to illustrate the essential physics rather than to describe any actual realization. The individual peaks of frame (a) have widths set by the atomic spontaneous emission lifetime; in practice those widths would be much less than the spacing, and the figure would show only vertical lines. The dashed-line envelope has a decay time set by the lifetime of a photon in the cavity; in practice this decay would be much more gradual than is shown. The spectral properties of frame (d) are similarly exaggerated. The widths of the individual peaks are set by the cavity decay time, while the dashed-line envelope expresses the spontaneous-emission lifetime.

4.2. Michelson interferometer with input from a passive cavity

Here we analyze the RF spectrum of the output of Michelson interferometer. For simplicity we consider the interferometer formed by an ideal beam splitter and two totally reflecting mirrors. We take the difference of interferometer arms to be the distance $L = cT/2$, where T is a total time delay.

The electric field in the output arm is

$$\mathscr{E}_{Mich}(t) = \frac{1}{2}[\mathscr{E}(t) + \mathscr{E}(t-T)]. \quad (52)$$

The interferometer output intensity,

$$I_{Mich}(t) = \frac{c}{32\pi}|\mathscr{E}(t) + \mathscr{E}(t-T)|^2, \quad (53)$$

can be written as a sum

$$I_{Mich}(t) = \frac{1}{4}[I(t) + I(t-T) + I_{int}(t, t-T)], \quad (54)$$

where $I(t)$ is the output intensity given by Eq. (39). The interference term

$$I_{int}(t, t-T) = 2\Re[\mathscr{E}(t)\mathscr{E}^*(t-T)] \quad (55)$$

makes no contribution to the mean intensity but, as we will show, it has important effects on the RF spectrum of the Michelson-interferometer output. The correlation function for the intensity of Eq. (54),

$$G^{(4)}_{Mich}(t,\tau) = \langle I_{Mich}(t) I_{Mich}(t+\tau)\rangle - \overline{I}^2_{Mich} \quad (56)$$

has two distinct contributions, which we denote as $G^{(4)}_{Mich}(t,\tau) = G^{(4)}_3(t,\tau) + G^{(4)}_{int}(t,\tau)$. The first of these is the sum of three individual correlation functions

$$G^{(4)}_3(t,\tau) \equiv G^{(4)}_3(\tau) = \frac{1}{16}\left[2G^{(4)}(\tau) + G^{(4)}(\tau+T) + G^{(4)}(\tau-T)\right], \quad (57)$$

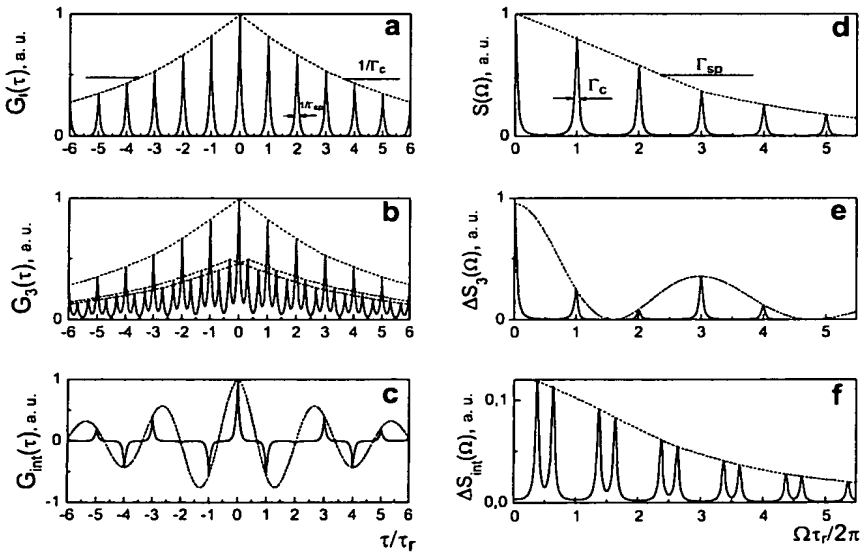

Fig. 2. Left-hand frames (a), (b), (c) show the correlation function, right-hand frames (d), (e), (f) show the resulting spectrum. Top row, frames (a) and (b) show the second-order correlation function of Eq. (44) and the corresponding optical spectrum of Eq. (47). Middle row, frames (b) and (e) show the correlation function $G^{(4)}_3$ of Eq. (57) and the corresponding RF spectrum $J^{(4)}_3$ of Eq. (62). Bottom row, frames (c) and (d) show the correlation function $G^{(4)}_{int}$ of Eq. (58) and the corresponding RF spectrum $J^{(4)}_{int}$ of Eq. (64). The observable spectrum is the sum of contributions (e) and (f).

and is independent of time. The second part originates with the interference intensities,

$$G^{(4)}_{int}(t,\tau) \equiv \frac{1}{16}\langle I_{int}(t,t-T)I_{int}(t+\tau,t+\tau-T)\rangle. \tag{58}$$

This interference term can be averaged in the same way as was done when obtaining $G^{(4)}(\tau)$ in the previous subsection. The result is

$$G^{(4)}_{int}(t,\tau) = G^{(4)}_{int}(\tau) = G_0 \sum_{M=-\infty}^{\infty} F(\tau - M\tau_r)^2 \mathscr{R}^{2|M|} \cos[M\Delta T]. \tag{59}$$

The additional phase shift ΔT between consecutive components in the cavity leads to some modulation of the correlation function with a period $2\pi\tau_r/\Delta T$.

The RF spectrum of the output from the interferometer receives contributions from two parts, corresponding to the two parts of the correlation function,

$$J^{(4)}_{Mich}(\Omega) = J^{(4)}_3(\Omega) + J^{(4)}_{int}(\Omega). \tag{60}$$

The contribution $J^{(4)}_3(\Omega)$ comprises a sequence of equidistant spectral profiles, each with the same profile $\mathscr{L}(\Omega)$ but with different amplitude:

$$\begin{aligned} J^{(4)}_{int}(\Omega) &= \frac{1}{32\pi} \\ &\quad \times \int_{-\infty}^{\infty} d\tau \left[2G^{(4)}(\tau) + G^{(4)}(\tau+T) + G^{(4)}(\tau-T)\right] \exp(-i\Omega\tau) \\ &= \frac{G_0}{32\pi} \sum_{M=-\infty}^{\infty} \mathscr{R}^{2|M|} \int_{-\infty}^{\infty} d\tau \exp(-i\Omega\tau) \cdot \\ &\quad \times \left[2F(\tau - M\tau_r)^2 + F(\tau + T - M\tau_r)^2 + F(\tau - T - M\tau_r)^2\right]. \end{aligned} \tag{61}$$

This function is expressible as the product of a scaling factor and three frequency-dependent functions [in contrast with the two functions of Eq. (48)],

$$J^{(4)}_3(\Omega t) = \frac{G_0}{4} L_{sp}(\Omega)\mathscr{L}(\Omega)\cos^2(\Omega T/2). \tag{62}$$

The first factor, $L_{sp}(\Omega)$, can be considered constant, in keeping with our assumption of large Γ_{sp}. The second factor, $\mathscr{L}(\Omega)$, is that of Eq. (48): it describes a set of narrow peaks, centered at the discrete frequencies $\Omega_q = 2\pi q/\tau_r$. In contrast to the previous section, here there occurs an additional frequency dependence: amplitudes of the narrow discrete components are weighted by the factor $\cos^2(\Omega T/2)$, evaluated at Ω_q. This revision occurs because the correlation function G_3 originates from an incoherent sum of three components delayed by time T. Fig. 2b illustrates the properties of the correlation function $G^{(4)}_3(\tau)$ of Eq. (57) and of the spectrum $J^{(4)}_3(\Omega)$ of Eq. (62). The latter exhibits an overall damped cosine modulation, as expected.

The contribution $J^{(4)}_{int}(\Omega)$ to the RF spectrum from $G^{(4)}_{int}$, discussed next, is qualitatively different. From the definition we obtain the expression

$$\begin{aligned} J^{(4)}_{int}(\Omega) &= \frac{1}{32\pi} \int_{-\infty}^{\infty} d\tau G_0 \sum_{M=-\infty}^{\infty} F(\tau - M\tau_r)^2 \mathscr{R}^{2|M|} \cos[M\Delta T] \exp(-i\Omega\tau) \\ &= \frac{G_0}{16} L_{sp}(\Omega) \sum_{M=-\infty}^{\infty} \mathscr{R}^{2|M|} \cos[M\Delta T] \exp(iM\Omega\tau_r). \end{aligned} \tag{63}$$

This spectral function therefore comprises a set of doublets,

$$\begin{aligned} J^{(4)}_{int}(\Omega) = \sum_{q=-\infty}^{\infty} \Big[&\frac{G_0}{32} L_{sp}(\Omega)\mathscr{L}(\Omega - 2\pi q/\tau_r - \gamma_c T) \\ &+ \frac{G_0}{32} L_{sp}(\Omega)\mathscr{L}(\Omega - 2\pi q/\tau_r + \gamma_c T)\Big]. \end{aligned} \tag{64}$$

Fig. 2f illustrates this spectral structure. The quantity $\gamma_c = \Delta/\tau_r$ appearing here is recognizable as the *chirp rate* used for optical ranging.

To summarize: the total RF spectrum of the Michelson-interferometer output consists of narrow discrete components centered at the frequencies $\Omega_q = 2\pi q/\tau_r$, each weighted by a factor $\cos^2(\Omega_q T/2)$. Each of these components is accompanied by a doublet of components shifted from Ω_q by $\pm\gamma_c T$ and whose amplitudes are almost independent of q. The frequency separation of these doublets incorporates information about the difference in length $cT/2$ of the interferometer arms that are used in ranging applications of FSF lasers [5–9]. Fig. 2 illustrates, on the third line of frames, these features.

It is worth noting that the existence in the RF spectrum of components shifted by $\pm\gamma_c T$ is readily understood from a model of a FSF laser seeded by a phase fluctuating CW laser [7]. Here we see that these components appear in a model of the passive FSF cavity seeded by uncorrelated spontaneous emission as a result of interference of cyclostationary stochastic processes.

4.3. Interferometer input from a frequency-dependent cavity

Here we consider a more realistic model of the FSF laser by including both gain and frequency-dependent losses. The field is given by Eq. (19). We will continue with assumptions made in Section 3.2: the width Γ_{sp} of the spontaneous-emission spectrum is much larger than the width Γ_f of the intracavity filter, so we idealize the spontaneous-emission process $\xi_{sp}(t)$ as a delta-correlated stochastic process; its correlation function is given by Eq. (33). In addition, we assume that the width Γ_f is much larger than both the frequency shift Δ and the cavity axial-mode frequency-difference $2\pi/\tau_r$.

Using the solution (19) for the FSF laser field and the condition $\Gamma_f \gg \Delta, 2\pi/\tau_r$ we obtain, after some complicated but straightforward algebra, the following expression for the intensity correlation function $G^{(4)}(t,\tau)$ defined by Eq. (40):

$$\begin{aligned} G^{(4)}(t,\tau) &= G^{(4)}(\tau) \\ &= \left| \frac{c}{8\pi}\xi_0^2 \int_{-\infty}^{\infty} \frac{d\varpi}{2\pi} \exp(i\varpi\delta\tau) \sum_{n=1}^{\infty} \exp[S(\varpi,n,M)] \right|^2. \end{aligned} \tag{65}$$

Here the argument of the exponent is zero unless $0 < \tau - M\tau_r < \tau_r$ when it is

$$S(\varpi,n,M) = \sum_{l=0}^{n-1} [g_{sat} - f(\varpi - l\Delta)] + \sum_{l=0}^{n-1+M} [g_{sat} - f(\varpi - l\Delta)]. \tag{66}$$

To simplify this expression, we use the condition $\Gamma_f \gg \Delta, 2\pi/\tau_r$ and replace the summation over n in (65) by integration. The exponent $S(\varpi,n,M)$ reaches a maximum at

$$n = n_{max} \simeq \frac{\varpi + \varpi_M}{\Delta} + M/2,$$

with $\varpi_M = \sqrt{\varpi_0^2 - M^2\Delta^2/4}$. In the Gaussian approximation justified in our earlier paper [19] the parameter $\varpi_0 = \sqrt{2(g_{sat} - f_m)\Gamma_f^2}$ is the frequency shift between the maximum of the Gaussian fit to the optical spectrum $J^{(2)}(\omega) = J_0 \exp\left[-(\omega - \varpi_0 - \omega_f)^2/\tilde{\Gamma}^2\right]$ and the filter frequency ω_f. As shown in [19], and justified experimentally in [20], the shift ϖ_0 and the width $\tilde{\Gamma}$ of the FSF-laser spectrum are related by the expression

$$\tilde{\Gamma}^2\varpi_0 = \gamma^3 \equiv \left(\Delta\Gamma_f^2\right). \tag{67}$$

Using the Gaussian approximation we then write

$$\sum_{n=1}^{\infty} \exp[S(\varpi, n, M)] \simeq A \exp[S(\varpi, n_{max}, M)]. \tag{68}$$

The phase and amplitude occurring on the right hand side are

$$S(\varpi, n_{max}, M) \simeq \frac{-\varpi^3 + 3\varpi_0^2\varpi + 2\varpi_0^3}{3\gamma^3} - \frac{M^2}{4M_0^2} \tag{69}$$

$$A \simeq \sqrt{\pi\gamma\tilde{\Gamma}}. \tag{70}$$

Here

$$M_0 = \tilde{\Gamma}/\Delta \gg 1 \tag{71}$$

is the effective number of round trips of a SE photon in the FSF-laser cavity. Integration over ϖ gives finally

$$G^{(4)}(\tau) = G_I \sum_{M=-\infty}^{\infty} F_I(\tau - M\tau_r)^2 \exp\left[-\frac{M^2}{4M_0^2}\right], \tag{72}$$

where

$$G_I = \frac{\pi\gamma^3}{\varpi_0}\left(\frac{c}{4}\xi_0^2\right)^2 \exp\left[-\frac{8\varpi_0^3}{\gamma^3}\right] \tag{73}$$

$$F_I(\tau) = \frac{\tilde{\Gamma}}{\sqrt{2\pi}} \exp\left[-\frac{\tau^2\tilde{\Gamma}^2}{4}\right]. \tag{74}$$

The correlation function (72) is very similar to the correlation function of the output intensity of the passive FSF cavity, Eq. (44), but there are two differences:

1. When gains and losses are present the width of the narrow function $F_I(\tau)$ is determined by the reciprocal of $\tilde{\Gamma}$, the width of the optical spectrum. In the passive cavity this width is fixed by the spontaneous-emission correlation time.
2. The successive maxima of the correlation-function decrease in keeping with a Gaussian law $\exp(-M^2/M_0^2)$ with $M_0\tau_r$ equal to the effective lifetime of a photon in the active FSF cavity.

It can be shown that the same is true for the correlation function of the Michelson-interferometer output excited by the active FSF laser: the contribution $G_3^{(4)}(\tau)$ is given by Eq. (57) with $G^{(4)}(\tau)$ defined by Eq. (59) and the interference term

$$G_{int}^{(4)}(\tau) = G_I \sum_{M=-\infty}^{\infty} F_I(\tau - M\tau_r)^2 \exp\left[-\frac{M^2}{4M_0^2}\right] \cos[M\Delta T]. \tag{75}$$

Thus we conclude that the RF spectrum of the FSF laser output intensity and the Michelson-interferometer output have the same behavior as in the passive cavity. The only difference is that the amplitudes of narrow discrete components centered at the frequencies $\Omega_q = 2\pi q/\tau_r$ and $\Omega_q^{(\pm)} = 2\pi q/\tau_r \pm \gamma_c T$ decrease according to the Gaussian law $\exp(-\Omega^2/\tilde{\Gamma}^2)$ and the shape $\mathscr{L}(\Omega - \Omega_q)$ of each narrow component is not Lorentzian but a Gaussian:

$$\mathscr{L}(x) \propto \exp\left[-x^2/(M_0\tau_r)^2\right]. \tag{76}$$

5. FSF laser with seeding by both spontaneous emission and continuous-wave radiation

5.1. The intensity equation

We consider here an FSF laser seeded simultaneously by spontaneous emission and a monochromatic seed laser. Because there is no nonlinearity in our model (only saturation of gain by the total intensity) the laser field is the sum of two fields described by Eqs. (19) and (20), each created by one of the sources. These sources are statistically independent and so the averaged intensity is also a sum of spontaneous and discrete spectrum intensities,

$$\bar{I} = \bar{I}_{sp} + \bar{I}_{seed}. \tag{77}$$

To evaluate the contribution of the external seed, $\bar{I}_{seed}$, we consider a monochromatic seed, meaning that its bandwidth is much smaller than either the axial mode spacing $2\pi/\tau_r$ or the frequency shift Δ. For such a seed the field $\mathscr{E}_{seed}(t)$ is [19]

$$\mathscr{E}_{seed}(t) = \varepsilon_s \sum_{n=0}^{\infty} a_n \exp[-i\Phi_n - i(\varpi_s + n\Delta)t], \tag{78}$$

where

$$\Phi_n \equiv -\tau_r n[\omega_s + (n+1)\Delta/2]. \tag{79}$$

We write the constant real-valued amplitudes as $a_n = \exp[S_{seed}(g_{sat}, n)]$, where

$$S_{seed}(g_{sat}, n) \equiv n\left[g_{sat} - f_m - \frac{6\varpi_s^2 + 6\varpi_s n\Delta + 6\varpi_s\Delta + 2n^2\Delta^2 + 3\Delta^2 n + \Delta^2}{12\Gamma_f^2}\right]. \tag{80}$$

The contribution $\bar{I}_{seed}$ of the discrete spectrum to the mean intensity $\bar{I}$ reads

$$\bar{I}_{seed} = \frac{c}{8\pi}\overline{|\mathscr{E}_{seed}(t)|^2} = \imath_{seed}\sum_{n=0}^{\infty}|a_n|^2 = \imath_{seed}F_{seed}(g_{sat}), \tag{81}$$

where the intensity of the seed laser radiation injected into the FSF laser cavity is

$$\imath_{seed} = \frac{c}{8\pi}|\varepsilon_s|^2 \tag{82}$$

and

$$F_{seed}(g_{sat}) = \sum_{n=0}^{\infty} \exp[2S_{seed}(g_{sat}, n)]. \tag{83}$$

The mean intensity of the spontaneous-emission spectrum,

$$\bar{I}_{sp} = \frac{c}{8\pi}\overline{|\mathscr{E}_{sp}(t)|^2} \tag{84}$$

has been evaluated earlier [19]. It can be written as

$$\bar{I}_{sp} = \imath_{sp}F_{sp}(g_{sat}). \tag{85}$$

Here

$$\imath_{sp} \equiv \frac{c\Gamma_f\xi_0^2}{8\pi^2} \tag{86}$$

is the intensity of spontaneous emission within the spectral interval Γ_f and

$$F_{sp}(g_{sat}) \equiv \frac{\pi^{1/2}}{2}\sum_{n=1}^{\infty}\exp[S_{sp}(g_{sat}, n)], \tag{87}$$

with

$$S_{sp}(g_{sat}, n) = n\left[2(g_{sat} - f_m) - \frac{\Delta^2}{12\Gamma_f^2}(n^2 - 1)\right] - \ln(n)/2. \tag{88}$$

Because the stochastic averaging removes any interference contribution the sum of the two terms (81) and (85) gives the total intensity $\bar{I}$. It is this intensity that saturates the gain $g_{sat} = g_0/(1 + \bar{I}/I_{sat})$. The determination of $\bar{I} = I_{sat}(\frac{g_0}{g_{sat}} - 1)$ requires the solution of the following transcendental equation for g_{sat}:

$$\frac{\imath_{sp}}{I_{sat}}F_{sp}(g_{sat}) + \frac{\imath_{seed}}{I_{sat}}F_{seed}(g_{sat}) = \left(\frac{g_0}{g_{sat}} - 1\right). \tag{89}$$

Our interest is with FSF lasers in which the output spectrum is both smooth and broad. Such conditions are possible if I_c, $I_0 \ll I_{sat}(\eta - 1)$ and if the spectral filter is sufficiently broad, $\Gamma_f \gg \Delta$. For these conditions the general operation of the FSF laser is readily understood from Fig. 3. The figure shows the cavity gain as a constant, and the loss as varying around the central frequency. The frequency shifter displaces any seed frequency toward the right. By contrast to the operation of a conventional laser, there exists a finite band of frequencies $\omega_f - \varpi_0 < \omega < \omega_f + \varpi_0$, symmetrically centered about the central frequency of the filter ω_f, where the frequency-dependent effective gain is positive, $g_{sat} - f_m - \frac{\varpi_0^2}{2\Gamma_f^2} > 0$. Any frequency component within this band will undergo growth as successive round trips increase the frequency by Δ. However, once the frequency exceeds $\omega_f + \varpi_0$ the losses dominate, and the frequency component will diminish as further frequency shifts occur. Thus we expect the saturated gain g_{sat} to be slightly greater than the minimum loss, f_m.

To proceed we make two approximations. First, because we expect the saturated gain g_{sat} to be slightly greater than f_m we approximate it as $g_{sat} = f_m$ on the right hand side of Eq. (89). Second, as in our earlier work [19], we assume that the seed frequency is far from the central frequency of the laser spectrum, so that the laser output spectrum is very close to a Gaussian form.

We express $S_{sp}(g_{sat}, n)$ and $S_{seed}(g_{sat}, n)$ as a Taylor series, centered around the value $n = n_i$, where $dS_i(n)/dt = 0$ ($i \equiv sp$ or $i \equiv seed$), and we retain only terms through second order in $(n - n_i)$. Within this Gaussian approximation the number of discrete components in the interval ϖ_0 is large, $\varpi_0/\Delta \gg 1$, and so we replace the summation over n in Eqs. (83) and (87) by an integration. We thereby obtain the results

$$F_{seed} \simeq \sqrt{\pi} M_0 \exp\left[\frac{2\varpi_0^3 + \varpi_s^3 - 3\varpi_s\varpi_0^2}{3\gamma^3}\right] \tag{90}$$

and

$$F_{sp} = \frac{\pi}{2}\frac{\Gamma_f}{\varpi_0}\exp\left[\frac{4\varpi_0^3}{3\gamma^3}\right]. \tag{91}$$

Eq. (89) now reads

$$\frac{\gamma}{\varpi_0}\exp\left[\frac{4\varpi_0^3}{3\gamma^3}\right] + \epsilon\sqrt{\frac{\gamma}{\varpi_0}}\exp\left[\frac{2\varpi_0^3 + \varpi_s^3 - 3\varpi_s\varpi_0^2}{3\gamma^3}\right] = \frac{1}{\beta}. \tag{92}$$

Here the small parameter β, defined as

$$\beta \equiv \frac{\pi}{2}\frac{I_0\Gamma_f}{I_{sat}(\eta - 1)\gamma}, \tag{93}$$

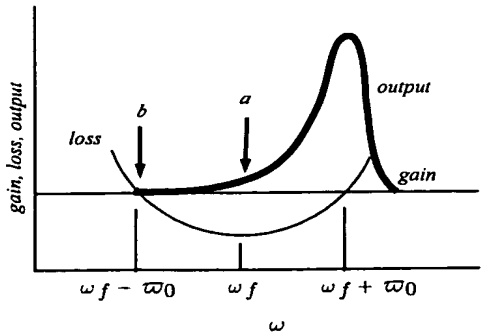

Fig. 3. Qualitative portrait of the magnitude of the FSF laser output-field spectral-density as a function of frequency, together with frequency dependence of the gain (constant) and loss (quadratic). Two choices of seed frequency are marked.

describes the spontaneous-emission source. The parameter

$$\epsilon \equiv \frac{2}{\sqrt{\pi}}\frac{\Gamma_f}{\gamma}\frac{I_c}{I_0}, \tag{94}$$

expressing the relative importance of the seed laser, is the ratio of the intensity of the seed laser to the spontaneous-emission intensity in the spectral interval $\sqrt{\pi}\gamma/2$. Using experimental data [20] we estimate that for an Yb^{3+}-fiber laser the parameter ϵ is equal to 1 when the power of the seed laser injected into the FSF cavity is about 50 μW.

5.2. Competition between spontaneous emission and continuous-wave seeding

In this subsection we discuss solutions to Eq. (92). We consider two specific choices for the seed frequency. In the first, marked *a* in Fig. 3, the seed frequency is at the minimum of the loss curve, $\varpi_s = 0$. In the second, marked *b* in the figure, the seed is near the frequency where growth first becomes possible.

5.2.1. Resonant seed, $\omega_s = \omega_f$

When the seed frequency coincides with the minimum of losses, $\varpi_s = 0$, Eq. (92) takes the form of a quadratic equation

$$Y^2 + \epsilon Y = \frac{1}{\beta} \tag{95}$$

involving the variable

$$Y = \sqrt{\frac{\gamma}{\varpi_0}}\exp\left[\frac{2\varpi_0^3}{3\gamma^3}\right]. \tag{96}$$

From the solution,

$$Y = \frac{2/\beta}{\epsilon + \sqrt{\epsilon^2 + 4/\beta}}, \tag{97}$$

we obtain the intensity of the continuous spectrum $\bar{I}_{sp}$ as

$$\bar{I}_{sp} = \frac{4/\beta}{\left[\epsilon + \sqrt{\epsilon^2 + 4/\beta}\right]^2} I_{sat}(\eta - 1) \tag{98}$$

and the intensity of the discrete spectrum as

$$\bar{I}_{seed} = \frac{2\epsilon}{\epsilon + \sqrt{\epsilon^2 + 4/\beta}} I_{sat}(\eta - 1). \tag{99}$$

We see that $\bar{I}_{seed} > \bar{I}_{sp}$ for $\epsilon > 1/\sqrt{2\beta} \gg 1$. This is to be expected: when the seed frequency is resonant with the loss minimum, $\omega_s = \omega_f$, then the seed laser must compete with spontaneous emission that has been amplified throughout the frequency interval from $\omega_f - \varpi_0$ to ω_f.

5.2.2. Seed at gain edge, $\omega_s = \omega_f - \varpi_0$

A better choice for the seed laser is $\omega_s = \omega_f - \varpi_0$. Eq. (92) then reads

$$\frac{\gamma}{\varpi_0}\exp\left[\frac{4\varpi_0^3}{3\gamma^3}\right] + \epsilon\sqrt{\frac{\gamma}{\varpi_0}}\exp\left[\frac{4\varpi_0^3}{3\gamma^3}\right] = \frac{1}{\beta}. \tag{100}$$

The solution to this equation for ϖ_0 with $\beta \ll 1$ gives the following expressions for the intensity $\bar{I}_{sp}$ of the continuous spectrum

$$\bar{I}_{sp} = \frac{1}{1 + \epsilon\sqrt{\sigma}} I_{sat}(\eta - 1) \tag{101}$$

and the intensity $\bar{I}_{seed}$ of the discrete spectrum

$$\bar{I}_{seed} = \frac{\epsilon\sqrt{\sigma}}{1 + \epsilon\sqrt{\sigma}} I_{sat}(\eta - 1) \tag{102}$$

where the parameter σ is defined as

$$\sigma \equiv \left(\frac{3}{4}\ln\frac{1}{\beta_{sp}}\right)^{1/3}. \quad (103)$$

This parameter is almost independent of laser parameters. In previously reported experimental work [20] the measured value of σ was $\sigma \simeq 2$. The discrete spectrum dominates in the case of a detuned seed laser starting with much smaller intensities: $\bar{I}_{seed} > \bar{I}_{sp}$ for $\epsilon > 1/\sqrt{\sigma} \sim 1$.

We see that even for optimal detuning of the seed laser there exists a large background of continuous radiation originating from spontaneous emission. For a strong seed laser, $\epsilon \gg 1$, the ratio of spontaneous to seed intensity is

$$\frac{\bar{I}_{sp}}{\bar{I}_{seed}} \simeq \frac{1}{\epsilon\sqrt{\sigma}}. \quad (104)$$

This means that, roughly speaking, the ratio of continuous to discrete spectra is equal to ratio of seed laser intensity to the intensity of spontaneous emission in the spectral interval ϖ_0.

6. Summary and conclusions

We provide here the first complete theory of the spontaneous-emission seeded FSF laser based on correlation functions. We present the second-order correlation function, from which one obtains the optical spectrum of the radiation emerging from the FSF cavity. Although the correlation function is not stationary, it is periodic, and so a period-averaged correlation function leads to a simple expression for the spectrum.

We also present the fourth-order correlation function analysis with which one can evaluate the RF spectrum of the laser output intensity and of the output of a Michelson interferometer, as is used in optical-ranging metrology. We show that even in a FSF laser seeded solely by spontaneous emission this spectrum comprises a set of doublets, whose spacing gives directly a measure of the length difference between the interferometer arms. The existence of this structure in the RF spectrum of a the Michelson-interferometer output results from correlation of interference terms of individual components of a cyclostationary stochastic processes, and is not seen in the optical spectrum of the FSF laser.

We discuss the operation of a FSF laser whose field originates from the joint action of spontaneous emission and a continuous-wave monochromatic laser seed. We show that in the FSF laser the competition between SE and external seed does not act in the usual way, of exponential growth of modes with greater gain. Instead, there occurs a balance between the two fields that is related linearly, rather than exponentially, to the control parameters. Although it would be desirable to suppress the spontaneous-emission component of the FSF laser output, thereby improving the signal-to-noise ratio for optical-ranging technique based on phase modulation of the CW seed laser, we show that this is not possible. This behavior differs from that of a normal laser.

We have not here discussed the temporal properties of the laser output. The statistical approach we have used in this paper, based on an analysis of the correlation functions and the spectral characteristics, is necessary because we consider a FSF laser seeded by spontaneous emission – a sequence of events that is completely chaotic. A time series of the laser output, just like the time series of the seeding spontaneous emission, is chaotic and conveys no information.

Acknowledgements

We acknowledge support by the Stiftung Rheinland-Pfalz für Innovation and by CNES, INTAS and NSAU (06-1000024-9075). LPY acknowledges support by the Deutsche Forschungsgemeinschaft (436-UKR-113/16).

References

[1] F.V. Kowalski, P.D. Hale, S.J. Shattil, Opt. Lett. 13 (1988) 622.
[2] I.C.M. Littler, S. Balle, K. Bergmann, J. Opt. Soc. Am. B. 8 (1991) 1412.
[3] I.C.M. Littler, S. Balle, K. Bergmann, Opt. Comm. 88 (1992) 514.
[4] I.C.M. Littler, J.H. Eschner, Opt. Comm. 87 (1992) 44.
[5] K. Nakamura, T. Miyahara, M. Yoshida, T. Hara, H. Ito, IEEE Photonics Technol. Lett. 10 (1998) 1772.
[6] K. Nakamura, T. Hara, M. Yoshida, T. Miyahara, H. Ito, IEEE J. Quant. Elect. 36 (2000) 305.
[7] L.P. Yatsenko, B.W. Shore, K. Bergmann, Opt. Comm. 242 (2004) 581.
[8] L.P. Yatsenko, V.M. Khodakovsky, V.V. Ogurtsov, G. Bonnet, B.W. Shore, K. Bergmann, Proc. SPIE 6054 (2005) 60540T.
[9] V.V. Ogurtsov, L.P. Yatsenko, V.M. Khodakovskyy, B.W. Shore, G. Bonnet, K. Bergmann, Opt. Comm. 266 (2006) 266.
[10] S. Balle, I.C.M. Littler, K. Bergmann, F.V. Kowalski, Opt. Comm. 102 (1993) 166.
[11] J. Martin, Y. Zhao, S. Balle, K. Bergmann, M.P. Fewell, Opt. Comm. 112 (1994) 109.
[12] F.V. Kowalski, S. Balle, I.C.M. Littler, K. Bergmann, Opt. Eng. 33 (1994) 1146.
[13] S. Balle, K. Bergmann, Opt. Comm. 116 (1995) 136.
[14] K. Kasahara, K. Nakamura, M. Sato, H. Ito, Opt. Rev. 4 (1997) 180.
[15] K. Nakamura, F.V. Kowalski, H. Ito, Opt. Lett. 22 (1997) 889.
[16] F.V. Kowalski, K. Nakamura, H. Ito, Opt. Comm. 147 (1998) 103.
[17] G. Bonnet, S. Balle, Th. Kraft, K. Bergmann, Opt. Comm. 123 (1996) 790.
[18] M. Stellpflug, G. Bonnet, B.W. Shore, K. Bergmann, Opt. Express 11 (2003) 2060.
[19] L.P. Yatsenko, B.W. Shore, K. Bergmann, Opt. Comm. 236 (2004) 183.
[20] V.V. Ogurtsov, L.P. Yatsenko, V.M. Khodakovskyy, B.W. Shore, G. Bonnet, K. Bergmann, Opt. Comm. 266 (2006) 627.
[21] I.C.M. Littler, H.M. Keller, U. Gaubatz, K. Bergmann, Zs. Physik D 18 (1991) 307.
[22] D.T. Mugglin, A.D. Streater, S. Balle, K. Bergmann, Opt. Comm. 104 (1993) 165.
[23] J.R.M. Barr, G.Y. Liang, M.W. Phillips, Opt. Lett. 18 (1993) 1010.
[24] M.J. Lim, C.I. Sukenik, T.H. Stievater, P.H. Bucksbaum, R.S. Conti, Opt. Comm. 147 (1998) 99.
[25] M. Cashen, V. Bretin, H. Metcalf, J. Opt. Soc. Am. B 17 (2000) 530.
[26] F.V. Kowalski, C. Ndiaye, K. Nakamura, H. Ito, Opt. Comm. 231 (2004) 149.
[27] A. Yoshizawa, H. Tsuchida, Opt. Comm. 155 (1998) 51.
[28] M.W. Phillips, G.Y. Liang, J.R.M. Barr, Opt. Comm. 100 (1993) 473.
[29] K.A. Shore, D.M. Kane, IEEE J. Quant. Elect. 35 (1999) 1053.
[30] W.A. Gardner, A. Napolitano, L. Paura, Signal Process. 86 (2006) 639.
[31] J.R. Klauder, E.C.G. Sudarshan, Fundamentals of Quantum Optics, W.A. Benjamin, Inc. New York, Amsterdam, 1968.

Optics Communications 282 (2009) 2212–2216

Contents lists available at ScienceDirect

Optics Communications

journal homepage: www.elsevier.com/locate/optcom

An intuitive picture of the physics underlying optical ranging using frequency shifted feedback lasers seeded by a phase-modulated field

L.P. Yatsenko [a], B.W. Shore [b,*], K. Bergmann [c]

[a] Institute of Physics, National Academy of Sciences of Ukraine Prospect, Nauki 46, Kiev-39, 03650, Ukraine
[b] 618 Escondido Circle, Livermore, CA 94550, USA
[c] Department of Physics and OPTIMAS Research Center at the Technical University, Kaiserslautern, 67653 Kaiserslautern, Germany

ARTICLE INFO

Article history:
Received 24 November 2008
Accepted 16 February 2009

PACS:
42.30.–d
42.55.–f
42.60.Da
42.62.Eh

ABSTRACT

Frequency shifted feedback (FSF) lasers have been demonstrated to have interesting and useful features when used for optical ranging. The use of a phase-modulated seed to the FSF laser dramatically improves the signal-to-noise ratio, enabling distance measurements with the accuracy expected of optical interferometry. We present here an intuitively accessible description of the physics that underlies this dramatic enhancement of optical ranging signals. Unlike a free-running FSF laser, each one of the many equidistant frequency components of the seeded FSF laser spectrum (typically $>10^4$) has a definite amplitude, and a phase which varies with component number and modulation frequency Ω of the seed radiation. Suitable adjustment of Ω gives all components a common phase; the resulting constructive interference enhances the signal by orders of magnitude.

1. Introduction

Many optical ranging technologies make use of interference between two ray paths, one of known distance and the other to a target object, to measure distances with subwavelength accuracy. Lasers have served well as the radiation sources for optical ranging. In particular, frequency shifted feedback (FSF) lasers have been proposed and demonstrated [1–7]; their properties offer potential advantages over other laser-based techniques for ranging [8–13].

In recent papers [10,11,13] we have proposed and demonstrated the use of a FSF laser whose seed frequency is phase modulated. This easily implemented modification improves the signal-to-noise ratio by many orders of magnitude and thus overcomes some recognized problems. Although the mathematics has been presented in detail [10], and experimental demonstrations have been published [11,13], the mathematical formalism has provided no intuitive picture of the role of phase modulation.

We here offer a very simple presentation of the principles involved in the phase-modulated FSF laser and its use for optical ranging. To explain the technology we first review the basic operation of a Michelson interferometer, because this forms the heart of the ranging measurement. We start by pointing out, as is well known, how classical interferometry with monochromatic light has an intrinsic ambiguity in measuring lengths: these are determined only within a multiple of the optical wavelength. One technique for overcoming this limitation is the use of phase-modulated light as interferometer input, but this technique has limitations that we mention.

Having presented this background, we discuss how a phase-modulated FSF laser, being the superposition of a very large number (typically more than 10^4) of mutually coherent components of a radiation field, overcomes the shortcomings of a conventional laser source when applied to ranging. It relies on a measurement of frequency, which is inherently more accurate than measurements of response amplitudes. As will be explained, the FSF laser with phase modulation greatly improves the signal-to-noise ratio.

1.1. Basic Michelson interferometer

The schematic diagram of Fig. 1 shows the essentials of a Michelson interferometer: from a source of collimated radiation two paths, whose lengths differ by L, recombine at a detector that produces a signal proportional to the power, i.e. proportional to the square of the local electric field. The two contributions to the detected field are derived from a common source field but differ by the delay time $T \equiv 2L/c$. Thus the detector signal has the form

$$S(t,T) = \mathcal{N}\{|E(t)|^2 + |E(t-T)|^2 + 2Re[E(t)E(t-T)^*]\}. \quad (1)$$

Here, the factor $\mathcal{N}$ expresses the efficiency of the detectionprocess as related to the square of the electric field. Note that when the material of the target differs from that of the reference there occurs upon reflection a difference in phase that acts as an increment of length [14]; we here ignore this phase difference.

* Corresponding author. Tel.: +1 925 455 0627.
E-mail address: bwshore@alum.mit.edu (B.W. Shore).

0030-4018/$ - see front matter © 2009 Elsevier B.V. All rights reserved.
doi:10.1016/j.optcom.2009.02.042

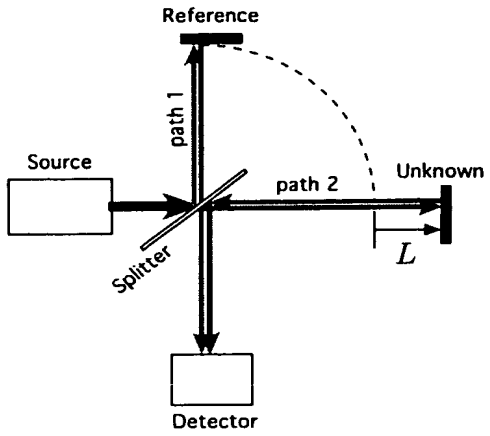

Fig. 1. Basic schematic layout of a Michelson interferometer, showing light source, power detector, and two arms. For clarity the overlapping beams are shown here as slightly offset spatially.

The simplest implementation of such a Michelson interferometer occurs when the source is monochromatic, of wavelength $\lambda = 2\pi c/\omega$. We write this field, at the position of the detector, in the complex form

$$E(t) = \mathscr{E}\exp[-i\omega t]. \tag{2}$$

Here, $\mathscr{E}$ is the amplitude of the source field and ω its frequency. It is this field that, after passing through the two paths of the interferometer, appears at the detector to produce a signal.

With such a field the detector signal is independent of time t and is expressible as

$$S(t,T) = \mathscr{G}[1+\cos(\omega T)], \tag{3}$$

where $\omega T = 4\pi L/\lambda$. The constant $\mathscr{G} = 2|\mathscr{E}|^2\mathscr{N}$ determines the size of the signal for a given electric field. Measurements of this signal, for varying optical frequency ω, provide values of $\cos(\omega T)$ and with that a measure of the ratio L/λ. Thus the technique is capable of providing values of L with an accuracy better than the optical wavelength λ, but with an ambiguity (of λ) arising from the periodicity of the cosine. When used for measurements of distance a classical interferometers cannot give values of absolute distance, only distances relative to some integer multiple of the wavelength. There are many methods capable of resolving this ambiguity [15–17]. One of them uses a phase-modulated light source. The following paragraphs review the operation of that technique, as a preliminary to the discussion of phase modulation in FSF lasers.

1.2. Absolute distance measurements using a phase-modulated light source

One of the suggestions for making absolute measurements of distance using an interferometer came from Webb et al. [18], who suggested the use of a phase-modulated laser as interferometer input. We here follow their approach and consider a light source upon which we impose a specified phase variation $\varphi(t)$,

$$E(t) = \mathscr{E}\exp[-i\omega t - i\varphi(t)]. \tag{4}$$

The detector signal is then expressible as

$$S(t,T) = \mathscr{G}\{1+\cos[\omega T + \varphi(t) - \varphi(t-T)]\}. \tag{5}$$

A particularly useful phase variation is a sinusoidal modulation, achievable using an electro-optical modulator driven at a radio frequency Ω,

$$\varphi(t) = \varphi_0 + \beta\sin(\Omega t + \vartheta). \tag{6}$$

Here, β is the modulation index, φ_0 is the initial optical phase and ϑ is the initial phase of the modulation signal.

For such harmonic modulation of the phase $\varphi(t)$ the phase difference $\varphi(t) - \varphi(t-T)$ is also sinusoidal

$$\begin{aligned}\varphi(t) - \varphi(t-T) &= \beta\{\sin[\Omega t + \vartheta) - \sin(\Omega(t-T) + \vartheta]\}\\ &= 2\beta\sin(\Omega T/2)\cos[\Omega(t - T/2) + \vartheta]\\ &\equiv z\sin(\Omega t + \phi),\end{aligned} \tag{7}$$

with the amplitude and phase

$$z = 2\beta\sin(\Omega T/2), \quad \phi = \vartheta - (\Omega T + \pi)/2. \tag{8}$$

The resulting interferometer signal is

$$\begin{aligned}S(t,T) &= \mathscr{G}\{1+\cos[\omega T + z\sin(\Omega t + \phi)]\}\\ &\equiv \mathscr{G}\{1+\cos(\omega T)\cos[z\sin(\Omega t+\phi)]\\ &\quad - \sin(\omega T)\sin[z\sin(\Omega t+\phi)]\}.\end{aligned} \tag{9}$$

By using the Jacobi–Anger identities

$$\sin(z\sin\chi) = 2\sum_{k=1}^{\infty} J_{2k-1}(z)\sin[(2k-1)\chi], \tag{10}$$

$$\cos(z\sin\chi) = J_0(z) + 2\sum_{k=1}^{\infty} J_{2k}(z)\sin(2k\chi), \tag{11}$$

we rewrite the signal as [18]

$$\begin{aligned}S(t,T) = \mathscr{G}\Bigg\{&1 + \cos(\omega T)J_0(z) + 2\cos(\omega T)\sum_{k=1}^{\infty} J_{2k}(z)\sin[2k\Omega t + 2k\phi]]\\ &-2\sin(\omega T)\sum_{k=1}^{\infty} J_{2k-1}(z)\sin[(2k-1)\Omega t + (2k-1)\phi]\Bigg\}.\end{aligned} \tag{12}$$

The signal of Eq. (12) is a superposition of the harmonics of the modulation frequency Ω, each weighted by an appropriate Bessel function. Viewed in the frequency domain these appear as discrete components. We can use a narrow-band filter to select any individual harmonic, using phase-locked detection or other means. In this way we can restrict consideration to a single value of k.

For example, consider a filter that selects just the first-harmonic, $k = \pm 1$. The signal responsible for this harmonic is

$$\begin{aligned}S_1(t,T) &= -2\mathscr{G}J_1(z)\sin(\omega T)\sin(\Omega t + \phi)\\ &\equiv \mathscr{G}J_1(z)[\cos(\Omega t + \phi + \omega T) - \cos(\Omega t + \phi - \omega T)].\end{aligned} \tag{13}$$

From the measured amplitude of this signal we obtain the value of a Bessel function $J_1(z)$. This gives information about z, from which we obtain information about the absolute value of the delay T. Because the modulation frequency Ω is radiofrequency (RF), it has a wavelength that is orders of magnitude longer than the optical wavelength of the light source. It is this long wavelength, rather than the optical wavelength, that determines the ambiguity with which we measure the distance L.

This method of ranging has two drawbacks. First, we have to adjust the interferometer to maximize $\sin(\omega T)$ in Eq. (13). Second, the method relies on a quantitative measurement of light intensity. From the magnitude of the signal we obtain the argument of the Bessel function z and, from Eq. (8), the time delay T. It is difficult to calibrate measurements of intensity, and hence the method has intrinsically low accuracy. These drawbacks have prevented practical application of the method for ranging using Michelson interferometer and phase-modulated light.

2. Optical ranging using a FSF laser

The development of frequency shifted feedback (FSF) lasers [1–13] offers a means of overcoming the previous limitations of

RF-modulated interferometry and of obtaining very high accuracy. The basic principles underlying a FSF laser are readily understood: it comprises an optical cavity (or closed loop) in which there occurs a frequency-shifting element, typically an acousto-optic modulator (AOM), and material that provides gain to a range of frequencies. A small portion of the cavity radiation emerges as output; see Fig. 2.

From a single seed field of frequency ω_s and phase $\varphi_s(t)$ a succession of round trips within the bounded laser cavity (or fiber loop) produce a set of frequencies, spaced equidistantly by the frequency shift Δ induced by the AOM. Typically the gain bandwidth is sufficient to amplify a large number ($>10^4$) of discrete frequency components, each with definite frequency and phase. These form a frequency comb spaced by the AOM frequency Δ.

As we explain below, instead of one laser field an FSF laser provides a large number of field components, each of which gives a similar contribution to the first-harmonic signal, but with different phases. One might expect that the averaging of so many signals would eliminate any interference effects. On the contrary, we will show that, when the modulation frequency matches a delay-dependent value, the signal is greatly enhanced; from a measurement of this frequency one obtains a very accurate value of the delay T and hence of the distance.

2.1. The FSF laser

The output field from a FSF laser is the sum of many components

$$E(t) = \sum_n \mathscr{E}_n \exp[-i(\omega_s + n\Delta)t - i\Phi_n - i\varphi_s(t - n\tau)], \tag{14}$$

Component n has a fixed frequency that has been shifted from ω_s by $n\Delta$. It has the phase of the seed laser taken at an early time $\varphi_s(t - n\tau)$ and it has undergone an additional phase shift,

$$\Phi_n = n\tau[\omega_s + (n+1)\Delta/2]. \tag{15}$$

where τ is the round-trip time within the FSF cavity. Gain from the amplifying medium and loss from the filter alter the original seed amplitude $\mathscr{E}_0$ to the value $\mathscr{E}_n$. As earlier work has shown [5], the distribution of amplitudes is well described by a Gaussian centered at a peak value n_{max} and of width n_W. In this approximation the amplitude $\mathscr{E}_n$ is

$$\mathscr{E}_n = \mathscr{E}_0 \exp\left[-\frac{(n - n_{max})^2}{n_W^2}\right]. \tag{16}$$

Fig. 3 illustrates the distribution of field components, showing the varying amplitudes, spaced by the AOM frequency Δ. The figure shows a representative distribution of gain and of loss from the filter. The peak of the Gaussian, parametrized by n_{max}, occurs close to the frequency at which gain equals loss.

2.2. Coherence properties of the FSF laser output

It is well known that the output of a multimode laser can, when the modes are phase-locked, appear as a periodic succession of very short pulses [19]. The frequencies contributing to this output are separated by the free spectral range (FSR) of the laser cavity, $2\pi/\tau$ for a round-trip time of τ, and their phases vary linearly with frequency. A FSF laser can also operate in a regime in which the output is a train of short pulses [20]. The field is then a set of mode-locked frequencies spaced by the FSR, $2\pi/\tau$.

However, for use in optical ranging, the operating regime of the FSF laser is such that no mode-locking occurs. The frequencies of the output field, are spaced by the AOM frequency Δ, and their static phases Φ_n vary quadratically with component number n. The temporal output is periodic with the period $2\pi/\Delta$ and appears as a train of frequency-chirped pulses [5].

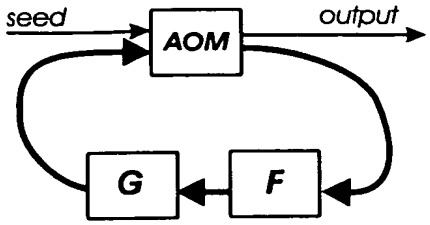

Fig. 2. Symbolic diagram of a ring cavity showing gain G, spectral filter F and frequency-shifter AOM, as well as seed and output (from [7]).

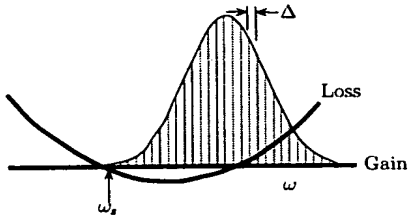

Fig. 3. Frequency components of FSF laser, spaced by Δ, as a function of frequency ω. Gain and filter loss are shown, as is the seed frequency ω_s.

2.3. Optical ranging using a FSF seed having sinusoidally modulated phase

The extension of the discussion of a single phase-modulated laser to a FSF laser is straightforward. Let us assume that the phase of the FSF seed laser is modulated as

$$\varphi = \beta \sin(\Omega t + \vartheta). \tag{17}$$

When such phase modulation of the seed is present the phase of a specific FSF component n reads

$$\varphi_n = \beta \sin(\Omega(t - n\tau) + \vartheta). \tag{18}$$

Therefore, we have

$$\varphi_n = \beta \sin(\Omega t + \vartheta_n), \quad \vartheta_n = \vartheta - n\Omega\tau, \tag{19}$$

meaning that each FSF component has, in addition to the static phase Φ_n, a modulated phase φ_n that originates with the seed-laser phase. The initial phase of that modulation varies linearly with component number n.

Eq. (12) has given the expression for the signal for a single modulated laser. With the FSF laser we have many such modulated components. The detector signal sums the results from each of them, appropriately phased.

For example, consider filtering that selects just the modulation frequency Ω (the first of the harmonics). Then the signal, generalizing Eq. (13), is the sum of all the individual components of the FSF field,

$$S_1(t,T) = 2\mathscr{N} J_1(z) \sum_n |\mathscr{E}_n|^2 \{\cos(\Omega t + \phi_n + [\omega_s + n\Delta]T) - \cos(\Omega t + \phi_n - [\omega_s + n\Delta]T)\}, \tag{20}$$

where

$$\phi_n \equiv \vartheta_n - (\Omega T + \pi)/2, \quad \vartheta_n = \vartheta - n\Omega\tau. \tag{21}$$

We rewrite this as two separate sums

$$S_1(t,T) = 2\mathscr{N} J_1(z) \sum_n |\mathscr{E}_n|^2 \cos[\Omega t - n(\Omega\tau - T\Delta) + \psi_+] - 2\mathscr{N} J_1(z) \sum_n |\mathscr{E}_n|^2 \cos[\Omega t - n(\Omega\tau + T\Delta) + \psi_-], \tag{22}$$

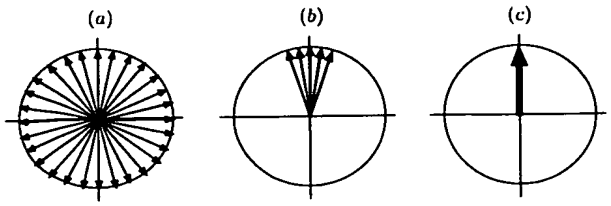

Fig. 4. Schematic distribution of vector phases. (a) a uniform distribution of vectors resulting from small constant phase increments between components of the radiation field. (b) A narrow distribution of phases, as occurs when the resonance condition is nearly but not exactly fulfilled. (c) All vectors have phases that obey the resonance condition.

where

$$\psi_{\pm} \equiv \pm\omega_s T - (\Omega T + \pi)/2 + \vartheta. \tag{23}$$

Each of these sums is responsible for a distinct resonance (an enhancement of the signal within a narrow frequency range) as noted in the following paragraphs.

2.4. Vector picture of interferometer output signal

Because the terms of the summation have amplitude and phase, they can be regarded as vectors. When the modulation frequency Ω obeys the resonance condition

$$\Omega\tau = \pm T\Delta + m2\pi, \quad m = 0, 1, 2, \ldots. \tag{24}$$

then all vectors in one of the sets are aligned in the same direction. The resulting vector has, as magnitude, the arithmetic sum of the amplitude of each of the many components. The resulting first-harmonic signal is

$$S_1(t,T) = \pm 2\mathcal{N}J_1(z)\sum_n |\mathscr{E}_n|^2. \tag{25}$$

Fig. 4c illustrates this situation. By contrast with the results of a single laser, here we have the sum of many components (typically $>10^4$), and so the signal is greatly enhanced by comparison with a single laser.

However, when the modulation frequency is nonresonant, so that the argument $(\Omega\tau \pm T\Delta)$ is nonzero, the vectors point, with angular increment $n(\Omega\tau \pm T\Delta)$, into different directions. Their summed amplitude will therefore typically be small, or zero. Fig. 4a illustrates this situation.

To evaluate the interferometer-arm delay T, from which we derive the ranging information, we must evaluate the modulation frequency Ω for which the resonance condition of Eq. (24) holds. This is recognizable as the modulation frequency which maximizes the interferometer output signal at a frequency

$$\Omega_m^{(\pm)} = \pm\frac{\Delta}{\tau}T + m\frac{2\pi}{\tau}. \tag{26}$$

The components will be in phase, and the signal will be large, only within a small interval

$$\delta\Omega \sim \frac{2\pi}{n_W}\frac{T}{\tau}\Delta. \tag{27}$$

of frequencies near such a resonance frequency, set by the width n_W of the component distribution, see Eq. (16). Fig. 4b illustrates this situation.

Our optical ranging procedure, using a phase-modulated seed for a FSF laser, is based upon identifying the frequency where the resonance occurs. We do not need to measure relative intensity and interpret this through a Bessel function. It is this change, from measuring relative intensity to measuring a frequency (facilitated by strong signal enhancement at resonance), that gives our method such an advantage.

Our procedure also dramatically enhances the signal observed with an unseeded FSF laser [8,9]. The phases of a FSF laser seeded by a phase-modulated input laser have well defined phases. By contrast, when the FSF grows from spontaneous emission the FSF field comprises a continuous distribution of frequency combs. Within any comb the phases are fixed by geometry, and are not adjustable, but the phases between different combs (started by spontaneous emission) are random. Our method uses the coherence of the various components to enhance the signal compared with growth from noise.

2.5. Observing higher harmonics

We remark that the resonances exist in the amplitudes of all harmonics of the output of Michelson interferometer excited by FSF laser with phase-modulated seed laser. For example, the signal of the second harmonic is

$$S_2(t,T) = 2\mathcal{N}J_2(z)\sum_n |\mathscr{E}_n|^2 \sin[2\Omega t - n(2\Omega\tau - T\Delta) + \psi_+^{(2)}] - 2\mathcal{N}J_2(z)\sum_n |\mathscr{E}_n|^2 \sin[2\Omega t - n(2\Omega\tau + T\Delta) + \psi_-^{(2)}], \tag{28}$$

where

$$\psi_{\pm} \equiv \pm\omega_s T - (2\Omega T + \pi)/2 + 2\vartheta. \tag{29}$$

The resonance condition is

$$\Omega\tau = \frac{1}{2}[T\Delta + 2\pi m]. \tag{30}$$

In a similar way one can show that for the kth harmonic the resonance condition is

$$\Omega\tau = \frac{1}{k}[T\Delta + 2\pi m]. \tag{31}$$

Each harmonic signal varies in proportion to a Bessel function whose argument z, defined in Eq. (8), varies with distance L. When a distance is such that the Bessel function $J_1(z)$ for order 1 is small, thereby limiting the signal strength, the Bessel function $J_k(z)$ of a higher order will then give a larger signal.

3. Summary and outlook

Phase modulation interferometry has been earlier suggested and is well understood [18]. The physics of FSF laser operation is equally well understood [5]. The concept of ranging with a free-running FSF laser has been described and demonstrated some years ago by Japanese researchers [8,9]. However, the free-running FSF laser is not a practical device for industrial applications.

The use of a phase-modulated FSF seed overcomes the drawbacks noted for a free-running FSF laser. As has been demonstrated, this technique provides dramatic enhancement of the interferometer output signal by orders of magnitude if, and only if, the modulation frequency Ω obeys the resonance condition of Eq. (24). The accuracy of the ranging technique stems from the accuracy with which frequency measurements can be made, in contrast to measurements of relative intensity.

Although the literature contains rigorous mathematical treatments of FSF lasers [10] the present discussion offers a simple straightforward picture of the physics behind the observation of the dramatic signal enhancement resulting from the phase modulation of the FSF seed.

Acknowledgements

We acknowledge support from the Stiftung Rheinland-Pfalz für Innovation and the Research Center OPTIMAS at the Technisches Universität Kaiserslautern.

References

[1] P.D. Hale, F.V. Kowalski, IEEE J. Quant. Electron. 26 (1990) 1845.
[2] K. Shimizu, T. Horiguchi, Y. Koyamada, Exp. Appl. Opt. 32 (1993) 6718.
[3] F.V. Kowalski, S. Balle, I.C.M. Littler, K. Bergmann, Opt. Eng. 33 (1994) 1146.
[4] K. Nakamura, F. Abe, K. Kasahara, T. Hara, M. Sato, H. Ito, IEEE J. Quant. Electron. 33 (1997) 103.
[5] L. Yatsenko, B.W. Shore, K. Bergmann, Opt. Commun. 236 (2004) 183.
[6] V.V. Ogurtsov, L.P. Yatsenko, V.M. Khodakovskyy, B.W. Shore, G. Bonnet, K. Bergmann, Opt. Commun. 266 (2006) 266.
[7] L.P. Yatsenko, B.W. Shore, K. Bergmann, Opt. Commun. (2008), doi:10.1016/j.optcom.2008.10.002.
[8] K. Nakamura, T. Miyahara, H. Ito, Appl. Phys. Lett. 72 (1998) 2631.
[9] K. Nakamura, T. Hara, M. Yoshida, T. Miyahara, H. Ito, IEEE J. Quant. Electron. 36 (2000) 305.
[10] L.P. Yatsenko, B.W. Shore, K. Bergmann, Laser Opt. Commun. 242 (2004) 581.
[11] V.V. Ogurtsov, L.P. Yatsenko, V.M. Khodakovskyy, B.W. Shore, G. Bonnet, K. Bergmann, Opt. Commun. 266 (2006) 627.
[12] K.A. Shore, D.M. Kane, IEEE Procc-Optoelectron. 153 (2006) 284.
[13] V.V. Ogurtsov, V.M. Khodakovskyy, L.P. Yatsenko, B.W. Shore, G. Bonnet, K. Bergmann, Opt. Commun. 281 (2008) 1679.
[14] L.P. Yatsenko, M. Loeffler, B.W. Shore, K. Bergmann, Appl. Opt. 43 (2004) 3241.
[15] P. de Groot, Appl. Opt. 30 (1991) 3612.
[16] P. de Groot, J. McGarvey, Opt. Lett. 17 (1992) 1626.
[17] B. Chen, X. Cheng, D. Li, Appl. Opt. 41 (2002) 5933.
[18] D.J. Webb, R.M. Taylor, J.D.C. Jones, D.A. Jackson, Opt. Commun. 66 (1988) 245.
[19] L. Dahlstrom, Opt. Commun. 5 (1972) 157.
[20] G. Bonnet, S. Balle, T. Kraft, K. Bergmann, Opt. Commun. 123 (1996) 790.